UNIVERSITY OF SOUTHAMPTON

# DYNAMICS OF SPACE CHARGE AND ELECTROLUMINESCENCE MODELLING IN POLYETHYLENE

By

JUNWEI ZHAO

A thesis submitted for
the degree of Doctor of Philosophy

Electronics and Computer Science
Faculty of Physical and Applied Science
University of Southampton
United Kingdom

April 2012

UNIVERSITY OF SOUTHAMPTON

## ABSTRACT

FACULTY OF PHYSICAL AND APPLIED SCIENCE
ELECTRONICS AND COMPUTER SCIENCE

Doctor of Philosophy

# DYNAMICS OF SPACE CHARGE AND ELECTROLUMINESCENCE MODELLING IN POLYETHYLENE

by Junwei Zhao

Space charge has been recognized as an important factor contributing to the electrical failure of the cable insulation. Extensive efforts have been made to investigate space charge dynamics within polymeric insulations under electric stresses. Basic information about space charge has been recognized resorting to modern charge mapping techniques but the underlying mechanisms for charge transport, charge trapping characteristics are not yet well understood. Hence theoretical modelling and numerical simulation are employed to simulate the space charge and provide an insight into the charge distribution in dielectrics. This thesis comprises the quantitative analysis of space charge through numerical modelling and experimental investigations of charge trapping in polymeric insulation materials.

A bipolar charge transport model which involves bipolar charge injection from the electrodes, charge transport with trapping and recombination in the bulk has been developed to simulate the dynamics of space charge in polyethylene. The build-up of space charge in polyethylene under dc electric fields has been modelled. The influence of parameters related to the properties of polyethylene on the formation of space charge has been recognized. Furthermore, this model is introduced to simulate the dynamics of corona charge decay in polyethylene. The formation of charge packets in polyethylene is also investigated using a numerical modelling approach.

A fast pulsed electro-acoustic system along with a data processing program has been developed to investigate the behaviour of space charge in polyethylene under ac voltages. The understanding of space charge under ac stresses has also been simulated using the further developed bipolar charge transport model. Experiments and simulation have also been expanded into understanding electroluminescence, which is an indication of pre-aging of polymers under ac stress.

# Contents

# List of Figures

# List of Tables

# Definitions and Abbreviations

## Symbols

| | |
|---|---|
| $E,F$ | Electric field, $Vm^{-1}$ |
| $\rho$ | Net Charge density, $Cm^{-3}$ |
| $\varepsilon$ | Permittivity of dielectric, $Fm^{-1}$ |
| $n$ | Density of mobile species, $Cm^{-3}$ |
| $\mu$ | Mobility of charge carrier, $m^2V^{-1}s^{-1}$ |
| $q, e$ | Electronic charge, C |
| $d$ | Sample thickness, m |
| $\sigma$ | Conductivity, $Sm^{-1}$ |
| $\varphi_m$ | Working function of the metal |
| $\varphi$ | Working function of the insulator |
| $\varphi_B$ | Potential barrier height at the interface |
| $E_{Fm}$ | Fermi level of the metal |
| $E_F$ | Fermi level of the insulator |
| $E_F'$ | Fermi level of the contact between the metal and an insulator |
| $\chi$ | Electron affinity of the insulator |
| $E_C$ | Lowest energy level of the conduction band of insulator |
| $E_V$ | Highest energy level of the valence band of insulator |
| $E_G$ | Band gap of the insulator |
| $\sigma_1, \sigma_2$ | Density of surface charge, $Cm^{-2}$ |
| $J, j$ | Current density, $Amm^{-2}$ |
| $A$ | Richardson constant, $A = 1.2 \times 10^6\ Am^{-1}\ K^{-2}$ |
| $k_B$ | Boltzmann constant, $k$=1.38 $\times 10^{-23}\ m^2kgs^{-2}K^{-1}$ |
| $h$ | Planck constant, $h$=6.626 $\times 10^{-34}\ m^2kgs^{-1}$ |
| $m_e$ | Effective mass of tunnelling electrons |

| | |
|---|---|
| $m_0$ | Mass of free electrons |
| $T$ | Temperature, K |
| $v$ | Attempt-to-escape frequency, $s^{-1}$ |
| $a$ | Separation distance of the potential barrier |
| $\theta_a$ | Ratio of free carrier density to the total carriers |
| $d_{eff}$ | Effective thickness due to the presence of traps in dielectrics |

## Abbreviations

| | |
|---|---|
| AC, ac | Alternating current |
| Al | Aluminium |
| Au | Gold |
| DC, dc | Direct current |
| EL | Electroluminescence |
| EVA | Ethylene-vinyl acetate |
| HDPE | High density polyethylene |
| HTS | High temperature superconducting cable |
| HVAC | High voltage alternating current |
| HVDC | High voltage direct current |
| Hz | Hertz |
| kV | Kilo volts |
| LDPE | Low density polyethylene |
| LLDPE | Linear low density polyethylene |
| LIMM | Laser intensity modulation method |
| LIPP | Laser induced pressure pulse method |
| MDPE | Medium density polyethylene |
| PC | Polycarbonate |
| PE | Polyethylene |
| PEA | Pulsed electro-acoustic method |
| PEI | Polyetherimide |
| PI | Polyimide |
| PP | Polypropylene |
| PS | Polystyrene |
| PTFE | Polytetrafluoroethylene |

| | |
|---|---|
| PVC | Polyvinyl chloride |
| PVDF | Polyvinylidene fluoride |
| PWP | Pressure wave propagation method |
| Semicon | Semiconducting polymer |
| SCLC | Space charge limited current |
| SEA | Step electro-acoustic method |
| TP | Thermal pulse method |
| TRR | Total recombination rate |
| TSP | Thermal step pulse method |
| XLPE | Cross-linked polyethylene |

# Publications

**Journal papers:**

J. Zhao, G. Chen and P. L. Lewin, "Space charge in polyethylene under combined ac and dc voltages," submitted to *Journal of Physics D: Applied Physics*, 2012.

J. Zhao, G. Chen and P. L. Lewin, "Investigation into the formation of charge packets in polyethylene: Experiment and Simulation," submitted to *Journal of Applied Physics*, 2012.

G. Chen and J. Zhao, "Observation of negative differential mobility and charge packet in polyethylene," *Journal of Physics D: Applied Physics*, 44 (21), pp. 212001, 2011.

J. Zhao, Z. Xu, G. Chen and P. L. Lewin, "Modelling of space charge in polyethylene under ac fields," *Journal of Applied Physics*, 108 (12), pp. 124107-1 - 7, 2010.

**Conference papers:**

1. J. Zhao, Z. Xu, G. Chen and P. L. Lewin, "Space Charge Behaviour in Polyethylene under AC Electric Fields," *2011 IEEE CEIDP*, 16-19 October 2011, Cancun, Mexico.
2. N. Hussin, J. Zhao and G. Chen, "The AC Breakdown and Space Charge Characteristics of LDPE in the Presence of Crosslinking Byproduct," 2011 International Symposium on Electrical Insulation Materials, 6-11 September, 2011, Kyoto, Japan.
3. J. Zhao, G. Chen and P. L. Lewin, "Investigation into the Formation of Charge Packets in Polyethylene under dc Electric Fields," 14$^{th}$ International Symposium on Electrets, 28-31 August, 2011, Montpellier, France.

4. J. Zhao, G. Chen and P. L. Lewin, "Measurement of Mobility of Positive Charge Carriers in Polyethylene," *Dielectrics 2011,* 13 - 15 April 2011, Canterbury, UK.
5. J. Zhao, D. H. Mills, G. Chen and P. L. Lewin, "Modelling of Electroluminescence in Polymers Using a Bipolar Charge Transport Model," *UHVnet 2011*, 18-19 January 2011, Winchester, UK.
6. J. Zhao, Z. Xu, G. Chen and P. L. Lewin, "Numerical Modelling of Space Charge in Polyethylene under AC Fields," 10th IEEE International Conference on Solid Dielectrics, 4-9 July 2010, Potsdam, Germany.
7. G. Chen, J. Zhao and Y. Zhuang, "Numerical Modelling of Surface Potential Decay of Corona Charged Polyethylene Material," 10th IEEE International Conference on Solid Dielectrics, 4-9 July 2010, Potsdam, Germany.
8. Z. Xu, J. Zhao and G. Chen, "An Improved Pulsed Electroacoustic System for Space Charge Measurement under AC Conditions," 10th IEEE International Conference on Solid Dielectrics, 4-9 July 2010, Potsdam, Germany.
9. J. Zhao, Z. Xu, G. Chen and P. L. Lewin, " Effect of field-dependent mobility on current density and dynamics of space charge in polyethylene," 2009 IEEE Conference on Electrical Insulation and Dielectric Phenomena, 18-21 October 2009, Virginia Beach, Virginia, USA.

# Acknowledgements

I would like to present my sincere appreciation to my supervisors, Dr George Chen and Prof. Paul L. Lewin. George gives me patient guidance and essential suggestions on the simulation of the space charge in solids. He also provides valuable comments and solutions to the oncoming experimental problems during the research. Paul provides me more chances to communicate with others especially on the electroluminescence modelling and gives valuable support on writing and publishing papers. I must thank them gratefully for their quality supervision.

Thanks are also given to Dr Zhiqiang Xu, who gave me training on the experimental techniques, especially the collaboration on the detection of space charge under ac voltages. Thanks to David H Mills who provides the measurement data of electroluminescence by which I could use to fit with the simulation. And I give my thanks to the Lab technicians for their support on experimental work in the Tony Davies High Voltage Laboratory.

Finally thank all my friends for their companies in Southampton and special thanks to my family for their keen support from China.

# Chapter 1 Introduction

## 1.1 Polymeric insulation materials

### *1.1.1 Polymers*

Polymers are a category of organic materials which are composed of long chain molecules and branching. The long chain molecule is a periodic structure of monomers (small molecules) connected by covalent bonds. The number of monomers in the long chain can be up to tens of thousands, leading to a large molecular weight of up to millions. The characteristics of the long chain and its branching structure determine the property of polymers. Polymers can be classified into two groups according to thermal performance (a) thermoplastics, which have linear or branched structures. They can be shaped and reprocessed when heated; (b) thermosets, which normally have molecular chains cross-linked together with covalent bonds in the form of a network. They cannot be reprocessed once cross-linked even after being heated. The linear, branched and cross-linked structures of polymers are shown in Figure 1-1 [1]. Polymers can be produced by stringing a series of monomers together under controlled pressure and chemical conditions. To tailor polymers to specific requirements or operational circumstances, different types of fillers, additives, e.g., plasticizers, flame retardants, are incorporated during the manufacturing process to achieve appropriate properties,

e.g. erosion resistance, chemical stability. Different types of monomers can also be polymerized together to form a copolymer, e.g., ethylene-vinyl acetate, which possesses improved properties to some extent. Polymer blends, which are a mixture of two compatible polymers and possesses the advantages of two materials, is another way of creating new materials for desired properties. In addition, polymer composites, which include a certain concentration of micro/nano or macro sized foreign particles in the polymer matrix, is a promising alternative to provide improved properties for engineering applications [2, 3].

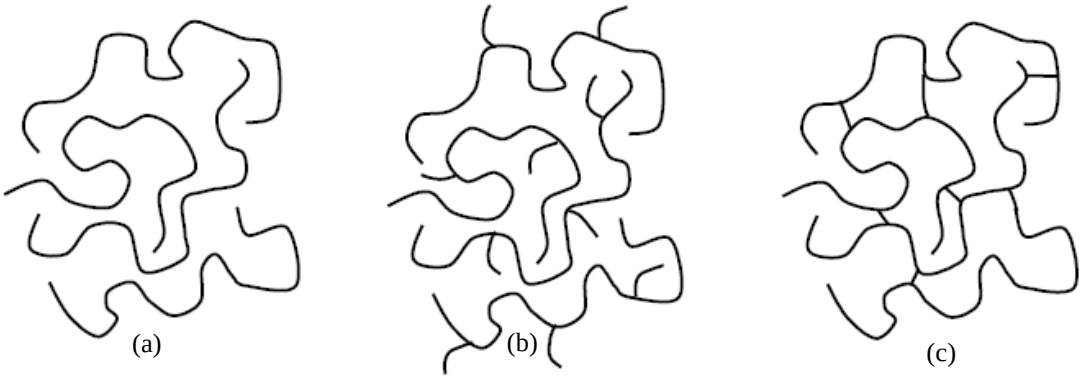


**Figure 1-1:** Linear, branched and cross-linked structure of polymers: (a) linear; (b) branched; (c) cross-linked.

Polymers play a significant role in human life since the beginning of the mankind. Natural polymers, such as protein in our food, cellulose for our clothing and coating and others have a great importance of building human history. In the 18$^{th}$ century, the natural resin extruded from the rubber tree Hevea brasiliensis was used to produce natural rubbers for the use of tyres and wheels [4]. In the 19$^{th}$ century, the modification of natural resins leaded to a prominent use of the cellulose derivatives. Celluloid from the nitration of cellulose, the first semi-synthetic polymer, was widely used for textiles and coatings [4]. It is not until the 20$^{th}$ century that synthetic polymers promoted the great development of polymers in the history. A variety of synthetic polymers was commercially produced and used in daily life and industries. In the 1930s, Wallace Carothers from Du Pont discovered nylon, which has been widely used as the replacement of silk. The development of polyethylene prepared from ethylene at the same time brought the largest volume of use in the world today.

Polymers used for electrical insulation typically have high dielectric strength, low dielectric loss along with ease of manufacturing. They have demonstrated good performance in electrical engineering. The first use of synthetic polymers in the electrical engineering is the phenolic resins as the insulation in the electrical applications [5]. Vulcanized fibre which has high mechanical strength is also one of the early insulating materials used in circuit breakers. Polyvinyl chloride (PVC), which has high electrical strength, volume resistivity and surface resistance, has been used as wire and cable insulation since the 1930s and used for cable sheath and wire covering due to its resistance to water and oxygen [6]. Polyethylene (PE) is a nonpolar polymer having low permittivity, low dielectric loss and high breakdown strength and has been developed into a variety of materials [7], such as low density polyethylene, high density polyethylene and cross-linked polyethylene and widely used for high voltage power cable insulations. Polypropylene (PP) has a melting point of up to 170℃ and is a good choice for the wire and cable insulations operated at high temperatures [8]. Polytetrafluoroethylene (PTFE) having the carbon-fluorine bonds has low dielectric loss, dielectric constant and exceptional chemical resistance and has been used for high temperature and space electrical insulations. Polystyrene (PS) prepared from the monomer styrene, has very high resistivity of $10^{19}$ Ωm and low loss factor and is normally used for producing low loss capacitors [8]. Polyvinyl carbazole has a high softening temperature and good dielectric properties and is preferably used as the impregnation for paper capacitors. Polyimide (PI) has excellent high temperature properties and oxidative stability and is normally used for wire enamel or impregnating resin in the rotating machines [1]. Rubber which is a vulcanization product of polymers, e.g. silicone rubbers, has high elastic extensions, sufficient dielectric strength and low dielectric loss factors for the use as the insulation of wires and cables in the distribution and medium voltage transmission lines as well as in coalmines, submarines and ship wiring. Epoxy resin is a thermosetting polymer, having good mechanical and insulating properties, and is particularly suitable for casting of the electrical components and also used for the impregnation of electrical machine insulation. Epoxy mouldings also act as insulation for instrument transformers and dry transformers. For outdoor applications, the polymeric insulators produced from ethylene propylene rubbers and silicone rubbers have demonstrated advantages over the traditional porcelain and glass insulators [9]. The dielectric properties of widely used polymeric insulating materials are given in Table 1-1[7, 10, 11].

**Table 1-1:** Dielectric properties of common polymeric insulation materials

| Polymer | Permittivity @60Hz | Volume resistivity (Ω·cm) | Dielectric loss factor @1MHz | Dielectric strength ($MVm^{-1}$) |
|---|---|---|---|---|
| PVC | 3.4-5.5 | $10^{15}$ | 0.006-0.019 | 25.6-34 |
| PP | 2.2 | $10^{16}$ | 0.0005-0.0018 | 25.6 |
| PTFE | 2.1 | $10^{16}$ | <0.0003 | 17.7 |
| PS | 2.5 | $>10^{14}$ | 0.0001-0.0004 | 19.7 |
| PC | 3.2 | $2\times10^{16}$ | 0.01 | 15 |
| PI | 4.1 | $3\times10^{15}$ | 0.009@106 Hz | 12.2 |
| Silicone rubber | - | $10^{14}$-$10^{16}$ | - | >20 |
| Epoxy | 4.6-5.0 @1MHz | $10^{16}$ | - | 14.1-15.7 |

### *1.1.2 Polyethylene*

Polyethylene (PE) is a hydrocarbon polymer which is polymerized from ethylene at high temperature and high pressure environment. The molecular structure of polyethylene may be represented simply as $(CH_2)_n$ where $n$ is the degree of polymerization as shown in Figure 1-2. Typically the number $n$ is in excess of 100 and can be as high as 250,000 or more, resulting in molecular weights ranging from 1400 to more than 3,500,000 [7]. However, the chemical structure of a polyethylene system is far more complex. Polyethylene is a semi-crystalline material, which is a mixture of crystalline regions and amorphous regions. An arrangement of chain folding is necessary to accommodate long chains within the crystal entity. Groups of these folded long chains form a single crystal block that is called a lamella. The thickness of the lamella is only 10 nm, which is remarkably less than its lateral dimension in the order of 10-20 μm. Polyethylene chains which form crystalline structures are often arranged to form larger aggregates, called spherulites, which radiate radially from the core until approaching others. These spherulites typically have a diameter of tens of micrometres. The spherulite structure comprises a folded chain crystalline lamella and the interlamellar amorphous region tying lamella together in a polymer bulk [12]. The schematic diagram of the polyethylene bulk is shown in Figure 1-3.

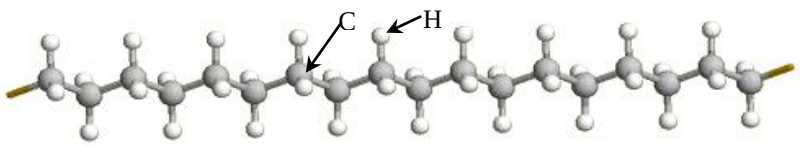


**Figure 1-2:** Molecular structure of polyethylene.

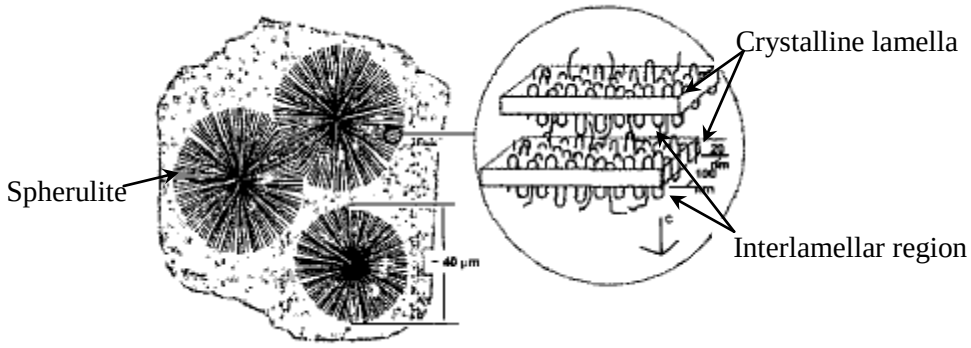


**Figure 1-3:** Morphology of semi-crystalline polyethylene [13].

Polyethylene is produced through polymerization of ethylene. The process can be realized by radical polymerization, anionic addition polymerization, ion coordination polymerization or cationic addition polymerization techniques. Each method results into a different type of polyethylene, as the manufacturing process is able to control the crystallinity, the branching of molecular chains hence the properties of polyethylene. Polyethylene is classified into a broad range of categories, such as high density polyethylene (HDPE), medium density polyethylene (MDPE), low density polyethylene (LDPE), linear low density polyethylene (LLDPE), which have variable mechanical properties, based mostly on its density (or molecular weight) and branching characteristics. Cross-linked polyethylene (XLPE) is a thermoset plastic produced by cross-linking polyethylene, mostly HDPE and MDPE, using free radicals generated by peroxides, ultraviolet or electron beam irradiation [14]. XLPE exhibits excellent mechanical properties and thermal resistance. The principle properties of different types of polyethylene can be found in [7].

In terms of electrical properties, polyethylene is a non-polar thermoplastic material that has lower permittivity, lower dielectric loss and higher electric strength than conventional paper insulation of power cables, and hence becomes a preferable insulation material for the high voltage and even extra high voltage cables. The advantages of polyethylene insulation system over paper/oil insulation are low cost of manufacturing, easier installation and maintenance other than the above superior electrical properties given in Table 1-2 [9-11, 13, 14]. Since the introduction of polyethylene as power cable insulation in the early 1950's, the designing, manufacturing and using polyethylene power cables for high voltage systems has advanced rapidly. In 1969, a 225 kV LDPE insulated cable was firstly installed in

France; followed by the application of 400 kV cables since 1985; the development of 500 kV cable has been under investigation since 1990's [15, 16]. However, polyethylene can only be operated at the maximum temperature of 70℃ below the average operating temperature of 90℃ for underground cables due to its low melting temperature and large thermal expansion coefficient [17]. The sustained current rating, overload and short-circuit temperature of this type of cables were limited. This was solved by cross-linking technology during polymerization of ethylene. And the resulted cross-linked polyethylene (XLPE) can sustain performance up to the temperature of 90℃ and has improved mechanical properties at elevated temperature. The reduced susceptibility to water treeing also favours the high voltage cable insulation. XLPE cable gradually presents its priority in newly constructed transmission or distribution lines and replacement of existing paper insulation HV cables. XLPE cable is free of maintenance that is pretty suitable for underground transmission in highly densely populated cities or urban areas. The first extruded 145 kV XLPE submarine cable was installed in 1973 by ABB. Since then with the significant improvement in producing clean polyethylene, highly advanced cable manufacturing technology and the new generation of extrusion systems, high voltage XLPE cables used at nominal voltages varying from 110 kV up to 500 kV have come into service [18, 19]. In the past decade, high voltage direct current (HVDC) cables with polymeric insulation have attracted growning attention over the world as the advantages of HVDC systems used for the interconnection of large power system and bulk power transmission using dc submarine cable links. The increasing development of wind farms is leading to increased installation of HVDC underground cables [20].

**Table 1-2:** Electrical properties of polyethylene

| Parameters | LDPE | HDPE | XLPE |
|---|---|---|---|
| Permitivity $\varepsilon_r$ (@ 1MHz) | 2.25-2.35 | 2.3-2.35 | 2.4 |
| Tan$\delta$ (@ 1 MHz) | $<5\times10^{-4}$ | $10^{-3}$ | $10^{-3}$ |
| Breakdown strength ($kVmm^{-1}$) | 20-160 | 20-160 | 50 |
| Volume resistivity ($\Omega$·cm) | $>10^{16}$ | $>10^{16}$ | $\sim10^{16}$ |
| Arc resistance (sec) | 135-160 | 200-250 | - |

### *1.1.3 Degradation of polymeric insulation*

When a polymer insulated cable comes into operation, the insulation experiences the combination of electrical stress, thermal and mechanical forces. The degradation of insulation could be initiated where high or divergent electrical stress occurs due to the influence of impurities, defects and microvoids in the bulk of insulation or at the interfaces of materials. The degradation in polymeric insulations may develop into different behaviours at different ageing stages such as electroluminescence, partial discharge, treeing and eventual breakdown. The trees growth in polymeric insulation are considered as a pre-breakdown phenomenon and can be classified into three types: electrical tree, water tree and electrochemical tree [21]. The electrical tree is one of the main reasons for long-term degradation of polymeric insulations used in high voltage ac system. Extensive research has investigated electrical trees in polymeric insulations, especially in polyethylene [22]. Typically electrical trees grow in regions of high stress, such as metallic asperities, conducting contaminants and structure irregularities. Microvoids inevitably exist in polymeric insulation materials. These voids have low permittivity and electrical strength, the electrical stress within voids could be higher determined by these low permittivity localizations and may initiate partial discharge due to the breakdown of gas in voids. Partial discharge can generate degradation structure from void surface which are essentially electrical trees [23]. These electrical trees probably evolve until breakdown of the polymer insulation. At the initiation stage of electrical trees, there are two precursory phenomena: one is formation of degradation region; the other is electroluminescence (EL) [24]. The relationship between EL and the degradation of XLPE under high fields has been investigated by Fan et al [25]. The results show that photo-degradation due to EL light is not the dominant mechanism of electrical degradation during the induction period of tree initiation. This suggests that the electron impact theory, i.e., electrons injected from electrode are accelerated in micro voids and/or polymer free volume by high electric fields, and collide with polymer molecules or chromophores which are excited or ionized, is probably responsible for EL and degradation. Although electroluminescence, partial discharge and electrical tree are investigated from experiments and analysed or even modelled by numerical approaches, the degradation of polymer insulation cannot be fully understood because the whole degradation/aging process involves multi-factors of electrical, thermal and mechanical stresses. However, the above degradation phenomena are all affected or related to electrical charges within polymeric insulations

or at interfaces when polymeric insulation is subjected to electric stress. No matter whether the charge is injected from electrodes or dissociated from ionization of impurities or particles within polymers, the low conductivity and trapping sites in the polymers both lead to the accumulation of this charge, referred as to space charge. This charge can distort the electric field distribution within dielectrics and initiate partial discharge, electrical trees, electroluminescence and/or other degradation processes.

## 1.2 Research aims and objectives

Extensive experimental efforts have been made to investigate the characteristics of space charge in the past decade in order to understand the correlation between space charge and the ageing process of the polymeric insulation materials. Substantial information of charge dynamics in polymers has been reported. However the behaviour of space charge varies in wide range of materials; it behaves differently over specific range of electric fields as well. It is also affected by the environmental conditions, such as temperature and humidity. In addition, the presence of charge packets in polymers reveals a new aspect of charge dynamics. This further complicates the understanding of the generation, transportation of charge carriers in the bulk of polymers. Therefore there is a research need to link the characteristics of charge carriers in polymers with molecular structure and properties of polymers, which may help improve the life expectation of high voltage power cables and assist cable manufacturing. The aim of this project is to examine the space charge characteristics in polymeric insulations under various electric fields and investigate the underlying physics behind space charge and finally to interpret the charge behaviours in polymers under electric stress.

Even though experiments can demonstrate dynamics of space charge in polymers under electric stress, it only provides the overall net charge distribution rather than detailed information of charge carriers. Therefore a numerical modelling approach has been employed to simulate the dynamics of space charge in solid dielectrics and to understand the effects of related physical parameters on charge behaviour and the consequent electric field distribution in the bulk of materials. The charge transport process is especially taken into consideration to examine the influence of different charge transport mechanisms on the build-up of space charge in polymers. The relaxation of space charge in dielectrics also needs to be examined through numeric simulation when the applied field is removed. The numeric model is also expected to be

extended into wide range of fields including the investigation into the space charge relaxation in the corona charged polymer films. In addition to the dc condition, the modelling work is expected to reproduce space charge behaviour under ac conditions and helps understand the characteristics of space charge and electroluminescence in polymers, which is originated by recombination of bipolar charge carriers in polymers under a non dc stress.

The phenomenon of charge packets in polymeric insulation materials complicates the classical understanding of space charge in solids. Further experimental investigation into the dynamics of charge packets in polymers has to be undertaken. The numerical modelling is expected to be able to reproduce the formation of charge packets and provide a theoretical knowledge of the nature of charge packets and the correlation between the formation of charge packets and the characteristics of charge carriers.

## 1.3 Contributions

This thesis contributes to the understanding of space charge characteristics in polymeric insulation materials through theoretical modelling and experimental investigations. The dynamics of space charge in polyethylene under dc electric stress is simulated using a bipolar charge transport model, which considers the bipolar charge injection, transport with trapping and recombination processes. From the simulation, the influence of charge injection, different conduction mechanisms together with the trapping dynamics and recombination of opposite charge carriers on the resultant space charge in polyethylene is understood.

The bipolar charge transport model is used to simulate the discharging and surface potential decay of corona charged polyethylene films. Numerical model reproduces the crossover phenomenon of the surface potential decay and reveals that bipolar charge recombination in the bulk of polyethylene and positive charge extraction from grounded electrode both contributes to the charge decay process.

The packet-like space charge phenomenon is observed in experiments, which reveal a reduction of charge carrier’s velocity with electric field or a negative differential mobility of charge carriers in polyethylene. Numerical simulation work

concludes that this decrease of velocity with electric field is substantial to the formation of charge packets in the polyethylene.

A fast pulsed electro-acoustic system along with a signal denoising & data processing program has been developed to examine space charge behaviours in polyethylene under ac electric stress. Experiments and numerical modelling both reveal that there is limited charge accumulation under ac stress mostly in the vicinity of the electrodes; and that hetero-charge can be accumulated near the electrodes at lower frequencies. But the combined ac and dc voltage has been found to be able to significantly affect the threshold and amount of space charge in polyethylene. In addition, the electroluminescence process in polyethylene under ac stress is reproduced using the numerical simulation based on a theory of bipolar charge recombination in the bulk of polyethylene and at the electrodes.

## 1.4 Structure of thesis

This thesis reports the research work on space charge in polyethylene under electric stresses completed by quantitative numerical modelling and experimental investigations. It is structured in several chapters describing the following work.

Chapter 2 describes the basics of space charge and existing research on space charge in polymeric insulation materials.

Chapter 3 reports the simulation of the dynamics of space charge in polyethylene under dc electric fields using a bipolar charge transport model.

Chapter 4 describes the characteristics of positive charge packets in polyethylene under dc electric fields and the analysis of the formation of the packet-like space charge through numerical modelling approach.

Chapter 5 describes the behaviour of space charge in polyethylene subjected to individual ac electric fields and combined ac and dc stresses using a fast pulsed electro-acoustic measurement system. The further understanding of the characteristics of space charge under ac stresses is achieved using the numeric simulation approach.

Chapter 6 reports the numeric modelling of electroluminescence in polyethylene under ac electric stresses and the discussion of the effects of voltage waveform, voltage amplitude and ac frequency as well as parameters on the electroluminescence.

Chapter 7 summarizes the conclusions from above work on the space charge dynamics and electroluminescence in polyethylene and discusses the limitations of the numerical model and future work.

# Chapter 2 Space Charge in Polymeric Insulation Materials

To achieve the understanding of the space charge in polymeric insulation materials, the basics of space charge has to be acknowledged. This chapter first introduces the definition of space charge in dielectrics. Classic physics of charge generation and transport are described to provide a general understanding of the behaviours of electrical charge carriers. Then a review of existing research work on space charge in polyethylene-based insulation is described. A variety of mapping techniques for space charge in solids, especially the pulsed electro-acoustic method is detailed as well.

## 2.1 Classification of space charge

Space charge can be defined as charges, such as electrons, ions and charged particles that accumulate in the bulk of dielectrics or at the interfaces between conductors and insulators or at the interfaces between different dielectric materials. These charges may be injected from electrodes by enhanced thermal electronic injection or generated from dissociation of impurities or additives within insulation materials when subjected to external electric fields. They can be mobile charges that

drift across a dielectric under the local electric field resulted from the external field and the effect of space charge. They can also be trapped in capture centres originated by chemical or physical defects within a dielectric, resulting trapped charges. Charges with opposite polarity can recombine and then effectively disappear in a process that often results in photonic emission.

Basically there are two types of space charge: homocharge and heterocharge. Charge carriers with the same polarity as the nearby electrodes are referred to as homocharge while those with the opposite polarity as the adjacent electrodes are called heterocharge, which is explained in Figure 2-1. Homocharge can be originated by the injection of charge carriers from the electrodes. Normally electrons are injected from the negative terminal (cathode) while positive electronic charge carriers from the positive terminal (anode). The positive electronic charge carrier is referred to as a hole which is a vacancy where an electron is absent and equivalently positively charged. On the other hand, ionization can lead to the formation of heterocharge. The impurities and additives that exist in the bulk of insulation materials could be dissociated due to thermal excitation enhanced by the application of an external voltage; additional charge carriers or ions are created and attracted to the electrode of opposite polarity, with negative charges to the anode and positive charges to the cathode [26-28].

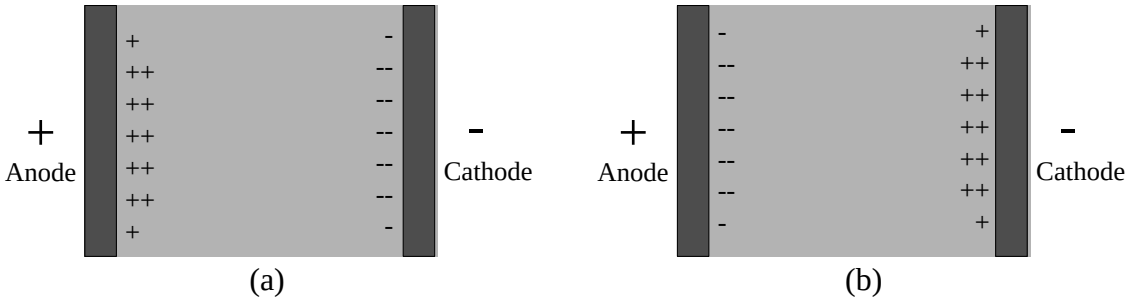


**Figure 2-1:** Space charge in dielectrics: (a) homocharge; (b) heterocharge.

## 2.2 Charge generation and transport

The conductivity of a dielectric material is normally less than $10^{-12}$ $Sm^{-1}$, and hence being electrically non-conductive; they provide good insulation for electrical application systems. Conductivity can be contributed by the movement of different types of charge carriers, electrons, holes and ions. The conductivity $\sigma$ is described by,

$$\sigma = q\mu n \tag{2-1}$$

Where $q$ is the electronic charge; $\mu$ is the drift mobility of charge carriers; and $n$ is the concentration of free charge carriers [26].

For polymeric insulation materials, for example, polyethylene has a typical conductivity of $10^{-15}$ $Sm^{-1}$, if the mobility $\mu$ is set to be $10^{-14}$ $m^2V^{-1}s^{-1}$ which is a typical value derived from experiments in polyethylene [29], the concentration $n$ can be calculated from equation (2-1) to be $6.25\times10^{18}$ $m^{-3}$. This is a huge number that definitely exceeds the intrinsic charge carrier's concentration in the insulator which typically has a large band gap between its valence and conduction bands. Therefore the pertinent question is what the charge carriers are and where they come from. A dielectric inevitably involves chemical and physical defects in its molecular structure; impurities and additives always occur during manufacturing and preparation processes; these could be both responsible for non-intrinsic sources of charge carriers in dielectrics. They have significant influence on the electrical performance of insulators when subjected to applied electric field.

### *2.2.1 Ionic processes*

Ions might already exist in insulators especially insulating polymers (e.g., ionomers and polyelectrolytes). For most insulating polymers, ions could also be created from the residual polymerization catalysts, degradation and aging products of polymer chains or side groups under the combination of electric and thermal stresses [30]. Ionic charge carriers can be classified into two types: (a) intrinsic ions which are created by the dissociation of the main polymer chain or side groups; (b) extrinsic ions which are not from the chemical structure of polymers but from the dissociation of additives or impurities incorporated during the fabrication process [23].

Chemical changes during the preparation process and low molecular weight chains of LDPE have been investigated to see if they are responsible for the formation of heterocharge in LDPE [31]. The effect of crosslinking byproducts on the accumulation of space charge has also been reported which suggests that cumyl alcohol introduces heterocharge under dc electric fields [32]. Inorganic nanofillers, which are introduced into the polymer matrix in order to achieve improved electrical properties of resultant nanocomposites, can also raise the accumulation of heterocharge [33].

### *2.2.2 Electronic injection*

With the significant improvement of fabrication and purification process in material production, the ionic process has been greatly reduced which lowers the dielectric loss of insulating polymers. Therefore the electronic process is dominantly responsible for the conduction, i.e., the power losses, and even breakdown of the polymeric insulations. The transport of electrons or holes in the bulk of polymers under low electric fields (where there is no occurrence of charge carrier injection from conductors) is negligible according to the classic band theory applied to polymers. Once the electric field exceeds a critical value, the injection of electrons or holes from electrodes (conductors) takes place; these form extra charge carriers and contribute to the extrinsic electronic conduction process in polymers.

All these processes begin at the interface of conductor/insulator. When an insulator is brought into contact with a conductor (electrode), free carriers will flow from the conductor to the insulator or vice versa until an equilibrium condition is established when the Fermi levels of both are equal. The flow of carriers depends on the work function of both materials and the surface states of the contact. There are three types of electrical contact between conductors (metal) and insulators. They are [30]:

- *Neutral contact* - which implies the regions adjacent to the contact are electrically neutral. In this case, the work function of the conductor $\varphi_m$ and that of the insulator $\varphi$ are equal before contact. When they are brought into contact, the carrier flow from the conductor to the insulator equals to the flow in the reverse direction, which finally leads to no net space charge accumulation at the interface.
- *Blocking contact* - which blocks the flow of electrons from the metal to the insulator. This is attributed to the situation where $\varphi_m > \varphi$. The electrons will flow from the insulator to the metal, leaving a positively charged region in the insulator.
- *Ohmic contact* - where $\varphi_m < \varphi$. Electrons flow through the interface to the insulator from the metal, which causes negative space charge accumulation at the interface and spreading into the insulator in the vicinity of the contact.

The explanation of these three types of contacts is based on the energy band theory and illustrated in Figure 2-2 where $E_{Fm}$ is the Fermi level of the metal; $E_F$ is the Fermi level of the insulator; $\chi$ is the electron affinity of the insulator; $E_C$ is the lowest energy level of the conduction band of insulator; $E_V$ is the highest energy level of the valence band of insulator; $E_G$ is the band gap of the insulator; $E_{F'}$ is the Fermi level of the contact system and $\varphi_B$ is the potential barrier height at the interface.

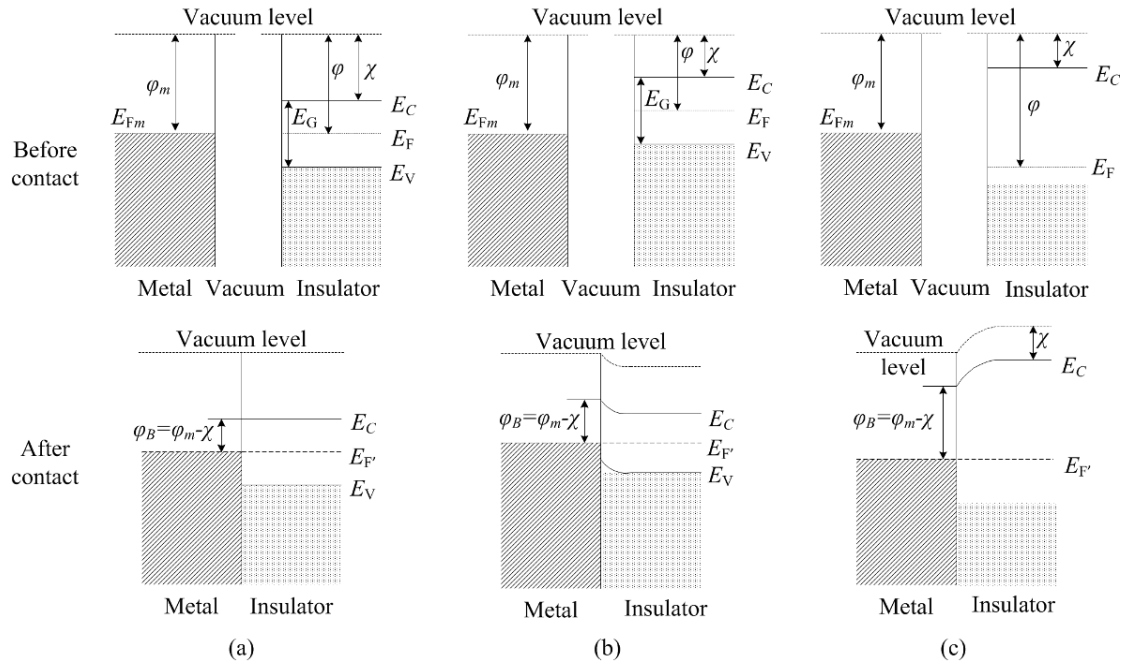


**Figure 2-2:** Energy diagram of the electrical contacts between metal and insulator: (a) neutral contact; (b) blocking contact; (c) ohmic contact [30].

However in practice the interface is not an ideal contact. It inevitably contains structural defects and contaminating impurities existing in the interface, which creates the surface states. The contact may be an intimate true contact established by strong short-range molecular forces; or an impeded contact with an impurity particle between the conductor and bulk dielectric. The surface states determine the exact potential barrier heights and greatly affect the electrical performance of the contact.

### (1) Richardson-Schottky injection

The potential barrier at the interface between a metal and an insulator prevents easy injection of electrons from the metal into the insulator. When an electric field is applied to the interface, this barrier height could be reduced by the applied field and the

image force so that enhanced electron injection can take place at the interface. The lowering of the potential barrier height in the case of the application of a uniform field to the neutral contact between a metal and an insulator is shown in Figure 2-3.

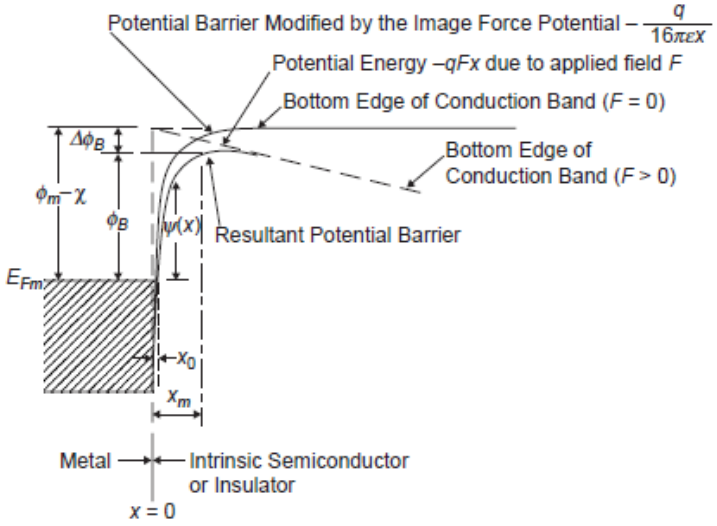


**Figure 2-3:** The lowering of potential barrier by the applied field and image force at the neutral contact between a metal and an insulator [30].

The original potential barrier height $\varphi_B$ at the interface without bias field is determined by the work function of the metal $\varphi_m$ and the electron affinity $\chi$ of the insulator, $\varphi_B = \varphi_m - \chi$. Once a uniform field $F$ is applied, a new barrier height is created by the combination of the field and the image force. The new potential barrier height $\psi(x)$ is given,

$$\psi(x) = \phi_m - \chi - \frac{q^2}{16\pi\varepsilon x} - qFx \tag{2-2}$$

Where the third term on the right is the contribution by the image force and the fourth is due to the applied field. The image force tends to attract emitted electrons back to the metal while the applied field drives the electrons away from the metal. There comes an optimal point where the net force on the electrons is zero and the potential $\psi(x)$ becomes minimal when the differential of the potential barrier height as a function of distance is zero. Hence the optimal point $x_m$ is obtained.

$$x_m = \left(\frac{q}{16\pi\varepsilon F}\right)^{1/2} \tag{2-3}$$

The lowering of the potential barrier height $\Delta\varphi_B$ can be calculated,

$$\Delta\phi_B = (\frac{q^2}{16\pi\varepsilon x}) + qFx = (\frac{q^3F}{4\pi\varepsilon})^{1/2} \qquad \text{when } x = x_m \tag{2-4}$$

Then the lowered potential barrier height becomes,

$$\psi = \phi_B - \Delta\phi_B = \phi_m - \chi - (\frac{q^3F}{4\pi\varepsilon})^{1/2} \tag{2-5}$$

The rate of thermionic emission of electrons from unit area (i.e., current density $J$) at the absolute temperature $T$ is given by Richardson-Dushman equation,

$$J = A_0T^2 \exp(-\frac{\psi}{k_BT}) \tag{2-6}$$

Where $A_0$ is a universal constant and $A_0$=1.2×10$^6$ Am$^{-2}$K$^{-2}$, $\psi$ is the potential barrier height and $k_B$ is the Boltzmann constant.

By introducing the potential barrier height calculated by equation (2-5) into equation (2-6), the Richardson-Schottky law of electron injection from a metal into an insulator is obtained by

$$J = A_0T^2 \exp(-\frac{\phi_B}{k_BT}) \exp(\frac{1}{k_BT}(\frac{q^3F}{4\pi\varepsilon})^{1/2}) \tag{2-7}$$

**(2) Fowler-Nordheim tunnelling**

Electrons can also transfer from a metal to an insulator through a potential barrier height by a field emission process, which is referred to as quantum mechanical tunnelling of electrons. The electrons have the probability of tunnelling through a barrier height into the conduction band of insulators at low temperature especially under an intense electric field. This depends on the shape of the potential barrier, the wave function of electrons and the applied field which can lower the potential barrier height. The Fowler-Nordheim tunnelling law is generally used to describe the field emission process. The current density of electron tunnelling is given by [34],

$$J(F) = \frac{q^3m_0F^2}{8\pi hm_e\phi_B} \exp(-\frac{8\pi\sqrt{2m_e}}{3qhF}\phi_B^{\frac{3}{2}}) \tag{2-8}$$

Where $q$ is the electronic charge; $m_0$ is the mass of free electron; $m_e$ is the effective mass of tunnelling electron; $F$ is the applied field; $h$ is the Planck constant; $\varphi_B$ is the potential barrier height. If assuming $m_e$ and $m_0$ are both equal to $m$, then the tunnelling current density can be simplified as,

$$J(F) = \frac{q^3F^2}{8\pi h\phi_B} \exp(-\frac{8\pi\sqrt{2m}}{3qhF}\phi_B^{\frac{3}{2}}) \tag{2-9}$$

### *2.2.3 Charge transport*

The nature of conduction in insulators is not as straightforward as that of metals or semiconductors since insulators have a low intrinsic conductivity and this conductivity is closely related to their chemical structure and bulk processes. Furthermore, conduction will have different field dependence over a specific range of electric fields. The typical current-field characteristic of a metal-insulator-semiconductor system is shown in Figure 2-4. The different slopes in region I, II, III, IV imply that there must be different conduction mechanisms occurring over the range of applied field. It is believed that defects and impurities in insulating materials both contribute to the conduction process. This is as important as the contribution by electronic carrier injection at the interface of a metal/insulator. The former is referred to as bulk limited conduction while the latter is electrode limited conduction which has been described as the electronic injection process. The combination of both normally complicates the experimental observations and theoretical analysis of the life expectation of insulation materials when undergoing electric stresses because the charge carriers involved in these conduction processes can both modify the electric field in the bulk of material which in turn affects the behaviours of charge carriers especially under high field stress. There are several classic theories describing the conduction process in dielectrics especially for the high field conduction process, such as hopping mechanism, Poole-Frenkel effect and space charge limited current (SCLC) which are described below.

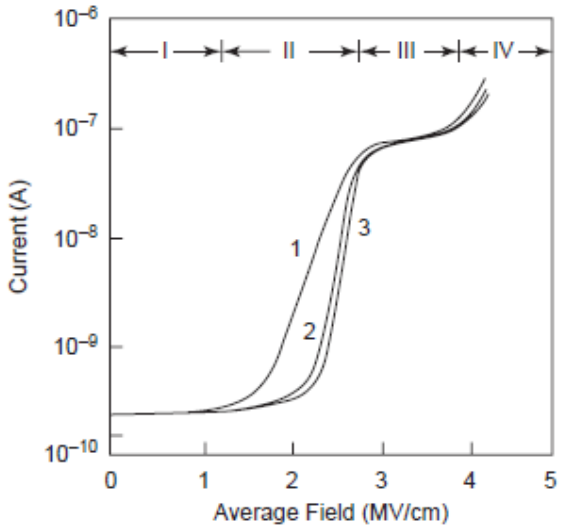


**Figure 2-4:** Typical current-field characteristics of the metal-polyimide-p-Si system [30].

### (1) Hopping mechanism

When considering the long polymer chain as a perfect periodical arrangement of monomer molecules by strong covalent bonding like a crystal, classic band theory can be applied to polymers. Polymers are believed to possess a wide band gap between their conduction and valence bands. For example, the band gap of polyethylene has been found to be 7.6-9.0 eV from experiments [23]. However the real picture of the chemical structure of polyethylene is a mixture of crystalline and amorphous domains in nature. The amorphous structure extends the wave tail of electrons into the band gap and creates some localized energy states below the conduction band for electrons or above the valence band for holes. Other chemical defects, such as structural disorders and foreign molecules, e.g., additives or impurities all introduce localized energy states in the band gap. These energy states localized in the forbidden energy band function as trap sites for available free charge carriers and restrict charge transport. A schematic diagram of the energy band diagram of polymers is shown in Figure 2-5. While electrons cannot be excited to get over the large band gap, on the other hand, they may hop over or tunnel through the potential barrier between the local energy states below the conduction band and this facilitates electron transfer in polymers as illustrated in Figure 2-6. Hole transport may also takes place by hopping over the potential barrier between the energy states located directly above the valence band. Whether it is a hopping or a tunnelling process depends on the energy of any exited electrons, the shape of the barrier height and the separation between the two energy sites. They both contribute to bulk conduction behaviour of polymers.

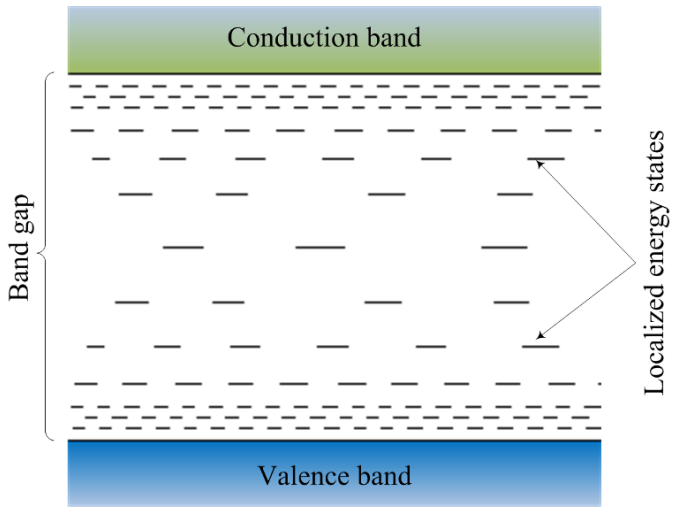


**Figure 2-5:** Schematic diagram of energy band in polymers.

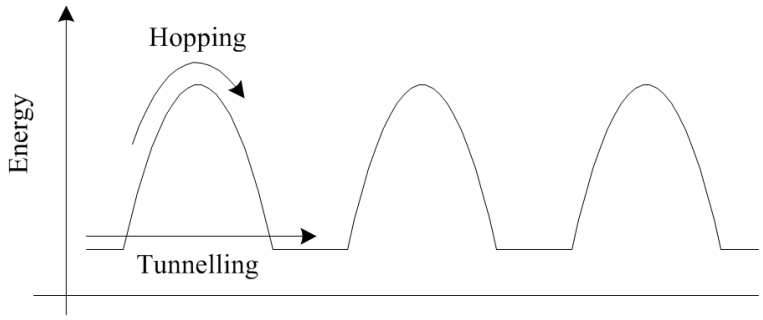


**Figure 2-6:** Hopping and tunnelling of electrons between two energy sites.

When a series of single level trap sites with an energy of $\varphi$ are localized in the band gap of polymers, electrons which are trapped in these sites can jump over the potential with a separation distance $a$ when receiving thermal excitation. The probability of electrons hopping through per unit time can be described as,

$$P = v\exp(-\frac{\phi}{k_B T}) \tag{2-10}$$

Where $v$ is the attempt-to-escape frequency in the order of $10^{12}$ to $10^{14}$ $s^{-1}$; $k_B$ is the Boltzmann constant and $T$ is the temperature. Then the mobility of hopping electrons can be expressed as,

$$\mu_H = \frac{qva^2}{k_B T}\exp(-\frac{\phi}{k_B T}) \tag{2-11}$$

When an electric field $F$ is applied, the potential barrier will tilt down in the direction of electric field and the potential barrier height will be lowered to be

$$\phi - \frac{1}{2}qaF \tag{2-12}$$

Finally the current density contributed by the hopping mechanism has the form

$$J = 2qnva\exp(-\frac{\phi}{k_B T})\sinh(\frac{qFa}{2k_B T}) \tag{2-13}$$

Where $q$ is the electronic charge; $n$ is the concentration of charge carriers.

**(2) Poole-Frenkel effect**

The electrons trapped in localized states can also transfer and even move into the conduction band in the bulk of insulators attributed to an internal Schottky effect, by which the potential barrier height is lowered by the columbic force due to a positively charged ionic centre which is generated by dissociation under high electric fields. As the columbic force in the Poole-Frenkel effect is due to a fixed positive charge while it

is resulted from a mobile image charge for the Schottky effect, the lowering of potential barrier for the Poole-Frenkel effect is twice of that for Schottky effect [35, 36], i.e.

$$\Delta\phi_{Sch} = \beta_{Sch} F^{1/2} = \left( \frac{q^3 F}{4\pi\varepsilon} \right)^{1/2} \tag{2-14}$$

$$\Delta\phi_{PF} = \beta_{PF} F^{1/2} = 2\beta_{Sch} F^{1/2} \tag{2-15}$$

Where $\beta_{Sch}$ is called the Schottky constant and $\beta_{PF}$ is the Poole-Frenkel constant.

Consequently the conductivity due to the Poole-Frenkel effect in the bulk of insulators can be expressed as,

$$\sigma = \sigma_0 \exp(\frac{\beta_{PF} F^{1/2}}{2k_B T}) \tag{2-16}$$

Where $\sigma_0$ is the low-filed conductivity of the material.

**(3) Space charge limited current (SCLC)**

The theory of space-charge-limited current (SCLC) in solids was proposed by Mott and Gurney [37]. The theory provides an analysis of current flow due to space chare injection into a perfect insulator without containing any traps in the bulk for charge carriers. This simplified analysis is based on several assumptions: (a) only one type of carriers (holes or electrons) is injected at the contact from a metal into an insulator; (b) the mobility of free carriers is independent of electric field; (c) the diffusion of carriers is not considered. With the single injection of holes into an insulator, a positive space charge is formed which in turn limits the rate of injection current flow. The current density through the material can be expressed as,

$$J = q\mu_h n_h(x) F(x) \tag{2-17}$$

Where $q$ is the electronic charge; $\mu_h$ is the mobility of free holes; $n_h(x)$ is the concentration of holes in the specimen; $F(x)$ is the electric field in the specimen and $x$ is the coordination axis in the direction of the specimen thickness.

The electric field in the specimen conforms to Gauss's law, such that

$$\frac{\partial F(x)}{\partial x} = \frac{q n_h(x)}{\varepsilon} \tag{2-18}$$

Where $\varepsilon$ is the permittivity of the specimen.

Thus the conduction current density can be rewritten by substituting equation (2-18) into equation (2-17) as,

$$J = \varepsilon \mu_h F(x) \frac{\partial F(x)}{\partial x} \tag{2-19}$$

By integrating the equation (2-19) and using the boundary conditions,

$$F(0) = 0 \text{ and } \int_0^d F(x)dx = V \tag{2-20}$$

Where $d$ is the specimen thickness and $V$ is the applied voltage.

The current density can be obtained, which is also called the square law,

$$J = \frac{9}{8} \varepsilon \mu_h \frac{V^2}{d^3} \tag{2-21}$$

At low applied voltages, if the density of thermally generated carriers $n_0$ is predominant, i.e.

$$J_\Omega = q n_0 \mu_h \frac{V}{d} \gg \frac{9}{8} \varepsilon \mu_h \frac{V^2}{d^3} \tag{2-22}$$

The ohmic conduction current will be dominant. Hence the whole picture of conduction current density through a perfect insulator over the voltage range is as shown in Figure 2-7. The transition from ohmic conduction to the space-charge-limited current comes at the voltage $V_\Omega$, when the injected space charge carriers exceed the thermally generated carriers.

$$V_\Omega = \frac{8 q n_0 d^2}{9\varepsilon} \tag{2-23}$$

This only deals with the trap free insulators. However, there always exist imperfections in insulators, e.g., structural disorders and impurities, which act as variety of trapping centres for electrons and holes. These all affect the transportation of charge carriers in the bulk of insulators, hence efforts have been made to extend the SCLC into insulators with a single level of discrete trapping energy, and even further into solids with quasi-continuous trapping energy having an exponential or Gaussian distribution. The resultant space-charge-limited current in solids with trap energy levels normally has a similar formula to equation (2-21) involving two extra parameters which are determined by the traps [30],

$$J = \frac{9}{8} \varepsilon \mu_h \theta_a \frac{V^2}{d_{eff}^3} \tag{2-24}$$

Where $\theta_a$ is the ratio of free carrier density to the total carriers (free and trapped) density and $d_{eff}$ is the effective thickness due to the presence of traps.

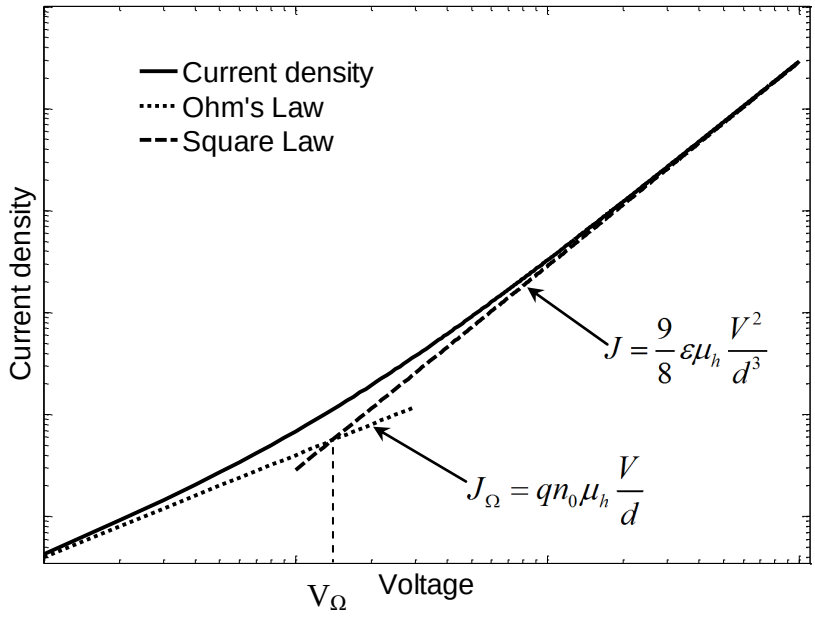


**Figure 2-7:** Log scaled current density for holes injection in a trap free insulator.

## 2.3 Space charge in polyethylene

Polyethylene is extensively used as an insulation material for dc/ac power cables due to its excellent electrical performance and good chemical/physical properties. Space charge has been regarded as one major component of the electrical aging process in polymeric insulations, such as low density polyethylene (LDPE), high density polyethylene (HDPE) and cross-linked polyethylene (XLPE), not only under dc fields but also in ac conditions [38, 39]. Space charge in the bulk or at the interfaces of insulator/electrode can increase the internal electric field up to several times higher than the applied field and accelerate the damage of dielectrics. This damage may be early degradation, electrical treeing or even complete insulation failure.

Within dc applications, space charge within polyethylene-based insulation materials of a power cable has been examined in order to understand the build-up, transport and trapping characteristics of charge under applied dc electric fields. This is greatly favoured by mapping the space charge in dielectrics by means of modern measurement techniques, such as laser induced pressure pulse (LIPP) method, pressure wave propagation (PWP) method and pulse electro-acoustic (PEA) method. G. C. Montanari et al. [29] investigated the space charge within LDPE, HDPE and XLPE using the PEA technique, observed charge injection, transport and analysed the trapping and detrapping characteristics of charge carriers. The results show that the

conductivity of LDPE is larger than HDPE and XLPE; the threshold field of space charge accumulation for LDPE and HDPE is smaller than XLPE; and that more charge can be accumulated in HDPE than the other two. The space charge distribution and threshold field for LDPE, HDPE and XLPE under dc fields are given in Figure 2-8 and Figure **2-9**. There is a remarkable effect of electrode materials on space charge build up in polyethylene since different electrode materials determine the distinct injection rate of charge carriers and then affect the internal stress and consequent charge behaviours. T. Hori [40] and G. Chen [41] have investigated experimentally how electrode materials, Aluminium (Al), Gold (Au) and semiconducting polymer (semicon) affect the space charge in LDPE, they conclude that charge are more easily injected from semicon than Al or Au, and that solid electrodes present a lower injection barrier than evaporated Al or Au electrodes. The presence of space charge at interface of polymer/polymer has also been investigated [41-43]. It is proposed that not only the discontinuity of conductivity and permittivity but also the surface states determine the polarity of charge density at the interface. Furthermore, directly probing of space charge in cable insulation has also been undertaken. Distribution of electric field in the presence of space charge in XLPE cable has been determined [44, 45] and the effect of temperature gradient and voltage reversal on charge accumulation in the cable insulation was also examined [46]. The phenomenon of charge packets was also observed under high electric fields greater than 100 $kVmm^{-1}$ at pre-breakdown of LDPE when K. Matsui et al. was to inspect the influence of space charge on the breakdown of insulation materials [47]. The formation of packet charges is believed to be caused by the higher conductivity in the reduced field region adjacent to the electrodes and the lower conductivity in the enhanced field region in the bulk.

Compared to dc conditions, space charge behaviour under ac electric fields has been less investigated because a more complicated measurement device is required to detect the dynamics of space charge in polymers subjected to the frequently reserving voltage. Different apparatus have been developed to examine space charge under ac voltages [48-51]. Research has been undertaken to understand the space charge characteristics under voltages at power frequency. With the changing amplitude and the frequently reversing polarity of applied voltage, the injected charges at the interface of electrode/polymer cannot easily travel across the polymer and mostly accumulate in the vicinity of the electrodes. X Wang et al. observed the space charge behaviour in XLPE

under ac voltages [52] and found that space charge can be developed at a very low frequency of 0.0002 Hz, and that homocharge and heterocharge coexisted at a critical electric stress due to the ionization of thermally unstable residuals and cross-linking byproducts. The amount of charge decreases with ac frequency. Z. Xu et al. investigated the space charge characteristic in LDPE under ac electric stress, and found that an applied ac voltage with a peak-to-peak of 10 kV could develop space charge which can travel into the bulk [53]. S. Bamji et al. detected the occurrence of heterocharge in LDPE under an ac electric field of 20 $kVmm^{-1}$ at 60 Hz [48].

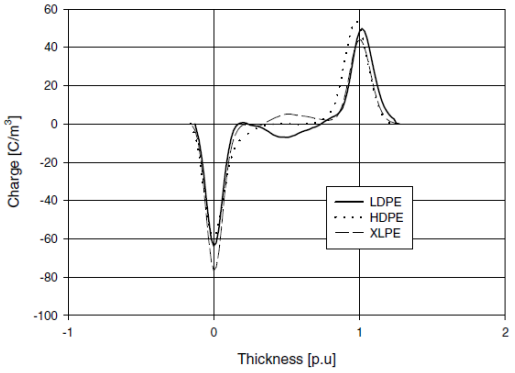


**Figure 2-8:** Space charge distribution in LDPE, HDPE and XLPE specimens at the stressing of 10000s under an applied dc field of 60 $kVmm^{-1}$ [29].

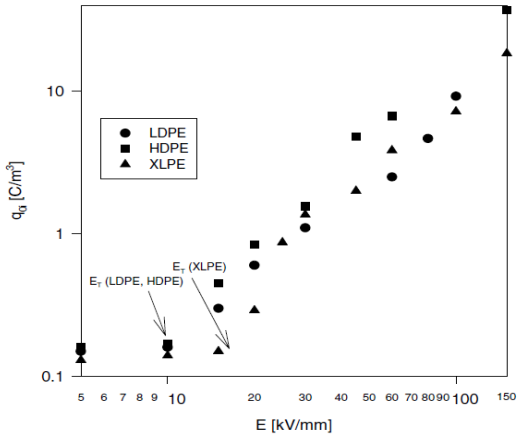


**Figure 2-9:** Threshold characteristics of space charge in LDPE, HDPE and XLPE specimens (the arrows indicate the transition from the ohmic to the quadratic regimes) [29].

## 2.4 Space charge detection techniques

A feasible detection method and a mature measurement system are of great importance for mapping space charge distribution in solid dielectrics and play significant roles in observation and understanding of behaviour of space charge in dielectrics subjected to electric fields and/or other conditions.

### *2.4.1 Evolution of space charge measurement techniques*

Since space charge has received attention from industry and research, extensive efforts have been dedicated to develop direct detection of the spatial distribution of charge within dielectrics over the past two decades. The early approaches, such as the dust figure method [54] and probe method [55], were inevitably destructive to an

experimental sample where cutting and sample preparation affected the charge distribution before any measurement. The first non-destructive technique for profiling space charge in solids was pioneered by Collins in the middle of 1970s [56] and has been considerably developed into modern multi-branch techniques over the following decades. Modern space charge measurement approaches are normally divided into two categories, namely thermal and acoustic methods. Thermal techniques generally involve a thermal expansion caused by varied temperature at one or two surfaces of the sample. Such thermal expansion (or disturbance) induces the movement of space charge in solid samples and consequently comes out a current that contains the charge information inside. The resulting current signals need to be processed by a mathematic deconvolution method and transformed into spatial distribution of charge inside the samples. The frequently used thermal techniques include laser intensity modulation method (LIMM) [57], thermal pulse (TP) method [58] and thermal step pulse (TSP) method [59]. The acoustic technique normally generates a pressure wave to travel through the charged dielectrics. The propagation of the elastic wave causes the displacement of the charge and then induces an external current which reflects the spatial charge distribution. Typical acoustic methods are the pressure wave propagation (PWP) method and laser induced pressure pulse (LIPP) method. The widely used pulsed electro-acoustic (PEA) method has its own unique principle, where an external pulsed electric field induces a perturbing columbic forces on the spatial charge and then generates an acoustic wave which contains the spatial distribution of charge in the material. The acoustic wave is detected by a piezoelectric transducer to be an electrical signal which is proportional to the acoustic signal. Comprehensive principles and the spatial resolution as well as comparison of performance of different space charge measurement techniques are detailed in [60-64].

### *2.4.2 Pulsed electro-acoustic method (PEA)*

Pulsed electro-acoustic method (PEA) was firstly developed in the 1980s [65] and since then has been continuously improved and implemented for mapping the charge distribution, charge injection and transport in solid dielectrics around the world. The principle of PEA method is illustrated in Figure 2-10. When a pulsed electric field is applied across a specimen that has internal charges, the pulsed electric field perturbs internal charge in the bulk, surface charge on the specimen and generates acoustic waves. These acoustic waves propagate through the specimen and are detected as

electrical signals by the attached piezoelectric transducer. The electrical signal contains the spatial distribution of charge layer in the bulk and at the surfaces of the specimen. If an appropriate calibration is applied to transform this electrical signal to charge density, the charge distribution in the specimen can be obtained. The PEA has a typical spatial resolution of 10 μm and a sensitivity of 0.1 $Cm^{-3}$ [66].

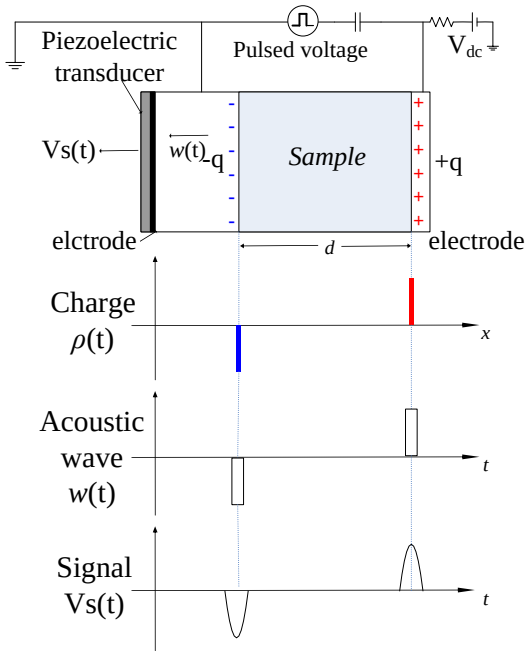


**Figure 2-10:** The principle of pulsed electro-acoustic method.

The experimental work described in this thesis was conducted using a PEA setup assisted with a user-defined acquisition and data processing LabVIEW program. The PEA setup is composed of the electrode system and the detection components as shown in Figure 2-11. The electrode system consists of a cylinder top electrode which is connected to a coupling capacitor and protective resistor casted in the epoxy insulation and surrounded by a copper screen to avoid flashover occurrence at high applied fields. The top electrode is extended by a thin layer of semiconducting polymer (Semicon) produced from carbon-loaded polyethylene pellets at a temperature of 150 ℃. The use of semiconducting polymer is to achieve a good acoustic wave transfer by matching acoustic impedance with test dielectrics. The ground electrode is flat aluminium (Al) which has a thickness of 10 mm. In the experiment, the test sample is sandwiched between the top electrode and the ground electrode. Biased dc voltage and pulse voltage are respectively applied through a protecting resistor and a coupling capacitor from the top electrode to the sample. The typical applied dc voltage ranges from 1 to 30

kV depending on the sample thickness and the experimental limitations. The pulse voltage has the amplitude of 0.1-2 kV and a width of 2-10 ns and works at the frequency of 400 Hz. The acoustic wave induced by the pulsed voltage is captured by the detection components composed of a piezoelectric sensor which is a polyvinylidene fluoride (PVDF) film (9 μm) attached to the ground electrode and two series amplifiers. The output electrical signal from the amplifier is acquired and averaged on a digital oscilloscope working at a sampling frequency of 2 $GSs^{-1}$. To minimize the reflection and attenuation of acoustic wave during propagation, a thin layer of silicone oil is filled in the interfaces of the Semicon/dielectric and dielectric/Al, and an absorber is placed beneath the sensor to delay and suppress any acoustic reflection.

As the result of the limitation of frequency response of the piezoelectric transducer and the unit of amplifier, the PEA output signal normally presents an overshoot peak immediately after the entry peak which represents the charge on the ground electrode as shown in Figure 2-12. This overshoot peak is not the real charge density and needs to be removed from the output signal for charge evaluation. Hence a calibration process, where a deconvolution method is used to gain the transfer function of the PEA system, is implemented to transform the output signal to its charge density value. The calibrated charge profile is shown in Figure 2-13.

All the PEA measurements were conducted on the nominally additive free low density polyethylene (LDPE) films supplied by GoodFellow Cambridge Ltd. The experiments were implemented using the same batch of LDPE products to make sure the consistence of the quality of the materials. LDPE films are stored in the dry condition at the room temperature without being exposed to light.

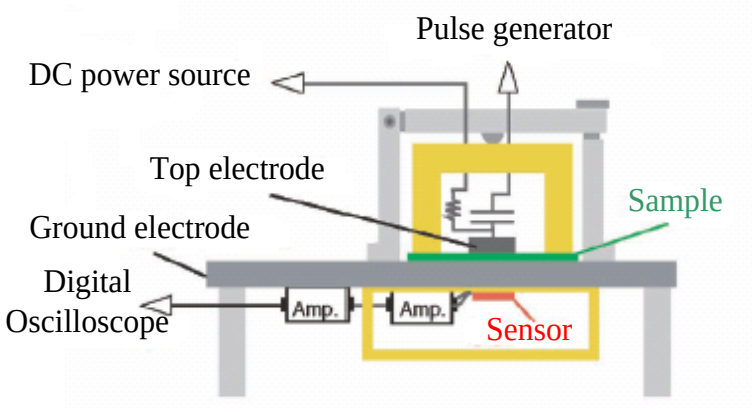


**Figure 2-11:** Configuration of PEA setup [66].

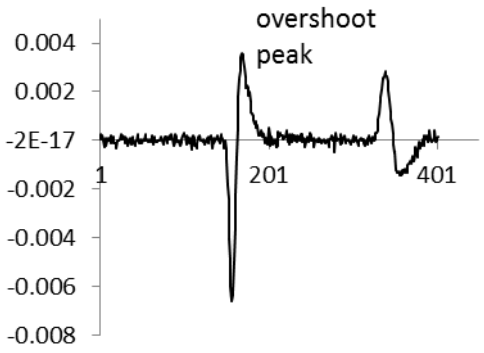


**Figure 2-12:** Typical PEA output signal.

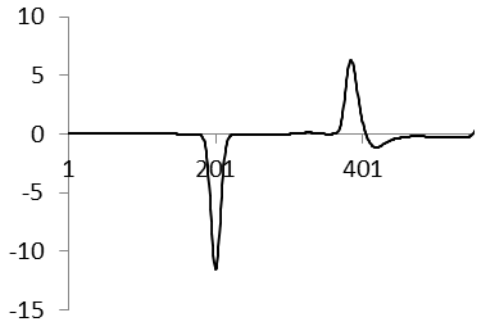


**Figure 2-13:** Calibrated charge profile.

## 2.5 Summary

The basics of space charge and fundamental physics describing the behaviours of electrical charge carriers in solids has been described to set a ground for future research into space charge. Existing research on space charge in polyethylene-based insulation material along with space charge measurement techniques have been reviewed.

# Chapter 3 Modelling of Space Charge under DC Electric Fields

Numeric modelling of a practical phenomenon is an approach of understanding underlying physics behind the experimental observations. This chapter first reviews the existing theoretical modelling of space charge in solids and then reports a bipolar charge transport model which is used to simulate the dynamics of space charge in polyethylene subjected to dc electric fields and to investigate the influence of charge carrier injection, transport, trapping and recombination on the resultant space charge behaviours. The relaxation of space charge in polyethylene after being stressed under dc fields or corona charged is also simulated using the bipolar charge transport model.

## 3.1 General theoretical approaches

As extensive research on space charge in solids has been conducted and knowledge gained from experiments, the dynamics of space charge within insulation materials has become more understood. But the underlying mechanisms behind the charge build-up, transport, trapping and recombination in the bulk of dielectrics or at the interfaces of materials are still an open question. The combination of these internal charge activities causes more complicated phenomena, such as electroluminescence,

early degradation and even breakdown of dielectrics. Hence the theoretical approach that involves classic knowledge of charge injection and charge transport process along with previously proposed models for charge trapping has been developed in order to recognize the characteristics of space charge under electric fields.

Several models describing charge transport in solid dielectrics have been developed in the last decade. The first was proposed by Alison and Hill in 1994; it simulated the behaviours of space charge in degassed XLPE [67]. This model features the double injection of charge carriers from the electrodes along with the extraction at both electrodes without potential barriers, and charge transport with a constant mobility while charge carriers can be trapped in deep trapping sites. In the same year, Fukuma et al. reported another model that involves Schottky injection of electrons and holes at the electrodes, and the charge transport by a hopping conduction mechanism [68]. In 1999 Kaneko et al presented a similar model but considering the extraction of charge at the boundaries without a barrier [69]. These models present reasonable charge profiles in the bulk of dielectrics and their evolution with time; they can also characterize the current density in the dielectric. These charge transport models have been further improved by many researchers across the world in order to achieve a good fit with experimental data and aid understanding of the charge dynamics in solids [70-73].

However the essential knowledge of charge transport in polymers under applied electric fields has not yet been realised. There are two typical categories of approach for characterizing the conduction process in the bulk of polymers: charge migration with a constant mobility or with a field-dependent mobility. Constant mobility is an average mobility extracted from the current characteristics obtained from experiments. But the experimental *I-V* curve indicates clearly a field dependence of the conduction process. Therefore the hopping mechanism by which charge carriers hop between sites of the same energy and phonon-assisted tunnelling [74] in which charge moves from site to site by a tunnelling process are taken into account in field-dependent alternatives. Poole-Frenkel effect is also used to describe the bulk conduction in polymers especially under high electric fields [75]. Furthermore the trapping and recombination of charge carriers both affect the conduction of polymers. These all make the modelling of space charge even more difficult.

## 3.2 Bipolar charge transport model

Cross-linked polyethylene (XLPE) has been widely used as the insulation materials of high voltage power cables. The produced XLPE inevitably involves additives, impurities and crosslinking by-products. These foreign molecules definitely affect the performance of XLPE insulation. The application of high voltage to XLPE may introduce the dissociation of some additives or impurities and generate additional charge carriers, such as ions other than the injected electronic charge carriers from the electrodes, which can both contribute to the space charge accumulation in reality. In contrast, the low density polyethylene (LDPE), considered being additive free, which has basic properties of polyethylene and well defined chemical structure is an easy object to inspect the characteristics of electronic charge carriers with the absence of ionization processes when subjected to applied electric fields. Furthermore, the experimental measurements are all conducted on the nominally additive free LDPE films. Therefore the simulation is focused on the low density polyethylene in which only electronic charge carriers, electrons and holes are considered. A bipolar charge transport model which involves the injection and extraction of electrons and holes from electrodes, electronic charge transport with trapping and recombination dynamics has been developed to describe the basic behaviours of space charge in polyethylene subjected to dc electric fields.

### *3.2.1 Model description and equations*

The bipolar charge transport model has three components which need to be considered. These are charge generation, the charge transport process and charge recombination. The model starts from the injection of positive and negative charge carriers at the interface of electrode/dielectric, with electrons injected from the cathode and holes from the anode. Subjected to an externally applied field, electrons and holes migrate in the bulk of the dielectric towards the opposite electrodes and hence come the conduction current. The trap energy levels localized in the band-gap of the dielectric, shallow trap centres originated by physical defects or deep trap centres due to chemical defects in the molecules can capture the mobile carriers and form trapped carriers inside. Hence there are four species considered in the model, mobile electrons/holes and trapped electrons/holes. Charge carriers in the shallow trap sites are normally considered to be able to detrap and migrate again while deeply trapped carriers cannot.

When the charge carriers of opposite polarity encounter each other in the bulk or at the interface of electrode/dielectric, they recombine and give out energy normally in the form of light emission, i.e., electroluminescence.

The dynamics of charge accumulation in solid dielectrics generally evolves with the stressing time and depends on the applied voltage and the temperature. The characteristics of space charge in solid dielectrics are governed by three essential equations. They describe the behaviour of charge carriers as a function of time and spatial coordinate $f(x,t)$. These three equations are Gauss's Law,

$$\frac{\partial E(x,t)}{\partial x} = \frac{\rho(x,t)}{\varepsilon} \tag{3-1}$$

Where $E$ is the local electric field, $Vm^{-1}$; $\rho$ is the net charge density, $Cm^{-3}$; $\varepsilon$ is the dielectric permittivity of solids, $Fm^{-1}$; $x$ is the spatial coordinate, m and $t$ is the stressing time, s. The transport of charge carriers is described as an ohmic conduction form in the media without considering the diffusion term for the sake of simplicity.

$$j(x,t) = \mu n(x,t) E(x,t) \tag{3-2}$$

Where $j$ is the conduction current density, $Amm^{-2}$; $\mu$ is the mobility of carriers, $m^2V^{-1}s^{-1}$ and $n$ is the density of mobile species, $Cm^{-3}$. Finally the continuity equation,

$$\frac{\partial n(x,t)}{\partial t} + \frac{\partial j(x,t)}{\partial x} = s \tag{3-3}$$

Where $s$ is the source term.

The local electric field in the dielectric is solved by direct discretization of equation (3-1) or by using an advanced finite element method. The continuity equation is solved using a splitting method. It is completed by first solving the equation,

$$\frac{\partial n(x,t)}{\partial t} + \frac{\partial j(x,t)}{\partial x} = 0 \tag{3-4}$$

And then solving a second equation using the solution of the above equation,

$$\frac{\partial n(x,t)}{\partial t} = s \tag{3-5}$$

Here charge recombination and trapping contribute to the source term illustrated in Figure 3-1. For each species, mobile or trapped, the equation (3-5) actually consists of four equations.

$$
\begin{aligned}
s_1 &= \frac{\partial n_{e\mu}}{\partial t} = -S_1 n_{ht} n_{e\mu} - S_3 n_{h\mu} n_{e\mu} - B_e n_{e\mu}(1 - \frac{n_{et}}{n_{0et}}) \\
s_2 &= \frac{\partial n_{h\mu}}{\partial t} = -S_2 n_{et} n_{h\mu} - S_3 n_{h\mu} n_{e\mu} - B_h n_{h\mu}(1 - \frac{n_{ht}}{n_{0ht}}) \\
s_3 &= \frac{\partial n_{et}}{\partial t} = -S_2 n_{h\mu} n_{et} - S_0 n_{ht} n_{et} + B_e n_{e\mu}(1 - \frac{n_{et}}{n_{0et}}) \\
s_4 &= \frac{\partial n_{ht}}{\partial t} = -S_1 n_{ht} n_{e\mu} - S_0 n_{ht} n_{et} + B_h n_{h\mu}(1 - \frac{n_{ht}}{n_{0ht}})
\end{aligned}
\tag{3-6}
$$

Where $s_1$, $s_2$, $s_3$, $s_4$ are the source term for each species; $S_0$, $S_1$, $S_2$, $S_3$ are the recombination coefficients for different opposite species; $B_e$, $B_h$ are the trapping coefficients for electrons/holes; $n_{e\mu}$, $n_{et}$, $n_{h\mu}$, $n_{ht}$ respectively indicate the densities of mobile electrons, trapped electrons, mobile holes and trapped holes; $n_{0et}$, $n_{0ht}$ are the trap densities for electrons and holes.

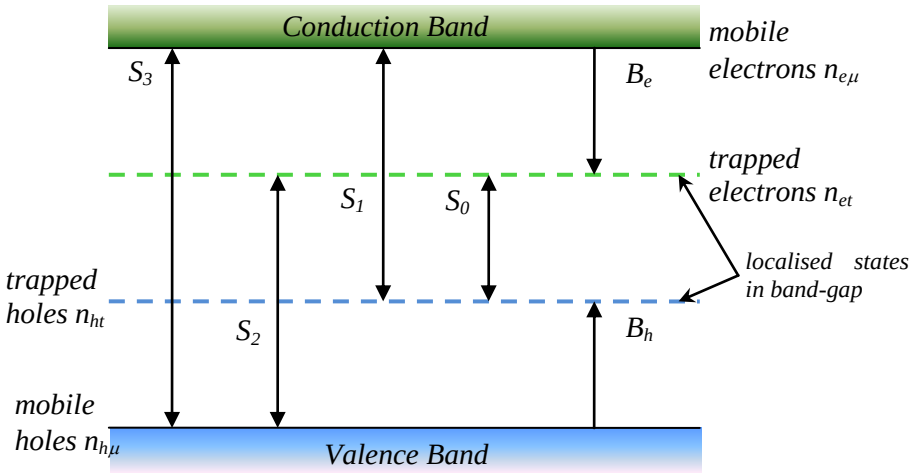


**Figure 3-1:** Trapping and recombination of bipolar charge carriers.

The boundary condition is defined by the Schottky injection at both electrodes,

$$
\begin{aligned}
j_e(0,t) &= AT^2 \exp(\frac{-ew_{ei}}{k_B T}) \exp(\frac{e}{k_B T}\sqrt{\frac{eE(0,t)}{4\pi\varepsilon}}) \\
j_h(d,t) &= AT^2 \exp(\frac{-ew_{hi}}{k_B T}) \exp(\frac{e}{k_B T}\sqrt{\frac{eE(d,t)}{4\pi\varepsilon}})
\end{aligned}
\tag{3-7}
$$

Where $j_e$ $(0, t)$ is the flux of electrons at the cathode while $j_h$ $(d, t)$ is the flux of holes at the anode; $T$ is the temperature; $A$ is the Richardson constant, $A = 1.2 \times 10^6$ $\mathrm{Am^{-1}\,K^{-2}}$; $w_{ei}$, $w_{hi}$ are the injection barrier heights for electrons and holes.

The extraction of charge carriers at the electrodes is also considered. If an extraction barrier is set, the current follows a Schottky law (with a barrier different from the one for injection). Otherwise, the extraction fluxes are:

$$\begin{aligned} j_e(d,t) &= \mu_e n_{e\mu}(d,t)E(d,t) \\ j_h(0,t) &= \mu_h n_{h\mu}(0,t)E(0,t) \end{aligned} \tag{3-8}$$

The total current density $J$ ($x$, $t$) is obtained from the second Maxwell equation (3-9), where the first item on the right is the conduction current density; the second is the displacement current density.

$$J(x,t) = j(x,t) + \varepsilon \frac{\partial E(x,t)}{\partial t} \tag{3-9}$$

Electroluminescence (EL) caused by recombination of opposite species can be represented using a total recombination rate (TRR) as shown below.

$$\text{TRR} = S_0 n_{ht} n_{et} + S_1 n_{ht} n_{e\mu} + S_2 n_{et} n_{h\mu} + S_3 n_{h\mu} n_{e\mu} \tag{3-10}$$

Where the TRR represents the EL intensity (arbitrary unit).

For the numerical computation, the dielectric specimen is discretized into $m$ ($m$=100) equal elements of width $\Delta x$ along its thickness, shown in Figure 3-2. $E$ is the local electric field at each element; $j_e$ is the flow of mobile electrons from the $k^{th}$ division into the $k$+1$^{th}$ division and $j_h$ the flow of mobile holes inversely. $E$, $j_e$ and $j_h$ of each element are computed progressively from the 1$^{st}$ division to the $m^{th}$ division at each time step $dt$ ($dt$=0.01s). The simulation procedure is explained in the flow chart as shown in Figure 3-3. The simulation is implemented using MATLAB coding and PDE solvers. Initial attempts have shown that the current time step of 0.01s is good enough to produce reasonable results compared with published simulation results. There is no difference in the simulated space charge profiles when choosing a larger time step of 0.1s. The spatial resolution of $d$/$m$ depends on the specimen thickness. For a thickness of 150 μm, the current spatial resolution of 1.5 μm produces enough resolution for the space charge accumulation in the bulk of polyethylene as the smallest penetration depth of space charge into the bulk of polyethylene is much larger than the spatial resolution. The smaller spatial resolution at $m$=1000 leads to no observable difference of computation results other than causing considerable time consumption, e.g. It takes more than 400 seconds running to simulate the equivalent one second.

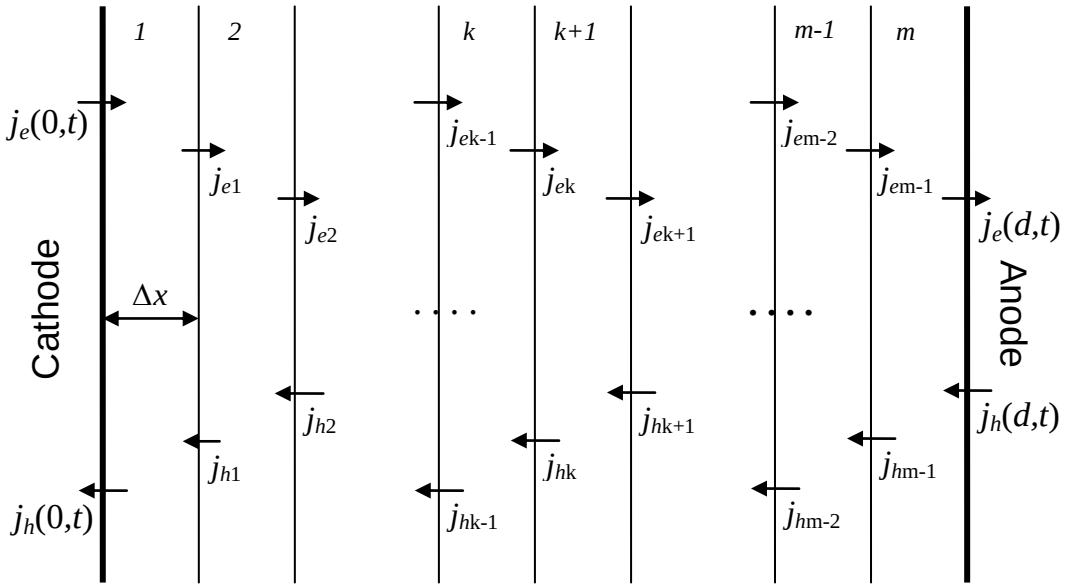


**Figure 3-2:** Discretization of the specimen.

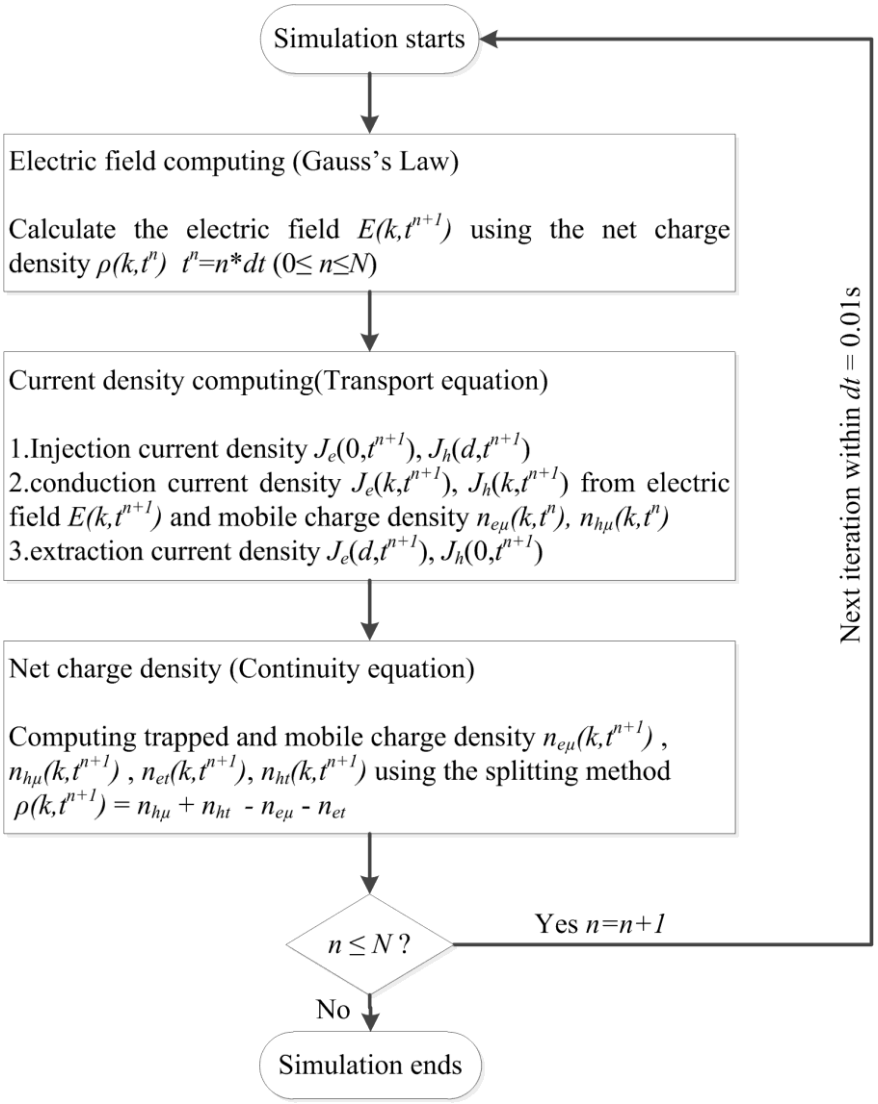


**Figure 3-3:** Flow chart of space charge simulation

### *3.2.2 Basic behaviours of simulated space charge*

A thin LDPE film with a thickness of 150 μm was subjected to a dc voltage of 9 kV in the simulation. The symmetric parameters, such as injection barrier height at the interface of electrode/dielectric, trapping and recombination coefficients as well as the constant mobility of electrons and holes have been used in the model for the sake of simplicity even though they are different charge carriers and have unique properties in reality. The detailed parameterization is given in Table 3-1. The build-up and evolution of space charge with stressing time in polyethylene has been simulated and the results are shown in Figure 3-4. It shows that charge carriers are injected from both electrodes and hence raise the electric field in the bulk of polyethylene and reduce the field strength at the electrodes; electrons (or holes) reach the middle of sample at around 100s, which indicates that the bipolar charge carriers take about 200s to travel across the sample. The charges are mainly trapped in the vicinity of electrodes when they are migrating towards the opposite electrodes. The overall charge density evolves in the same manner as it does experimentally. These results are in agreement with previous publications [72, 73].

**Table 3-1:** Symmetric parameterization for dc space charge modelling.

| Parameter | Value | Unit |
|---|---|---|
| Barrier height for injection | | |
| $w_{ei}$ (electrons) | 1.2 | eV |
| $w_{hi}$ (holes) | 1.2 | eV |
| Mobility | | |
| $\mu_e$ (electrons) | $9\times10^{-15}$ | $m^2V^{-1}s^{-1}$ |
| $\mu_h$ (holes) | $9\times10^{-15}$ | $m^2V^{-1}s^{-1}$ |
| Trap density | | |
| $N_{0et}$ (electrons) | 100 | $Cm^{-3}$ |
| $N_{0ht}$ (holes) | 100 | $Cm^{-3}$ |
| Trapping coefficients | | |
| $B_e$ (electrons) | $7\times10^{-3}$ | $s^{-1}$ |
| $B_h$ (holes) | $7\times10^{-3}$ | $s^{-1}$ |
| Recombination coefficients | | |
| $S_0$ trapped electron-trapped hole | $4\times10^{-3}$ | $m^3C^{-1}s^{-1}$ |
| $S_1$ mobile electron-trapped hole | $4\times10^{-3}$ | $m^3C^{-1}s^{-1}$ |
| $S_2$ trapped electron-mobile hole | $4\times10^{-3}$ | $m^3C^{-1}s^{-1}$ |
| $S_3$ mobile electron-mobile hole | 0 | $m^3C^{-1}s^{-1}$ |

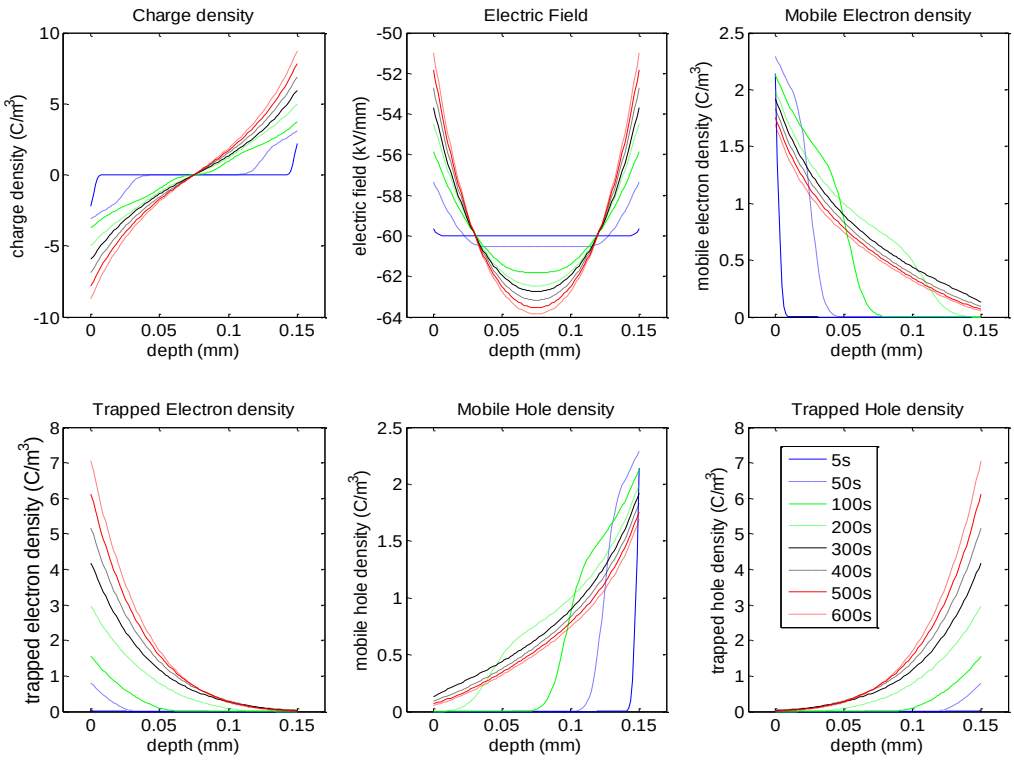


**Figure 3-4:** Simulated space charge in polyethylene under 9kV dc voltage

Apart from the simulated charge density, the conduction current density is also calculated and shown in Figure 3-5. The conduction current reaches a maximum when the bipolar charges arrive at the opposite electrodes after around 200s, and then drops gradually achieving a stable value as the stressing time progresses. The total recombination rate is calculated to characterize the electroluminescence due to bipolar charge recombination in this model. The result indicates a step increase starting around 130s and a peak before 400s in the evolution of recombination rate with stressing time as shown in Figure 3-6. This shows that electroluminescence starts to occur around 130s and it reaches a maximum before 400s.

The general trends of the simulated evolution of space charge and current densities seem to be consistent with the published results [72, 73, 76], which indicates the possibility to interpret the dynamics of space charge in polyethylene under constant dc voltages using this bipolar charge transport model.

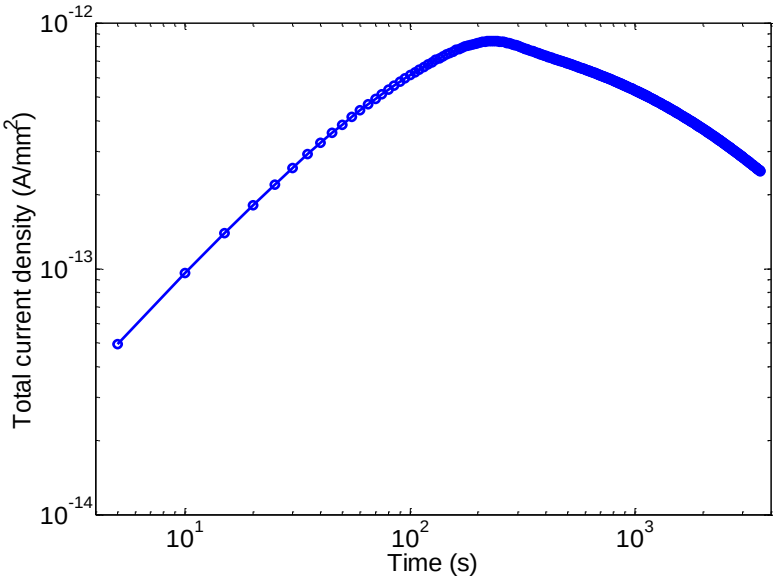


**Figure 3-5:** Conduction current density in polyethylene under 9kV dc voltage

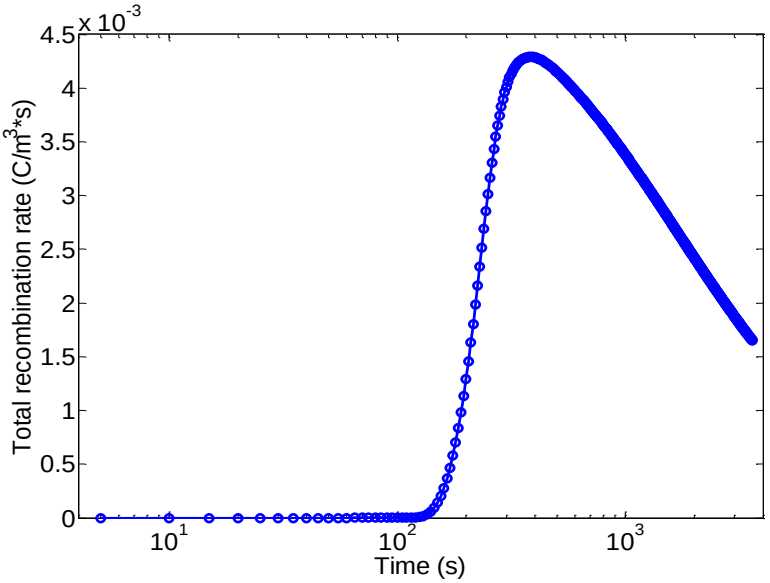


**Figure 3-6:** Total recombination rate in polyethylene under 9kV dc voltage

## 3.3 Influence of parameters

The bipolar charge transport model involves many parameters which are linked with the generation, transport, trapping and recombination of charge carriers in the dielectric when subjected to electric fields. All these processes contribute to the overall space charge accumulation, which hence complicates any analysis. Therefore it is necessary to examine the individual influence of each physical parameter on the resultant space charge behaviours from the simulation approach. By understanding the

sensitivity of the model to variation of key parameters, it helps to establish potential correlations between space charge and the dielectric properties of the material.

The effects of the injection barrier height, mobility of carriers, trapping coefficient, trap density and the recombination coefficient on space charge in polyethylene under dc electric fields have been investigated using the simulation. Each parameter is increased by step and used in the simulation when other parameters maintains as they are in Table 3-1. It is notable that symmetric parameters for electrons and holes are still used. The change of test parameters is explained in Table 3-2.

**Table 3-2:** Test physical parameters in the simulation

| Parameter | Unit | Value | | |
|---|---|---|---|---|
| | | 1st | 2nd | 3rd |
| Injection barrier height<br>$w_{ei}$ (for electrons)<br>$w_{hi}$ (for holes) | eV | 1.1 | 1.2 | 1.3 |
| Mobility of carriers<br>$\mu_e$ (for electrons)<br>$\mu_h$ (for holes) | $m^2V^{-1}s^{-1}$ | $9\times10^{-16}$ | $9\times10^{-15}$ | $9\times10^{-14}$ |
| Trapping coefficients<br>$B_e$ (for electrons)<br>$B_h$ (for holes) | $s^{-1}$ | $7\times10^{-4}$ | $7\times10^{-3}$ | $7\times10^{-2}$ |
| Trap density<br>$N_{oet}$ (for electrons)<br>$N_{0ht}$ (for holes) | $Cm^{-3}$ | 10 | 100 | 500 |
| Recombination coefficients<br>$S_0$ (trapped electrons-trapped holes)<br>$S_1$ (mobile electrons-trapped holes)<br>$S_2$ (trapped electrons-mobile holes)<br>$S_3$ =0 (mobile electrons-mobile holes) | $m^3C^{-1}s^{-1}$ | $4\times10^{-4}$ | $4\times10^{-3}$ | $4\times10^{-2}$ |

- Injection barrier height

The lower the injection barrier height, the more mobile charge carriers are injected into the polyethylene and hence more homocharge accumulation in the bulk as shown in Figure 3-7. This leads to substantial electric field distortion in the bulk of polyethylene.

- Mobility of charge carriers

As shown in Figure 3-8, the increase of mobility causes a big change in the charge distribution in the bulk of polyethylene under dc electric fields. At a low mobility of $9\times10^{-16}$ $m^2V^{-1}s^{-1}$, charge carriers move slowly, leading to a large quantity of charge accumulation adjacent to the electrodes but less charge moving into the bulk.

When the mobility is increased to $9\times10^{-15}$ $m^2V^{-1}s^{-1}$, the injected charge carriers spread quickly across the bulk, leading to a reduction in the total amount of charge. For a large mobility of $9\times10^{-14}$ $m^2V^{-1}s^{-1}$, the rapid transport of charge carriers across the polymer leads to much less accumulation of space charge in the polyethylene sample.

- Trapping coefficients

The trapping coefficients control the rate of mobile charge carriers being trapped in the deep trap centres and hence affect the density of mobile and trapped charge carriers. As shown in Figure 3-9, a lower trapping coefficient $B_e$ leads to more mobile electrons and a quicker spread of electrons into the bulk than a larger $B_e$. This causes a relatively large accumulation of charge carriers in the middle of polyethylene rather than in the vicinity of electrode/polymer interfaces.

- Trap density

The trap density indicates the maximum amount of trapped charge in the deep trap sites. A large trap density implies a large probability of trapping occurring. However the simulation does not demonstrate any significant difference of charge profiles at increased trap densities but results indicate a few more trapped charges and a slight reduction of mobile charge density, as shown in Figure 3-10.

- Recombination coefficient

In the simulation, a change of recombination coefficient from $4\times10^{-4}$ to $4\times10^{-2}$ does not influence the space charge distribution as shown in Figure 3-11.

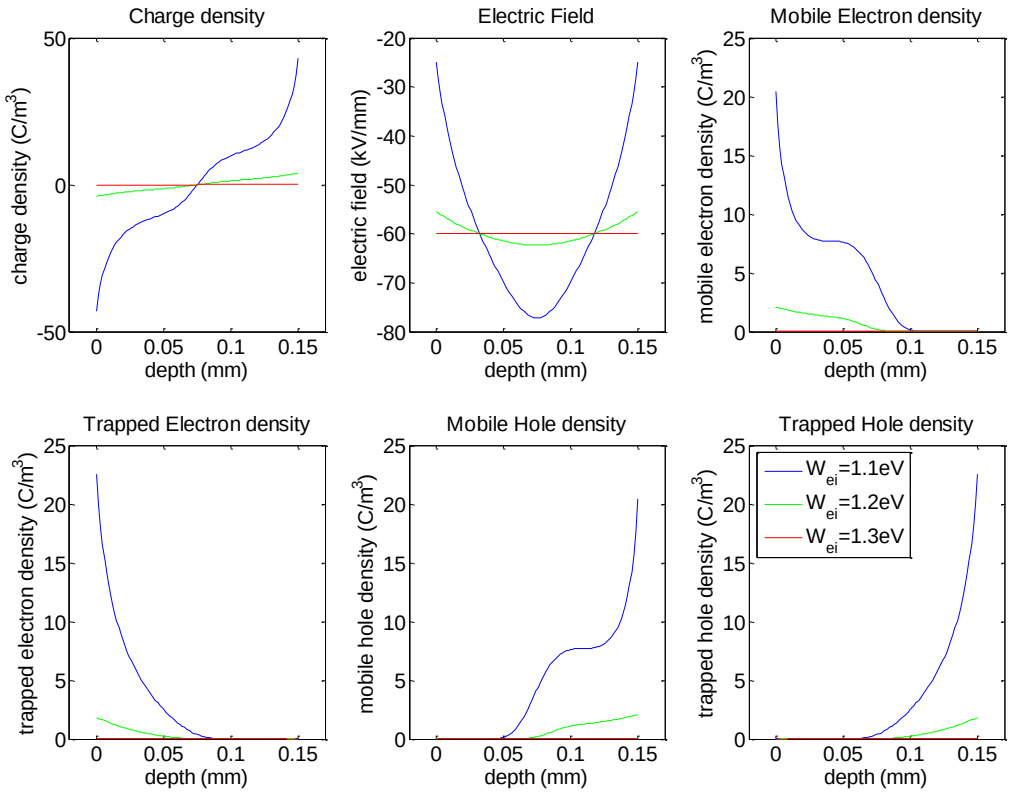


**Figure 3-7:** Simulated space charge at various injection barrier heights.

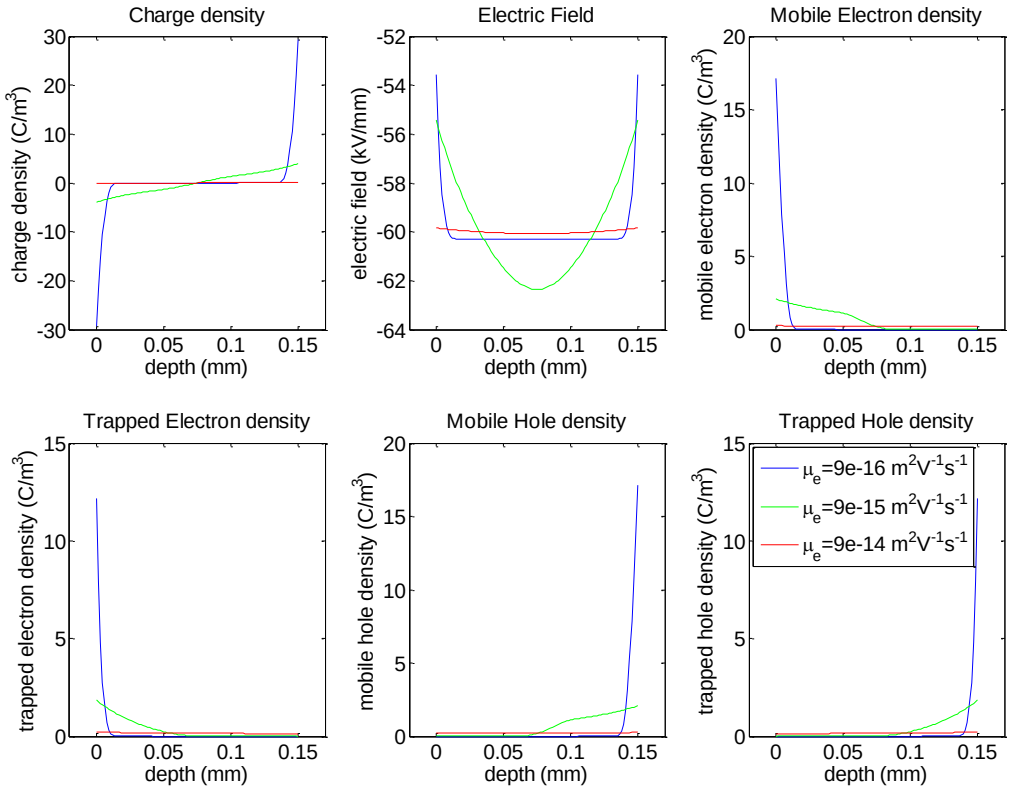


**Figure 3-8:** Simulated space charge at various constant mobilities.

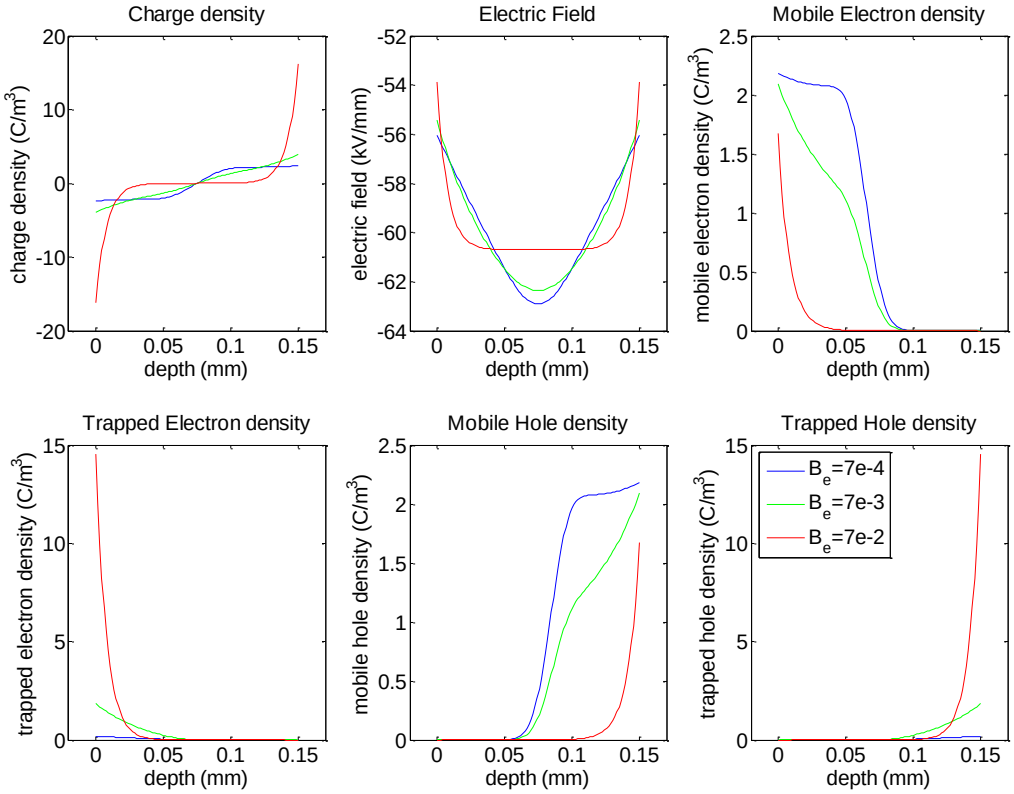


**Figure 3-9:** Simulated space charge at various trapping coefficients.

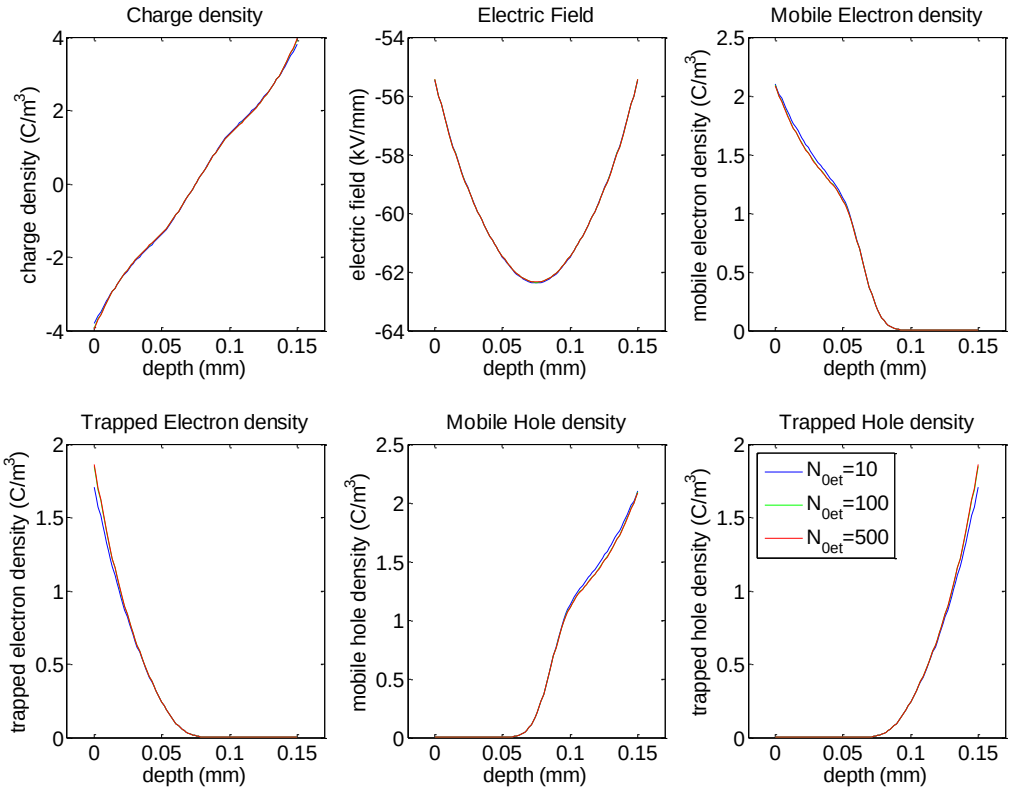


**Figure 3-10:** Simulated space charge at various trap densities.

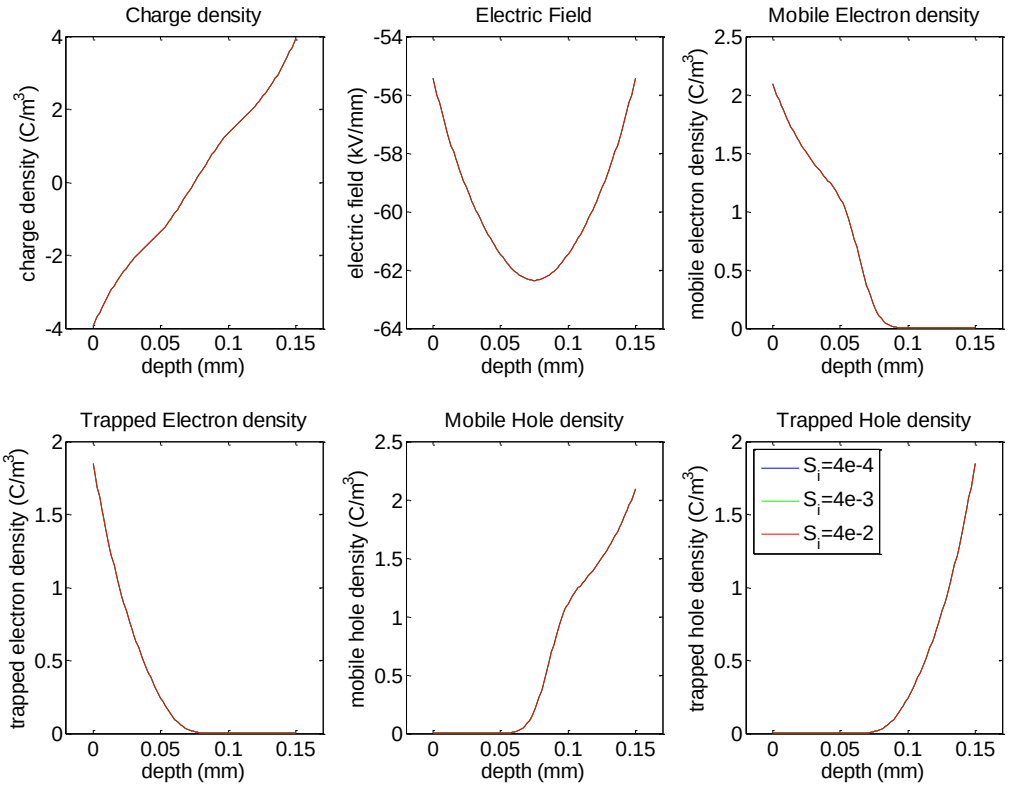


**Figure 3-11:** Simulated space charge at various recombination coefficients.

## 3.4 Effect of field dependent mobility

The transport of electrons and holes in polymers has not yet been well understood. Different transport mechanisms may lead to different charge behaviours in polymer matrix especially in the presence of electric stresses. This section focuses on the investigation of the effect of field dependent mobility of charge carriers on the dynamics of space charge in polyethylene.

### *3.4.1 Field dependent mobility*

The constant mobility used in the modelling might not be accurate for describing electronic charge transport. Hence a field-dependent mobility may be assumed. Three types of field-dependent carrier mobility have been considered as possible candidates. For simplicity, the equal mobility of electrons and holes are generally used in space charge modelling [72, 73] although the real situation is likely to exhibit different mobilities for holes and electrons.

The first model is hopping mobility, which describes the transport of electrons or holes by hopping over the trap sites localized in the band gap and even into the conduction or valence band of polymers. It is expressed as,

$$\mu = \frac{2va}{E}\exp(-\frac{w}{k_B T})\sinh(\frac{eEa}{2k_B T}) \tag{3-11}$$

Where $v$ is the attempt-to-escape frequency; $a$ is the separation between trap sites; $w$ is the energy level of trap depth; $E$ is the local electric field; $e$ is the electronic charge; $k_B$ is the Boltzmann constant and $T$ is the temperature.

The second is a power-law mobility, which describes the mobility of carriers as a power function of the electric field,

$$\mu = \mu_0 E^{(n-1)} \tag{3-12}$$

Where $\mu_0$ is the mobility under low electric field [77]; $n$ is the power index and $E$ is the local electric field.

The third approach is the Poole-Frenkel mobility,

$$\mu = \mu_0^{'}\exp(\sqrt{\frac{e^3 E}{4\pi k_B^2 T^2 \varepsilon_0 \varepsilon_r}}) \tag{3-13}$$

Where $\mu_0$ is the zero-field mobility [78]; $e$ is the electronic charge; $\varepsilon_0$ is the permittivity of free space; $\varepsilon_r$ is the relative permittivity of dielectrics; $k_B$ is the Boltzmann constant and $T$ is the temperature.

These three field-dependent mobilities for electrons and holes have been used in the charge transport process of the model. The constant mobility of $9\times10^{-15}$ $m^2V^{-1}s^{-1}$ and the resultant simulated space charge and current density in polyethylene under an applied dc electric field of 60 $kVmm^{-1}$ were selected as the reference. All the parameters in the equation of field-dependent mobility, such as the power index $n$ in power-law mobility and zero-field mobility $\mu_0$ in the Poole-Frenkel mobility, are determined by achieving the objective that charge carriers must travel across polyethylene in the same time, i.e., transit time, as that in the case of a constant mobility under a dc field of 60 $kVmm^{-1}$. Then the dynamics of space charge in polyethylene under various dc electric fields is modelled using the field-dependent mobilities and the results are evaluated by comparing them with the simulated space charge obtained for a constant mobility.

### *3.4.2 Transient space charge*

Space charge in a polyethylene film of 150 μm under dc voltages ranging from 1.5 to 21 kV, where the applied field ranges from 10 to 140 kVmm$^{-1}$, is simulated in the case of the field-dependent mobility. Most of the parameters for electrons and holes remain the same as that in the case of a constant mobility as given in Table 3-1 except the mobility equations and values. The transient dynamics of space charge over a stressing time of up to 240s is discussed below.

**(1) Hopping mobility**

By achieving an equal transit time of around 200s under a dc field of 60 kVmm$^{-1}$, the parameters in the hopping mobility equation have been determined and given in Table 3-3. The transient space charge in the polyethylene film under various dc electric fields is obtained through the simulation using hopping mobility. The evolution of space charge under an applied dc field of 60 kVmm$^{-1}$ is shown in Figure 3-12. The symmetric parameters of electrons and holes lead to an equal amount of homocharge formed on both sides of polyethylene causing a reduction of the electric field at the electrodes along with enhancement of the field in the middle of the sample.

**Table 3-3:** Parameters for hopping mobility

| Parameter | Value | | Unit |
|---|---|---|---|
| | Electrons | Holes | |
| Attempt-to-escape frequency $v$ | $v_e$=4×10$^{13}$ | $v_h$=4×10$^{13}$ | s$^{-1}$ |
| Separation between trap sites $a$ | $a$=2.6×10$^{-10}$ | $a$=2.6×10$^{-10}$ | m |
| Trap depth $w$ | $w_{et}$=0.6 | $w_{ht}$=0.6 | eV |

The resulting conduction current density $J$ during the build-up of space charge in polyethylene under dc electric fields is also computed and plotted in Figure 3-13. The conduction current density varies from 10$^{-16}$ to 10$^{-11}$ Amm$^{-2}$ with an increase of applied field from 10 to 120 kVmm$^{-1}$ and the maximum current density occurs earlier at higher electric fields. The dependence of conduction current density on the applied electric field is shown in Figure 3-14. The log scale of current density shows three slightly different field dependence regions: (I) the increase of current at a small slope when the field is below 20 kVmm$^{-1}$; (II) the current increases with field at a larger slope; (III) the current reaches a relative saturated level when undergoing a stressing time of longer than 120s. This curve resembles the space-charge-limited-current (SCLC) and the

experimental *I-E* curve described previously in Chapter 2. In other words, the simulated *J-E* curve may support the assumption that the conduction process is strongly related to space charge and trapping characteristics of charge carriers in polyethylene.

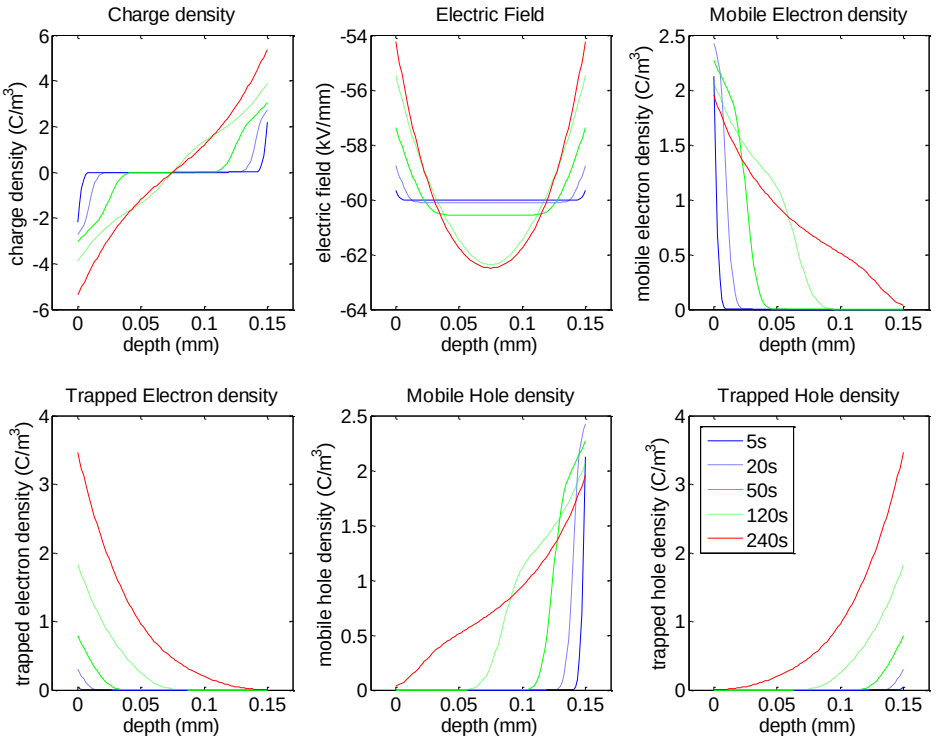


**Figure 3-12:** Simulated space charge with hopping mobility.

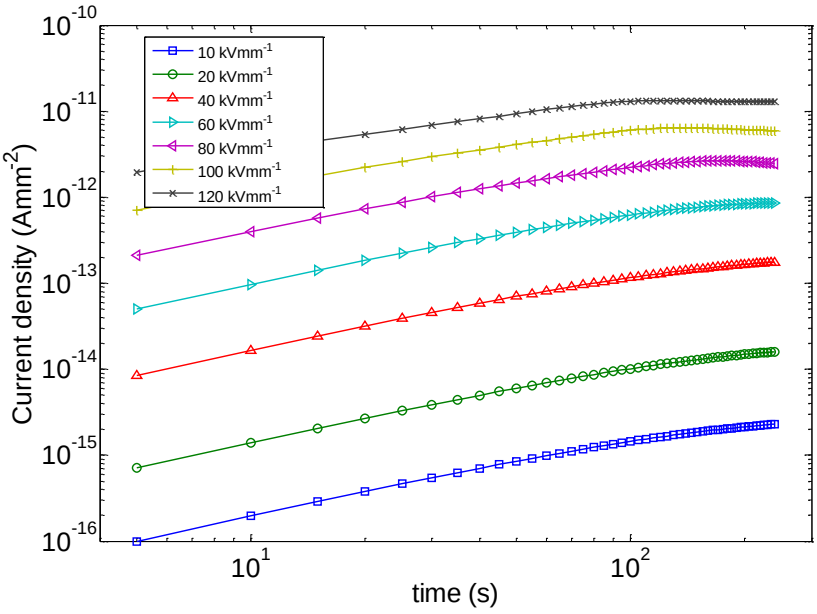


**Figure 3-13:** Simulated current density with hopping mobility under dc fields.

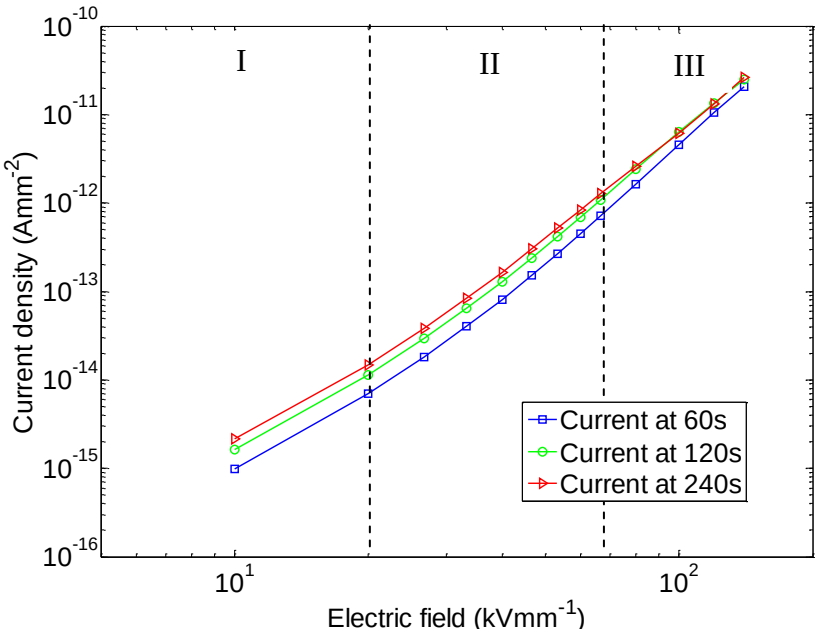


**Figure 3-14:** Current density vs. electric field in hopping mobility model.

### (2) Power-law mobility

As power-law mobility involves two important parameters, the low field mobility $\mu_0$ and the power index $n$, they need to be calibrated for the expected modelling procedure. The low field mobility value of $\mu_0=4.5\times10^{-16}$ has been used by other researchers [77]. To obtain an appropriate value of $n$, the dependence of space charge evolution on the power index $n$ has to be examined from simulation results. The conduction current densities under a different power index $n$ during the build-up of space charge within a 150 μm polyethylene film under 9 kV dc voltages are shown in Figure 3-15. The maximum conduction current density occurs earlier for higher power indexes $n$. There is a peak value occurring at around 200s, i.e., the transit time of charge carriers, when the power index $n$=1.165. This agrees with the situation of the constant mobility under the same dc voltage. Hence a value of $n$=1.165 was selected for power-law mobility for the following simulations.

The space charge evolution in a polyethylene film under a 9 kV dc voltage has been modelled and results are shown in Figure 3-16. It shows similar charge profiles in the sample compared with the charge profiles obtained under a constant mobility and the hopping mobility. The dependence of space charge on the applied dc voltage has also been investigated using the simulation. The resulting conduction current density under various applied dc fields is shown in Figure 3-17. To simplify the analysis, log

scaled current density as a function of electric field is plotted in Figure 3-18. It also demonstrates three slightly different field dependence regions and the threshold fields at the transition between regions are close to those observed for a hopping mobility.

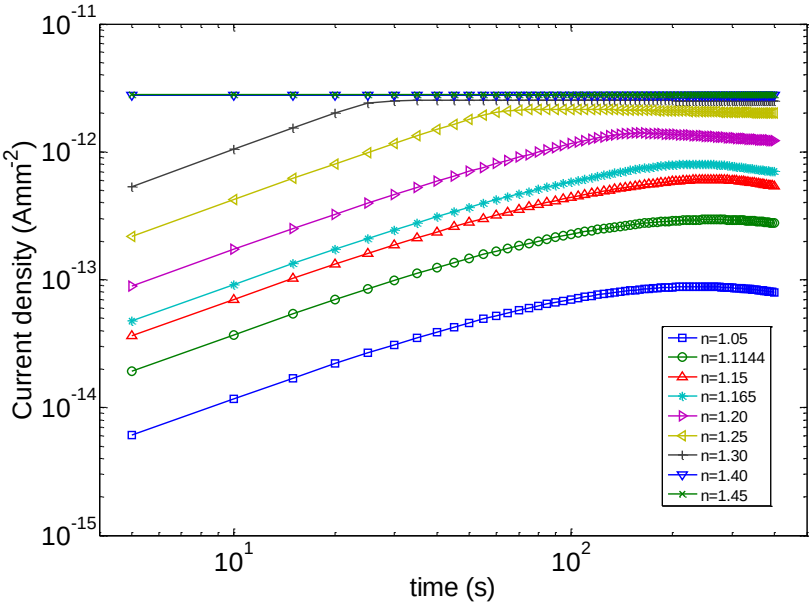


**Figure 3-15:** Simulated current density at different power index *n*

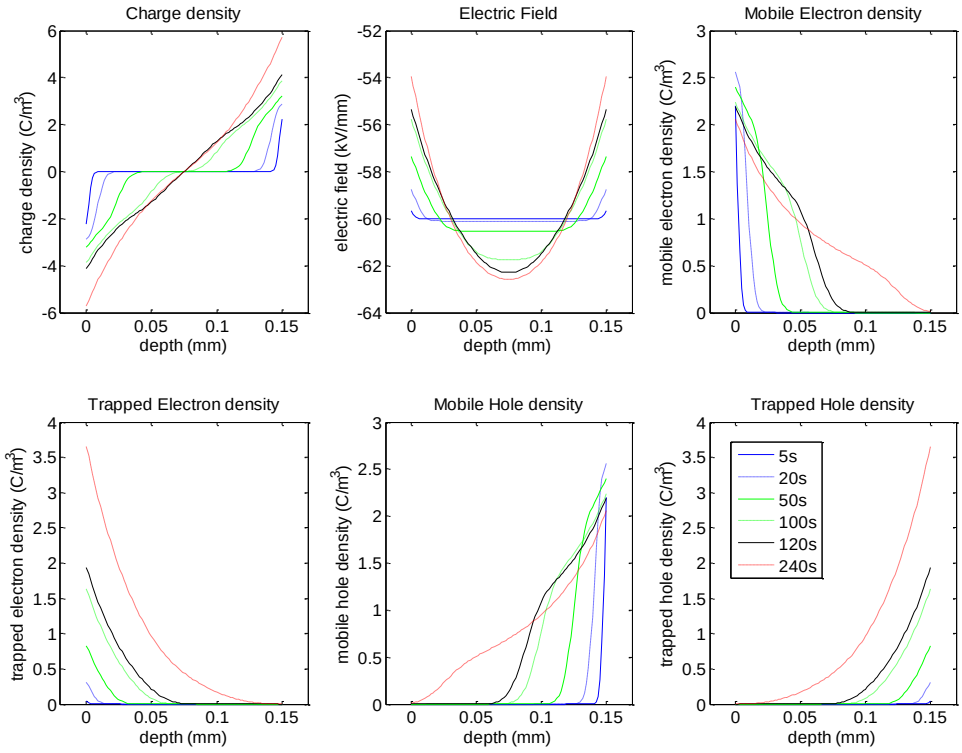


**Figure 3-16:** Simulated space charge with power-law mobility (*n*=1.165)

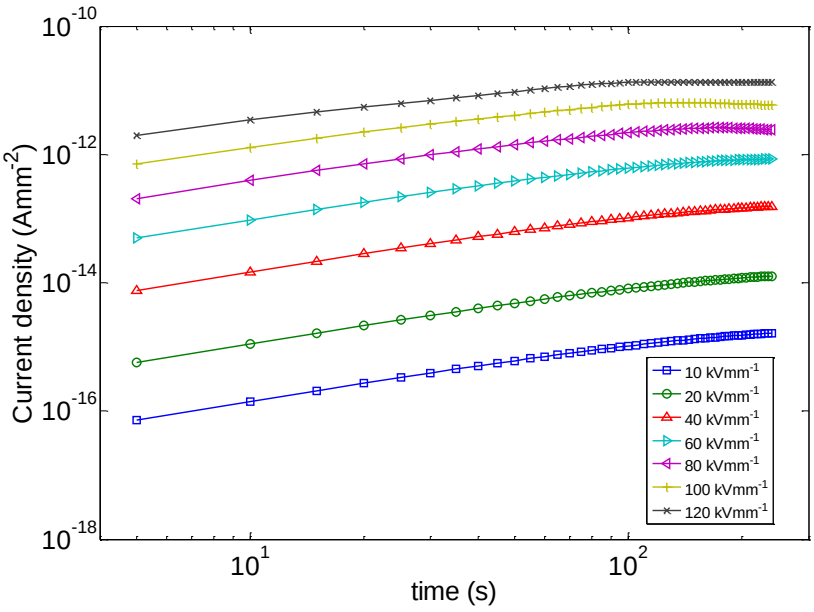


**Figure 3-17:** Simulated current density with power-law mobility under dc fields

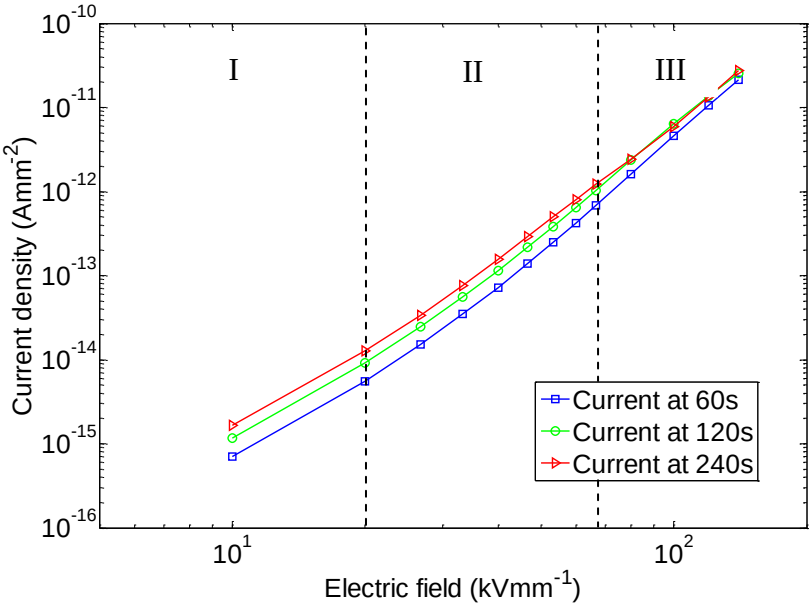


**Figure 3-18:** Current density vs. electric field in power-law mobility model

### (3) Poole-Frenkel mobility

The Poole-Frenkel mobility also involves two parameters, the permittivity of polyethylene $\varepsilon_r$ =2.3 and the zero-field mobility $\mu_0$. The zero-field mobility was determined to be $\mu_0$=5.0×10$^{-18}$ by achieving an equal transit time of charge carriers in the case of constant mobility. The simulated space charge evolution in polyethylene under a 9 kV dc voltage is shown in Figure 3-19. The conduction current densities

under different electric fields are plotted in Figure 3-20. The logarithmic current density vs. electric field demonstrates clearly a nonlinear dependence on electric fields as shown in Figure 3-21. The slope change is more significant. The current saturates earlier within 60s. The transition occurs at a higher field of 80 kVmm$^{-1}$ from region II to III when compared with results obtained from the other approaches.

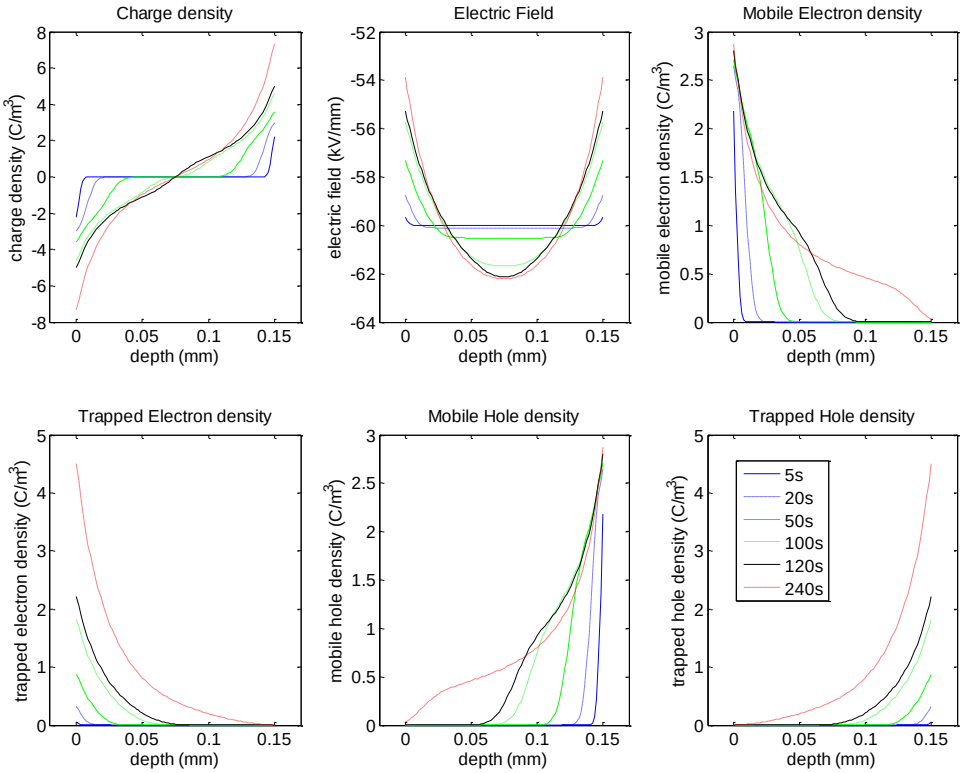


**Figure 3-19:** Simulated space charge with Poole-Frenkel mobility

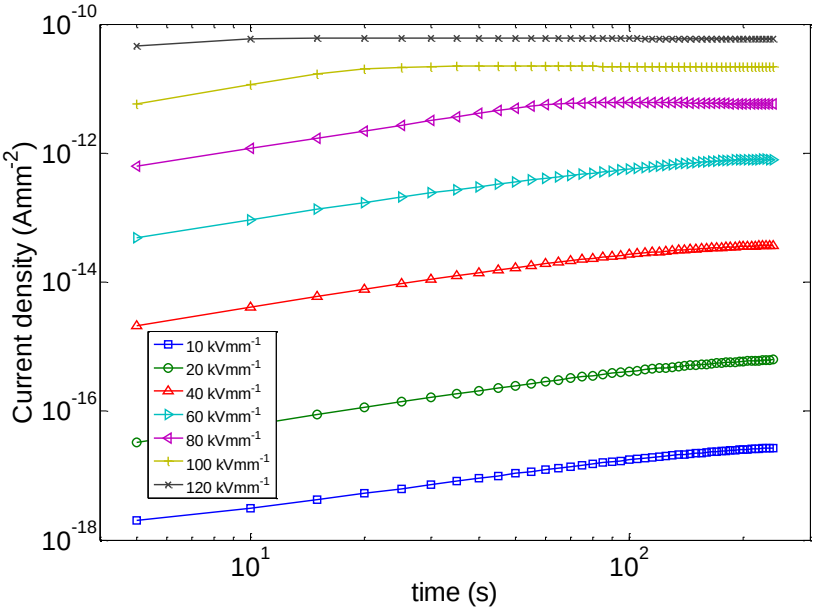


**Figure 3-20:** Simulated current density with Poole-Frenkel mobility under dc fields

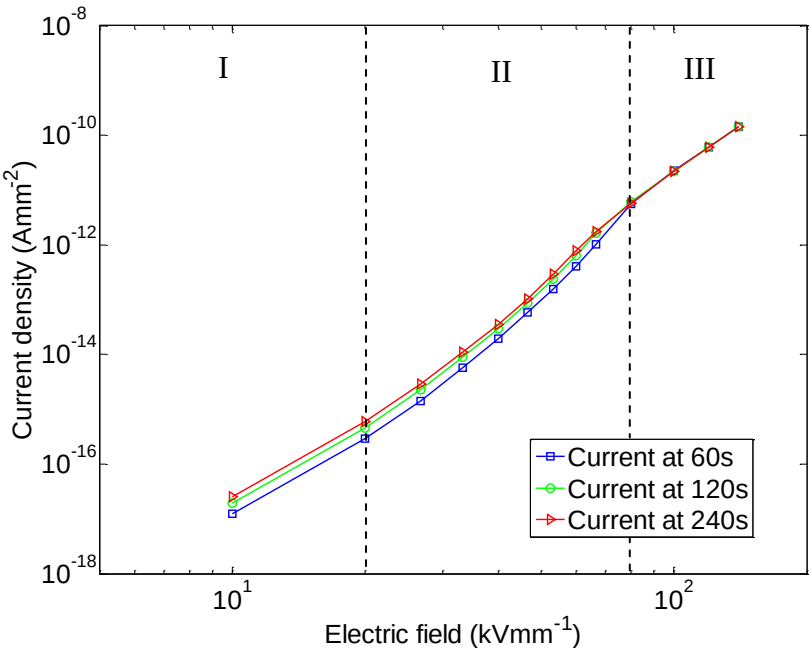


**Figure 3-21:** Current density vs. electric field in Poole-Frenkel mobility model

### *3.4.3 Discussion*

#### (1) Influence of field-dependent mobility on charge dynamics

The influence of involved parameters in the bipolar charge transport model on the dynamics of space charge in solids has been examined using the simulation described in Section 3.3. The results suggest that charge injection and charge transport play more significant roles than trapping and recombination processes. The simulated space charge profiles in polyethylene with field-dependent mobilities under equal dc electric fields have been compared. At a low electric field of 20 kVmm$^{-1}$, the obtained space charge profiles for a stressing time of 240s are shown in Figure 3-22. Charge distributions in polyethylene at 240s for a medium electric field of 60 kVmm$^{-1}$ are shown in Figure 3-23. Charge densities at 240s for a high electric field of 140 kVmm$^{-1}$ are shown in Figure 3-24. Each graph compares the charge profiles in polyethylene simulated using the field-dependent mobilties, i.e., hopping mobility, power-law mobility, Poole-Frenkel mobility and the constant mobility.

Under an applied dc field of 20 kVmm$^{-1}$, charge carriers with Poole-Frenkel mobility move slowly into the bulk of the polyethylene, leaving a large charge accumulation near the electrodes, while charges with constant mobility, hopping

mobility and power-law mobility already travelled further into the bulk. When the applied field is increased to 60 kVmm$^{-1}$ and the charge carriers have an equal transit time, the space charge with the first three mobility models behaves in a similar way. But in the case of Poole-Frenkel mobility, charges still move slower, leaving more charge near the electrodes (in the region of reduced electric fields) and less charge in the middle where the field is enhanced due to the presence of space charge; the density of the mobile electrons or holes front is however higher than that of the other three mobility models. This indicates that charge transport modelled using a Poole-Frenkel mobility is more sensitive to the electric field than the other three mobility models. With a high applied field of 140 kVmm$^{-1}$, the velocity of charges with Poole-Frenkel mobility is greatly promoted by the local electric field and thereby bipolar charges travel across the polyethylene film very quickly, leaving far less charge accumulation in the bulk of the sample. In contrast, there is a fairly large charge accumulation in the bulk for the other three mobility models. Carriers with power-law mobility or hopping mobility drift with nearly the same velocity as those with a constant mobility.

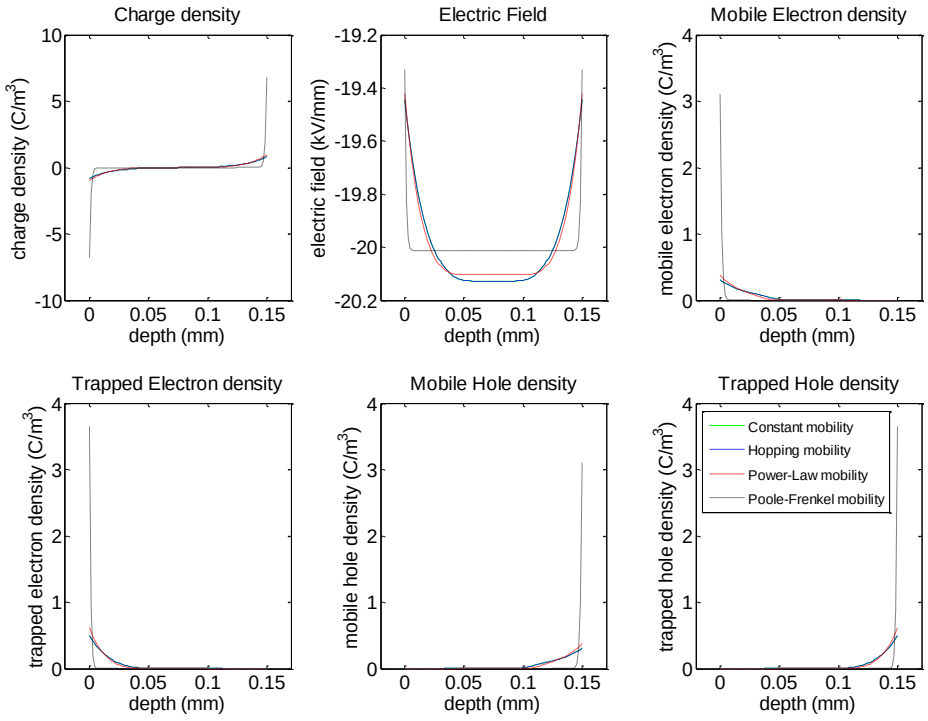


**Figure 3-22:** Space charge profiles with different mobility under 20 kVmm$^{-1}$ field

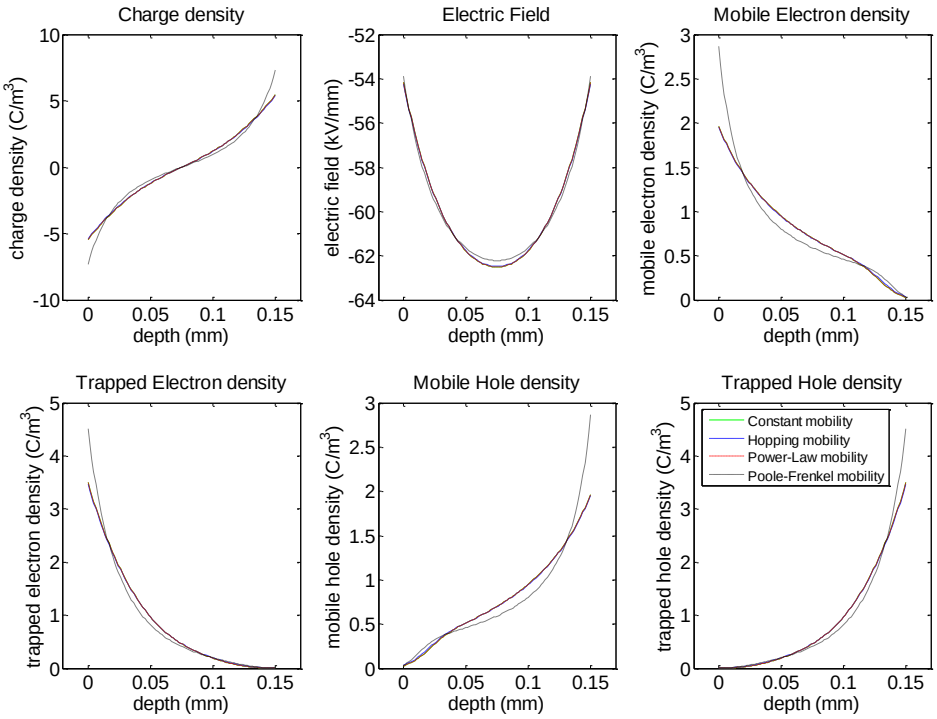


**Figure 3-23:** Space charge profiles with different mobility under 60 kVmm$^{-1}$ field

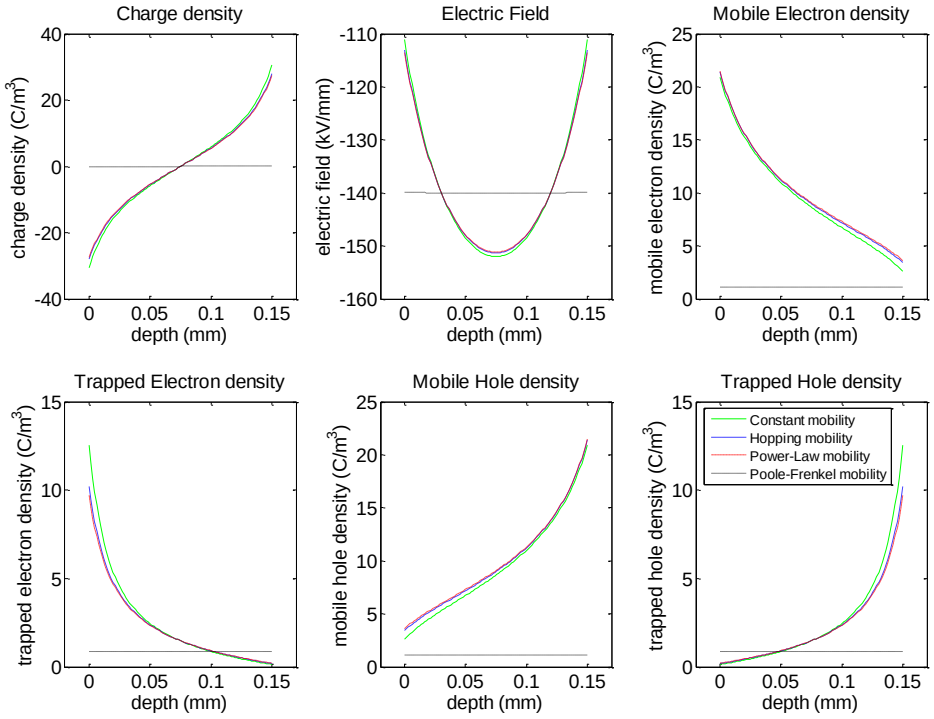


**Figure 3-24:** Space charge profiles with different mobility under 140 kVmm$^{-1}$ field

The conduction current generated during the charge injection and charge transport in polyethylene subjected to the applied dc field reveals the relationship

between the charge movement and the applied field. The variation of current densities with the electric field under the different field-dependent mobility models is shown in Figure 3-25. The conduction current densities in the constant mobility model and hopping mobility model overlap each other; the current using the power-law mobility model almost increases with the electric field in the same way as charge carriers with a constant mobility. However the conduction current increases to a higher value than in the other mobility models when the field is above 60 kVmm$^{-1}$. The *J-E* curve in the case of Poole-Frenkel mobility demonstrates a typical SCLC pattern than those of the other three mobility models; but it does not result in the large accumulation of space charge in the bulk of polyethylene under high electric fields.

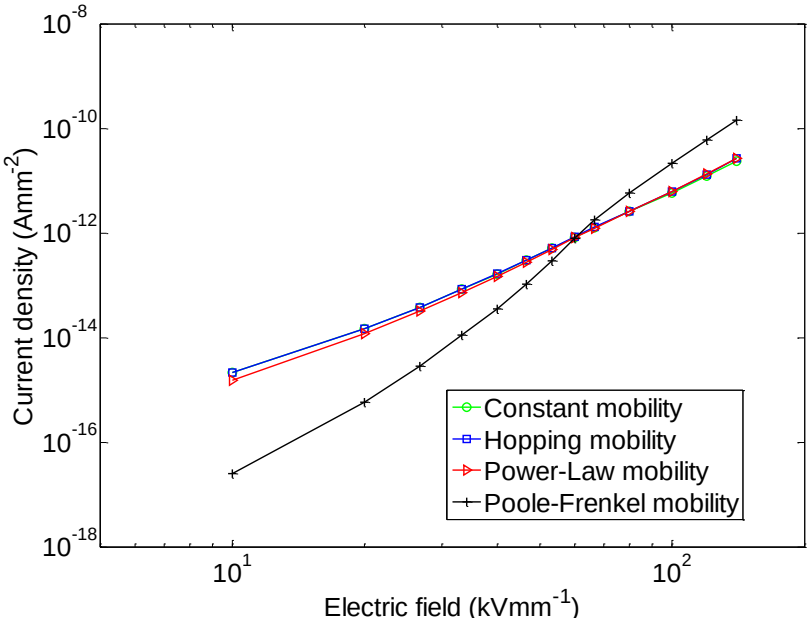


**Figure 3-25:** Current density vs. electric field with field-dependent mobility

### (2) Influence of field-dependent mobility on the recombination rate

The recombination rate of charge carriers in polyethylene in the case of field-dependent mobility models at various electric fields is shown in Figure 3-26. The recombination rate in the case of a constant mobility, hopping mobility and power-law mobility is almost the same for a low applied field of 20 kVmm$^{-1}$ and for the medium field of 60 kVmm$^{-1}$; the intensity of recombination in the case of a constant mobility is slightly lower than that with a hopping mobility or power-law mobility. For the Poole-Frenkel mobility model, due to far less charge accumulation under the high field of 140 kVmm$^{-1}$, the recombination rate is quite low.

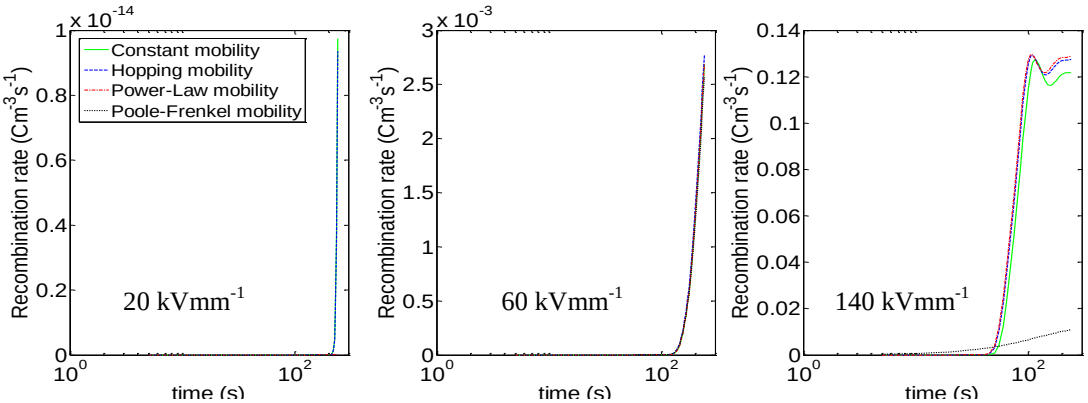


**Figure 3-26:** Total recombination rate with field-dependent mobility

## 3.5 Fitting with experimental data

Numeric modelling provides a theoretical approach to analyse the dynamics of space charge in solid dielectrics; and it is quite helpful to identify the factors that contribute to the formation of space charge under the application of electric fields. This allows an optimized numerical model that can be validated using experimental observations, which will assist in the understanding of the origin of space charge and the correlation between the physical/chemical properties linked with the models multi-parameters and the physics behind the formation of space charge in polymers.

In the experiment, the characteristics of space charge in polyethylene have been detected using the pulsed electro-acoustic (PEA) technique. The test sample is a film of nominally additive free low density polyethylene with a thickness of 180 μm, supplied by GoodFellow Ltd. It is sandwiched between a top electrode (semiconducting polymer) and a bottom electrode which is the flat Aluminium. The LDPE film is polarized under a constant dc voltage of 8 kV for one hour. The space charge measurements start on the application of the voltage and cease after one hour of dc stressing. All the measurements were undertaken at room temperature.

The simulation only describes the space charge in the bulk of polyethylene but does not contain any representation of the surface charge at the electrodes. Surface charge at the electrodes is composed of capacitive charge due to the applied voltage and induced charge (image charge) due to the formation of space charge in the bulk of polyethylene. To fit the simulated space charge with the measurement data in experiments, it is necessary to combine the surface charge at the electrode with the

simulated space charge in the bulk to construct an intact charge profile comparable to the experiment. The surface charge at the electrodes was calculated as [76],

$$\begin{aligned} \rho_{cath} &= -\frac{1}{dx}\int_0^d \frac{d-x}{d}\rho(x,t)\partial x - \frac{\varepsilon_0\varepsilon_r V}{dx\cdot d} \\ \rho_{anod} &= -\frac{1}{dx}\int_0^d \frac{x}{d}\rho(x,t)\partial x + \frac{\varepsilon_0\varepsilon_r V}{dx\cdot d} \end{aligned} \tag{3-14}$$

Where the first term on the right is the induced charge density at the electrode and the second is the capacitive charge density; $dx$ is the discrete element size; $d$ is the thickness of the polyethylene film; $\rho(x,t)$ is the charge density in the bulk of polyethylene; $\varepsilon_0$ is the permittivity of free space; $\varepsilon_r$ is the relative permittivity of polyethylene; $V$ is the applied voltage.

Finally for the obtained simulated space charge in a polyethylene film of 180 μm subjected to a dc voltage of 8 kV, to be comparable to the measured space charge, a series of optimized parameters in the bipolar charge transport model have been obtained. A comparison of the simulation result with experimental data is shown in Figure 3-27. It shows space charge distribution in polyethylene undergoing a dc stressing time of 20 minutes. In the simulation, power-law mobility was used to describe the charge transport process; even though the Poole-Frenkel mobility demonstrates strong field dependence, it cannot reproduce the accumulation of space charge. In reality, the transport of electrons or holes depends on the morphology of polyethylene and the distribution of electric field. The electrons and holes both have unique properties and they are not identical. The symmetric parameterization in modelling is not able to represent the exact processes occurring in the polymer. Therefore asymmetric parameters for electrons and holes are employed to fit the simulated space charge in polyethylene under dc electric fields with measurement data. The parameter values of power-law mobility and charge injection, trapping and recombination processes for electrons and holes are defined in Table 3-4.

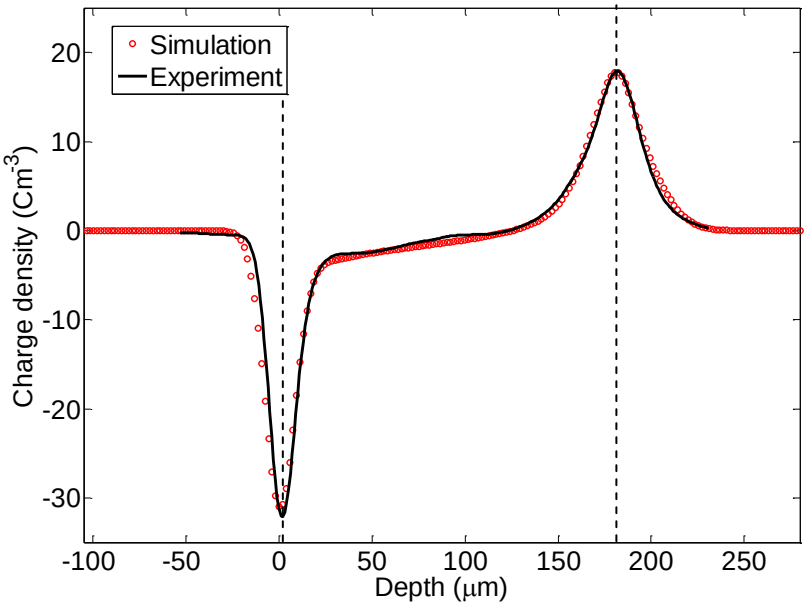


**Figure 3-27:** Comparison of simulated space charge with experimental data.

**Table 3-4:** Optimized parameters for fitting model with experiment.

| Parameter | Value | | Unit |
|---|---|---|---|
| | Electrons | Holes | |
| Injection barrier height $w_{ei}$ / $w_{hi}$ | 1.20 | 1.21 | eV |
| Power-law mobility ($n$=1.165) $\mu_{0e}$ / $\mu_{0h}$ | $1.095\times10^{-14}$ | $5.472\times10^{-15}$ | $m^2V^{-1}s^{-1}$ |
| Trapping coefficients $B_e$ / $B_h$ | 0.1 | 0.2 | $s^{-1}$ |
| Trap density $N_{oet}$ / $N_{0ht}$ | 100 | 100 | $Cm^{-3}$ |
| Recombination coefficients $S_0$ (trapped electrons-trapped holes) $S_1$ (mobile electrons-trapped holes) $S_2$ (trapped electrons-mobile holes) $S_3$ =0 (mobile electrons-mobile holes) | $4\times10^{-3}$ | | $m^3C^{-1}s^{-1}$ |
| Permittivity of polyethylene $\varepsilon_r$ | 2.3 | | |
| Temperature $T$ | 300 | | K |

## 3.6 Relaxation of space charge

The decay of space charge in polymers is considered to be linked with the trapping/detrapping characteristics of charge carriers [79-81]. The bipolar charge transport model is also used to simulate the relaxation of charge in polyethylene and try to understand the behaviour of space charge during the decay process.

### *3.6.1 Discharge of space charge in polyethylene*

When the polymeric material is short circuited through electrodes after being stressed under dc electric fields, the charged polymeric film is able to discharge through the electrodes. The accumulated space charge in the bulk gradually decays with the progressing of time. This is driven by the local electric field induced by the space charge in the bulk, the diffusion of charge carriers and the detrapping of trapped charges. The discharge process normally reflects the trapping/detrapping information of charge carriers in the bulk of polymers. Hence the decay of space charge has been investigated to extract the mobility of charge carriers and the activation energy of trapping dynamics [80]. The relaxation of space charge in polyethylene has been simulated using the bipolar charge transport model. The diffusion of charge carriers is not taken into account and only a single level of deep trapping regardless of detrapping is considered in the model to simulate the decay process.

The model includes an equation that constrains the space charge decay under the short circuit condition, i.e., the removal of the applied voltage,

$$\int E(x,t)dx = 0 \tag{3-15}$$

This equation is incorporated into Gauss's Law equation (3-1) to calculate the electric field distribution in the specimen during the decay process.

In the simulation, the discharge process takes place immediately after the polarization of a 150 μm polyethylene film under a dc voltage of 9 kV for a stressing time of 600s. The space charge built at 600s is set to be the initial charge density for the decay stage. The simulated space charge decay within the polyethylene film is shown in Figure 3-28. It shows that the space charge in the bulk of polyethylene decays very slowly under the present bipolar charge transport model with the same parameters as those used for the volts on condition described in Table 3-1. The evolution of local electric field is also plotted. It is notable that the electric stress in the bulk is in the opposite polarity to the field adjacent to the electrodes, which defines the flow of charge carriers in opposite directions. Due to the presence of space charge in the bulk, the overall discharging current density could appear in the same direction as the charging current density, which results in an anomalous discharging current as observed in polyethylene [82] and shown in Figure 3-29. It presents a peak at around

500s, which suggests a slow movement of charge carriers as well. This peak occurs later than the peak-time of discharging current reported in [72] even though they are of the same order of magnitude. The overall slow dynamics of space charge decay is due to the limitation of the bipolar charge transport model where only the recombination of opposite charge carriers and extraction at the electrodes are considered to release the accumulated space charge in the bulk of polyethylene. The detrapping process of trapped charge carriers was not taken into the model so that the discharging process is not significant as the recombination and extraction process are weak at the very low local electric fields in the bulk when the charged specimen is short-circuited.

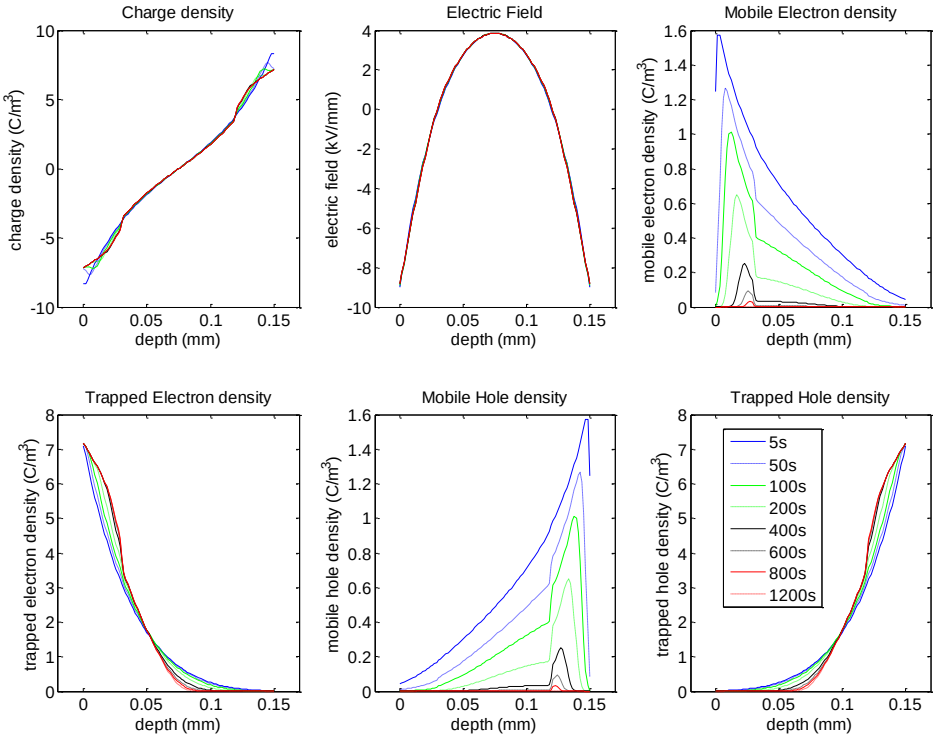


**Figure 3-28:** Simulated space charge decay in polyethylene

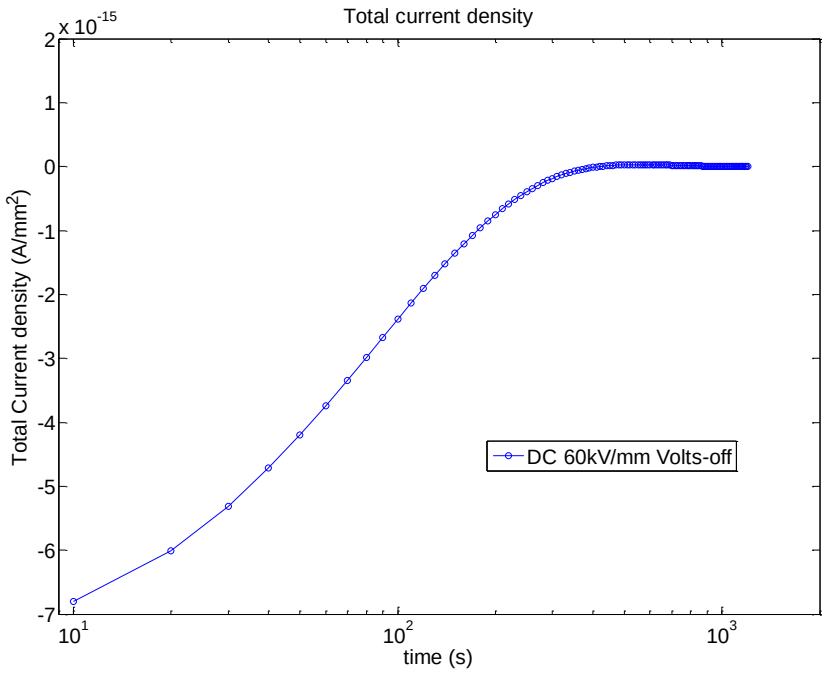


**Figure 3-29:** Simulated discharging current during space charge decay in polyethylene

### *3.6.2 Decay of negative corona charge*

The surface potential decay of corona charged polymer films has been investigated by experiments [83]. The decay curves with higher initial potentials always cross the decay curves at lower initial potentials. What causes this crossover to happen and what determines the decay process of the corona charge are still not well understood. Extensive efforts have been dedicated into exploring this crossover phenomenon and its origin. A theoretical approach which considers single type of charge carriers injection and transport has been used to model the crossover phenomenon [84]. However the experiment of using the pulsed electro-acoustic (PEA) technique to measure the space charge distribution in the corona charged additive free LDPE films reveals the bipolar charge accumulation in the bulk of LDPE films after being negatively corona charged [85] as shown in Figure 3-30. Hence the assumption that the bipolar charge injection and transport could be developed during the corona charging process and involved in the decay process is proposed. However the electric charge deposited on the surface of corona charged LDPE films might also play a significant role in the surface potential decay process. Assuming that there is a penetration of charge carriers from the surface into the bulk as soon as the corona charging starts and that surface charge continuously enters into the bulk even during the decay process, then the bipolar charge transport model could provide a way to examine

the behaviours of charge carriers in the corona charged specimen during the decay process. The bipolar charge model has been modified to simulate the corona charging process providing electric charge to the LDPE film and then the consequent charge decay on the surface and in the bulk of polymer films are also simulated.

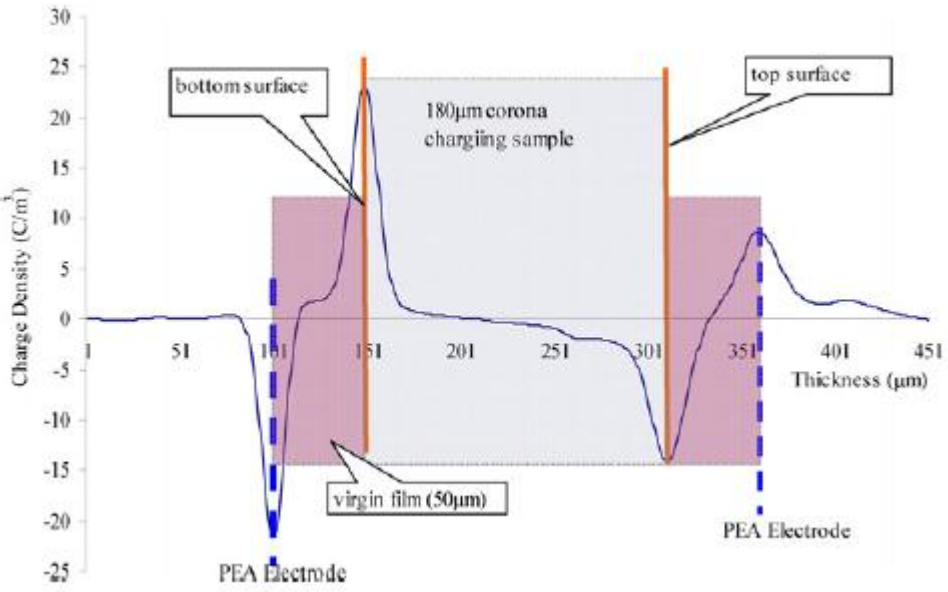


**Figure 3-30:** Space charge distribution in the corona charged 180 μm LDPE film (corona charging at -8 kV for 2 minutes) [85]

The negatively corona charging setup is shown in Figure 3-31. The additive free LDPE film is charged through a no-contact needle electrode with negative potential. The bottom surface of LDPE film is grounded. In the modelling, the supply of charge carriers to the specimen during the charging process is assumed to be the Schottky injection at the electrodes with electrons injected from the top electrode (cathode) and holes injected from the grounded electrode (anode). This injection is able to develop the bipolar charge accumulation in the bulk of corona charged polyethylene as observed from experiments. This bipolar charge transport model only simulates the charge in the bulk rather than that on the surfaces. Surface charge can be worked out using the conservation law. The simulation task is to charge the specimen firstly and then simulate the negative corona charge decay in a polyethylene film of 50 μm at different initial charging potentials. The simulation is based on the symmetric parameterization for electrons and holes and thus it can only be used for the qualitative analysis. The simulated charge distribution within a polyethylene film of 50 μm after

being negatively corona charged for 120s at different initial potentials is shown in Figure 3-32. The magnitude of the charge density in the vicinity of cathode is obviously larger than near the anode as would be expected for negative corona charging. The amount of charge in the bulk increases at higher applied potentials.

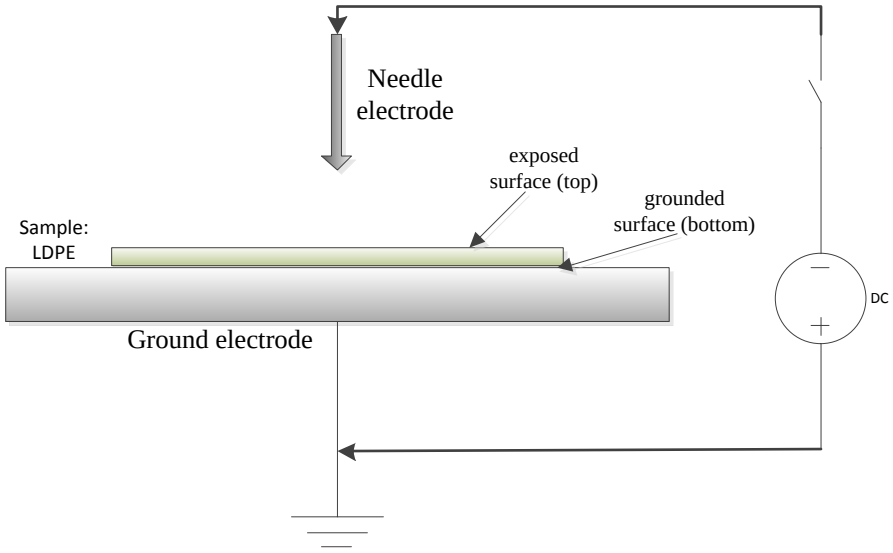


**Figure 3-31:** Setup of negatively corona charging system

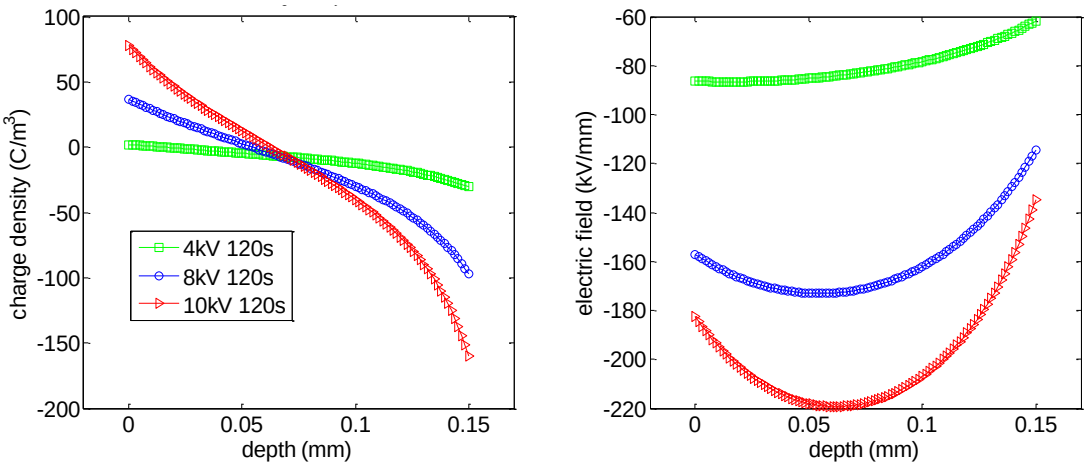


**Figure 3-32:** Simulated corona charge in polyethylene film under different potentials

The decay starts immediately after the corona charging is finished at 120s when the applied potential is removed but the circuit is still open. The set of equations governing the decay procedure introduces the open circuit condition except the typical three equations involved in the bipolar charge model. These are Gauss's Law,

$$\frac{\partial E_b(x,t)}{\partial x} = \frac{\rho_b(x,t)}{\varepsilon} \tag{3-16}$$

Where $\rho_b$ is the net charge density in the bulk of the polyethylene film, $Cm^{-3}$. The electric field calculated from $\rho_b$ is referred to as the bulk field $E_b$.

The transport equation:

$$j(x,t) = \mu n(x,t) E(x,t) \tag{3-17}$$

The continuity equation:

$$\frac{\partial n(x,t)}{\partial t} + \frac{\partial j(x,t)}{\partial x} = s \tag{3-18}$$

The open circuit condition:

$$\varepsilon \frac{\partial E(x,t)}{\partial t} + j(x,t) = 0 \tag{3-19}$$

The overall local electric field $E$ is the summation of the bulk field $E_b$, the field induced by the charges on the negatively charged surface (Cathode) $E_1$ and the field induced by charges on the positively charged surface (Anode) $E_2$. The induced fields $E_1$ and $E_2$ can be computed from the surface charge density.

$$E_1 = \frac{\sigma_1}{2\varepsilon} \qquad E_2 = \frac{\sigma_2}{2\varepsilon} \tag{3-20}$$

Where $\sigma_1$ is the charge density on the negatively charged surface, $Cm^{-2}$, $\sigma_2$ is the charge density on the positively charged surface, $Cm^{-2}$ and $\varepsilon$ is the permittivity of polyethylene. The charge densities on both surfaces $\sigma_1$ and $\sigma_2$ conform to the charge conservation law. They both contribute to the surface potential which is the integration of the local electric field. Hence the surface charge densities can be solved from the following equations. They are the charge conservation law,

$$\rho_b \cdot d + \sigma_1 + \sigma_2 = 0 \tag{3-21}$$

The initial surface potential condition,

$$-\int [(\sigma_1 + \sigma_2)/2\varepsilon + E_b] dx = V_0 \tag{3-22}$$

Where $d$ is the thickness of the specimen and $V_0$ is the initial surface potential.

The charge on the top surface of the negatively charged polyethylene film is assumed to exchange from the surface to the bulk by a reduction rate. The reduction rate is described by a Schottky injection current density.

$$\sigma_1(t) = \sigma_1(t-1) + J_{inj} \cdot dt \quad (\sigma_1 < 0) \tag{3-23}$$

Where $\sigma_1(t)$ is the charge density on the top surface at time instant $t$ and $J_{inj}$ is the Schottky injection current density. Positive charges at the grounded (bottom) surface can be calculated from the conservation law in equation (3-21) for each time step.

By solving the above equations, the corona charges on the surfaces and in the bulk of polyethylene film are numerically computed through the simulation. The surface potential decay of negatively corona charged polyethylene films under different initial potentials are shown in Figure 3-33. The decay of surface potential of corona charged polyethylene at higher initial potentials of 8 kV and 10 kV both cross the decay curve of lower initial potential 4 kV. The decay line at 10 kV also crosses the decay line at 8 kV. The higher the initial potential is, the earlier the crossover occurs.

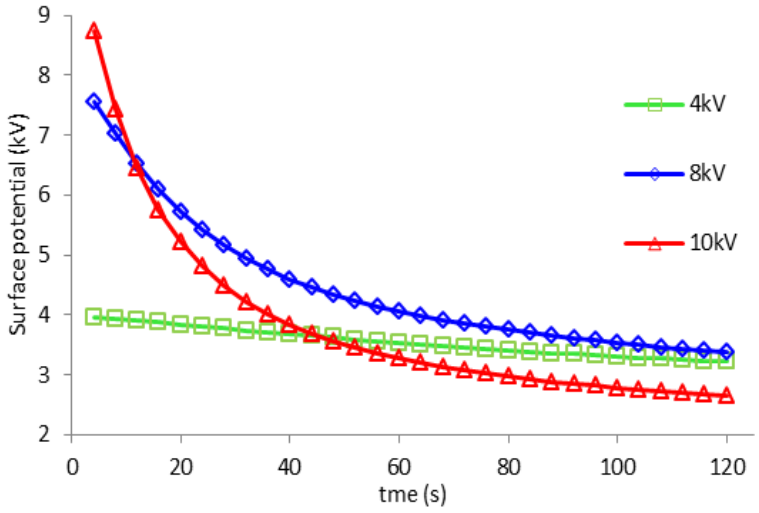


**Figure 3-33:** Simulated surface potential decay of corona charged polyethylene film

The decay of charges on the surfaces and in the bulk of corona charged polyethylene film is shown in Figure 3-34. The decay of surface charges crossover as well. This suggests that the surface potential decay must be closely related to the surface charge decay process. The absolute value of the bulk charge density $\rho_b \cdot d$ is less than one third of both surface charge densities.

In experiments, the decay of surface potential of longer charged films at the same initial potential is faster than those shortly charged. This feature is also reproduced in the simulation of corona charge decay within a polyethylene film of 50 μm at dc potential of -8 kV as shown in Figure 3-35. It indicates that the surface potential of the

specimen charged for 6 minutes decays faster than the one charged for 2 minutes and 30 seconds. Charges on the surfaces also decay similarly to the surface potential showing a faster slope for longer charged sample and surface charge density is larger than bulk charge density. Noticeably the decay of bulk charge for the shortly (30s) charged sample behaves differently from long charged samples. It decreases very fast in the first 20s followed by a small increase for a short period and then decays gradually like the longer charged samples. This is because a stable distribution of charge in the bulk has not been achieved at the end of corona charging for 30s prior to its discharging. It takes time to reach the stable status within the first 30s and then the decay behaves in the same way of longer charged samples.

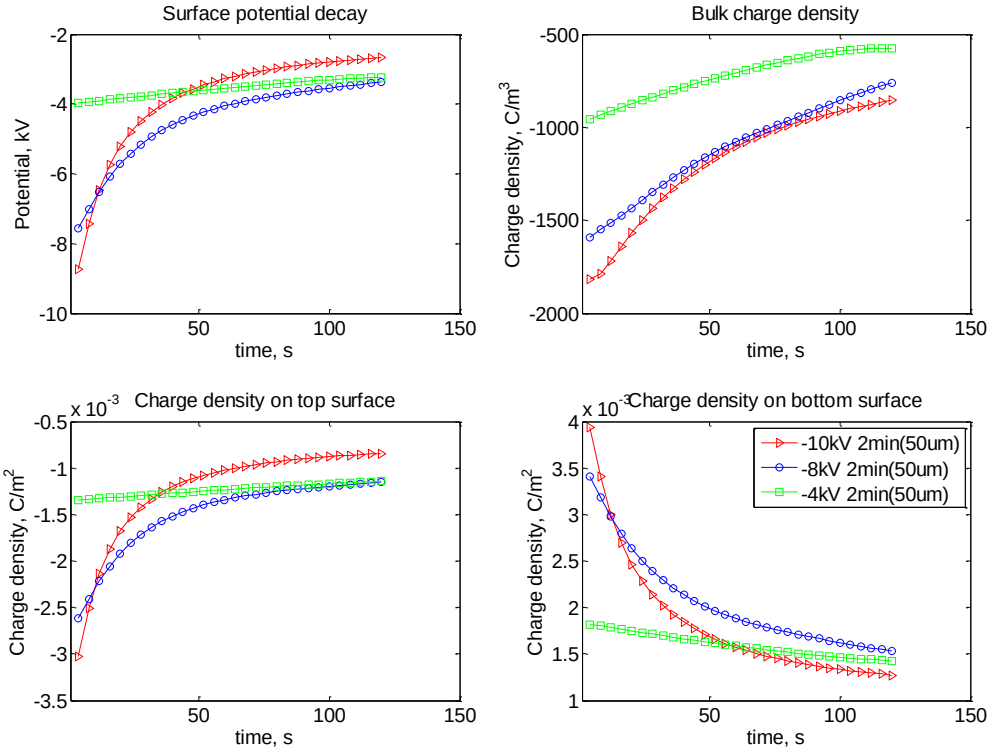


**Figure 3-34:** Surface charges and bulk charges decay of corona charged LDPE films

All the simulation results show that the decay of surface charges contributes predominantly to the surface potential decay rather than the bulk charge in terms of the amount of charge and the slope of decay.

In respect of the non-contact between the needle electrode and the exposed surface of polyethylene film in corona charging and decay, the exchange of charges from the surface to the bulk described by the Schottky injection might not be practical

while it is reasonable if the contact is in solid contact with the surface as the Schottky injection is normally accepted to describe the exchange of charge carriers at the contact of a dielectric/metal. Tunnelling injection, hence, is considered an alternative for the charge exchange at the exposed surface and has been introduced into the model. The simulation involving tunnelling injection also reproduces the fast decay of surface potential at higher initial potential and longer charged samples [86].

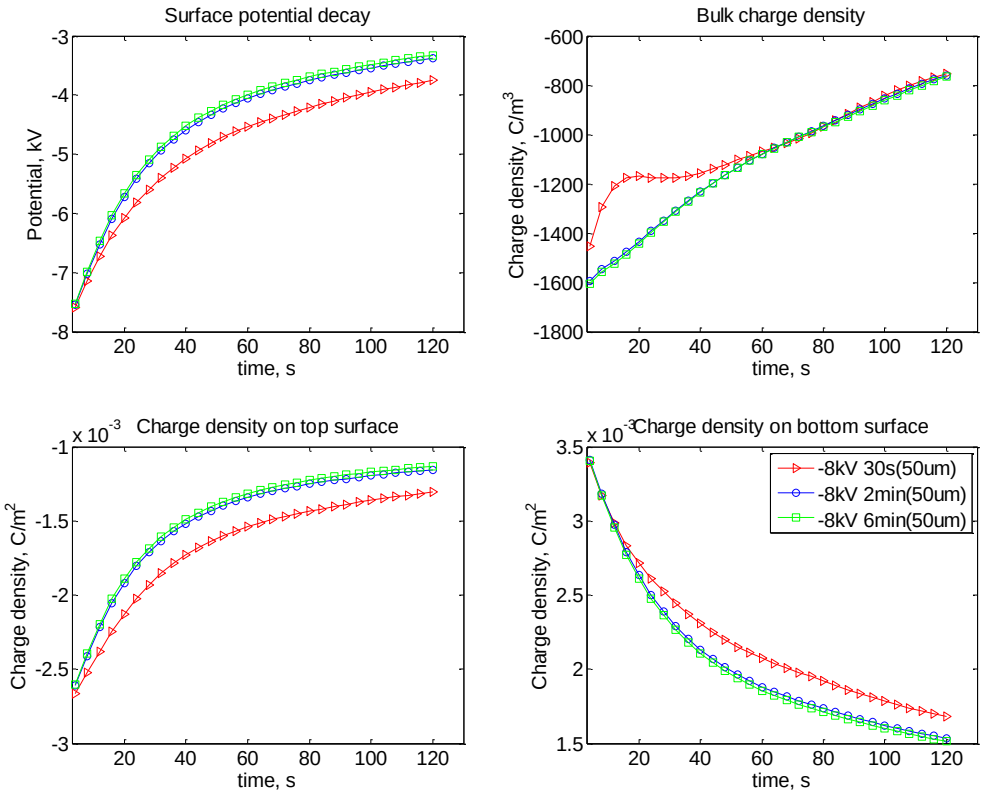


**Figure 3-35:** Corona charge decay after various stressing duration at -8kV initial potential

## 3.7 Summary

The dynamics of space charge in polyethylene under applied dc electric fields has been modelled and simulated using a bipolar charge transport model. Influence of charge carrier injection, especially the field-dependent mobility, trapping and recombination processes on the behaviour of space charge in polyethylene subjected to dc stresses has been recognized using the simulation approach. The optimized parameter values describing these physical processes have been obtained by fitting the simulated space charge profiles with experimental data. This simulation work helps the understanding of the behaviours of electronic charge carriers in polyethylene and the effect of space charge on the electric field distribution in the bulk of polyethylene. The

decay of space charge in polyethylene has also been simulated using this model, which reveals that the anomalous discharging current is due to the presence of space charge. The relaxation of corona charge in polyethylene film is also simulated using this bipolar charge transport model, which reveals that the crossover of the surface potential decay is closely related to the decay of charge on the surfaces of the sample.

# Chapter 4 Charge Packets in Polymers

A phenomenon of charge packets has been observed in polymers under dc electric fields during the latest decade. A variety of charge packets has demonstrate different dynamics, which opens a new approach of understanding the behaviours of electric charge carriers in polymers subjected to electric stresses. This chapter first reviews the existing experimental evidence of charge packets in polymers and related theories that explains the possible underlying mechanism. Then an experimental investigation of positive charge packets in polyethylene using the pulsed electro-acoustic technique is described. The velocity and mobility of positive charge carriers are both evaluated and introduced into a bipolar charge transport model to reproduce the dynamics of charge packets and to reveal the influence of essential parameters.

## 4.1 Charge packets

The first observation of charge packets was reported in the measurement of space charge in XLPE cable using the pulsed electro-acoustic (PEA) method by N. Hozumi et al in 1994 [45]. A packet form of positive charge was injected from the conductor (anode) at an applied dc field of 116.7 $kVmm^{-1}$; it travelled towards the opposite

electrode (cathode) but still retained its packet shape and it repeatedly occurred. In the following decade, the phenomenon of charge packets has been reported in polyethylene based cable insulation materials [47, 69, 87-89] and epoxy based nanocomposites [90] over a wide range of electric field conditions. The characteristics of the charge packets vary from material to material and depend on the electric field, the temperature and the presence of contamination. This packet-like space charge can cause substantial field distortion and accelerates the ageing and breakdown of the insulation material. However the origin of the charge packets has yet to be fully established.

Charge packets can be classified into two categories: (a) fast charge packets, which have a high mobility in the order of $10^{-11}$ to $10^{-10}$ $m^2V^{-1}s^{-1}$; this is normally linked with heterocharge accumulation as it appears in both polarities, i.e., negative and positive charge packets both exist simultaneously in the material [90]. Normally fast charge packets are observed at relatively low electric fields of 30-50 $kVmm^{-1}$. (b) slow charge packets, which have a low mobility in the order of $10^{-16}$ to $10^{-14}$ $m^2V^{-1}s^{-1}$; are linked with homocharge injection and normally appear to be unipolar, i.e., positive charge packets or negative charge packets. The required electric fields to observe slow charge packets are relatively higher and generally ranges from 110 to 200 $kVmm^{-1}$ in XLPE cables or from 100 to 400 $kVmm^{-1}$ in LDPE films [89]. The common features of charge packets are: the packet shape is maintained as they travel across the insulation and the behaviour can be repeatedly generated and observed.

Three theories have been proposed to explain the formation of charge packets in polymeric insulation materials under the application of electric fields.

- Hysteresis of injection current

In the very beginning of the observation of charge packets in XLPE cables under high electric fields, the generation of charge packets was believed to be associated with charge injection and transportation in polymers. A hysteresis of electronic injection at the electrodes has been proposed as illustrated in Figure 4-1. When the electric field at the electrode exceeds the threshold electric field $E_2$, the injection rapidly acquires a high rate and the electrode field is consequently reduced due to the injected space charge. When the field drops below $E_1$, the injection finally reverts to the low rate again. This injection hysteresis eventually leads to pulse-like charge carriers, i.e., the charge packet [45]. The enhancement of the injection rate may be attributed to the

occurrence of tunnelling injection of holes in the case of a dramatic change in the molecular chain compression at the electrode. The high electric field brings the chain sections close enough to the electrode and hence reduces the tunnelling distance. An intense tunnelling of injection change consequently takes place. Due to space charge, the electrode field is reduced and hence the compression is released, which therefore increases the tunnelling distance and leads to lower rate of injection [91].

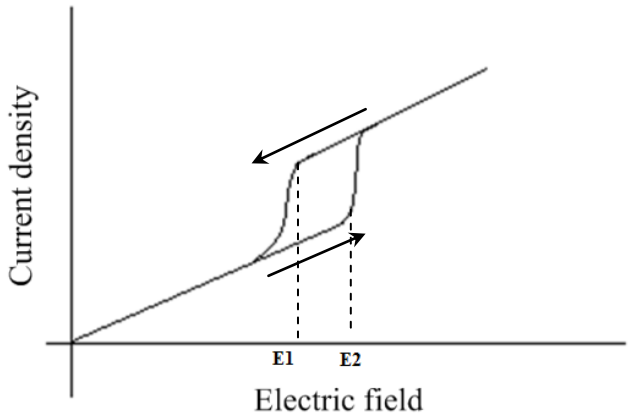


**Figure 4-1:** Hysteresis of injection current as a function of electric field.

- Field-induced ionization

On the other hand, the formation of charge packets is also related to the dissociation of cross-linking by-products in XLPE [87]. There is a limited region of ionization in the vicinity of anode as shown in Figure 4-2. The ionization is initiated in this region due to the electric field; the charges generated by the ionization are then separated at the effect of the field stress. The negative charges may vanish from the electrode leaving a packet of positive charge carriers travelling in the bulk of dielectrics towards the opposite electrode. The travelling charge packet creates a new ionization area in front of it due to the raised electric field forward of the packet; the present positive charges are neutralized by the newly generated negative charges, leaving a new positive charge packet in front. This leads to the propagation of the charge packet. Once the first charge packet arrives at the cathode, the next ionization in the vicinity of the anode starts again, which causes the repetitive nature of charge packets.

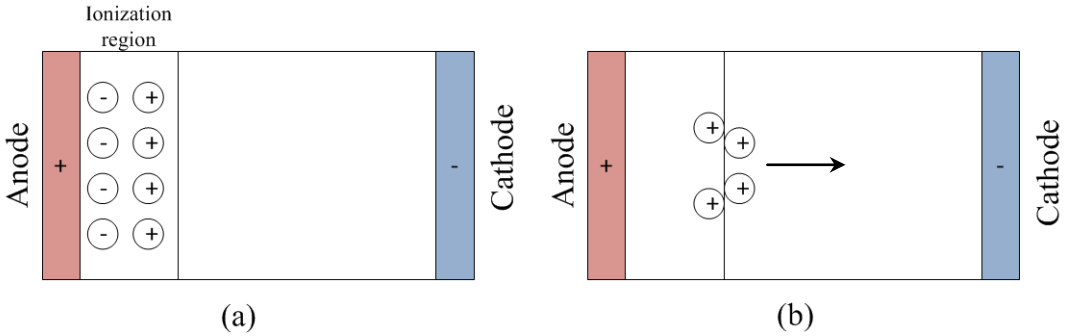


**Figure 4-2:** Formation of positive charge packet due to ionization

- Negative differential resistance

The slowdown and even stopping of positive charge packets has been observed in low density polyethylene under very high electric fields greater than 100 $kVmm^{-1}$ [47]. The decrease of the velocity of charge packets with increased applied field has also been observed. Thereby a concept of the negative differential resistance of polyethylene, which results into a decrease of the velocity of charge carriers when the electric field exceeds a threshold value as shown in Figure 4-3, is proposed to explain the characteristics of positive charge packets that have been observed in experiments. In the field region lower than $E_T$, the velocity of carriers increases with the electric field; it starts to decrease when the field exceeds $E_T$. Once positive charge carriers are injected from the anode, the electric field in the bulk away from the anode is raised while it is reduced in the region close to the electrodes. If the electric field in the bulk exceeds the threshold value $E_T$, it will lead to a slow transport of carriers in the bulk (the high field region) and quick transport near the electrode (the low field region). Eventually a packet of positive charge carriers can be formed. Similarly a discontinuity of the conductivity in the front and in the rear of a charge packet is proposed to account for the formation of the positive charge packets. There is a low conductivity in the front of the positive charge packet where the field is raised while a high conductivity exists in the rear of the charge packet where the field is reduced [89]. The mechanism behind the decrease of the velocity or the low conductivity under high electric fields is not known yet. It is proposed that when the field is above a threshold value, the recombination centres and the trapping centres near the electrode become saturated so that charge carriers travel rapidly in the rear of the charge packet. In contrast, charge carriers tend to be captured by these defect centres leading to slow charge transport in the front of the charge packet.

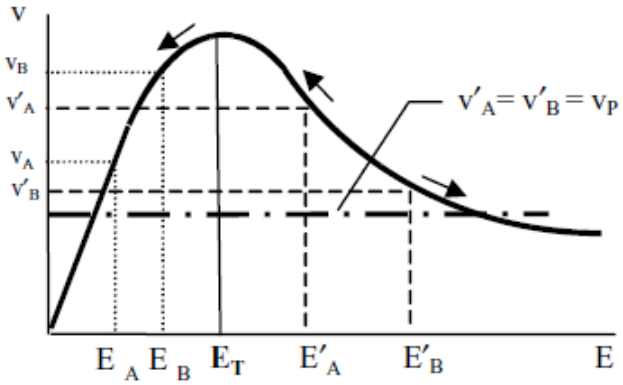


**Figure 4-3:** Field dependence of carrier velocity in the case of a negative differential resistance.

## 4.2 Experimental observations

To investigate the characteristics of charge packets, space charge measurement has been conducted on polyethylene under dc voltages ranging from 1 to 12 kV. Test samples of additive free low density polyethylene films with a thickness of 100 ± 5 μm, supplied by GoodFellow Ltd, were used for all experiments. They are sandwiched between the semiconducting polymer electrode (anode) and the flat aluminium electrode (cathode). Each sample is polarized under a dc electric field for a couple of minutes and the space charge profiles recorded at specific time steps. All the measurements are performed at a room temperature of around 22 ℃.

### *4.2.1 Pulse excitation method*

Under low electric fields, only a normal space charge distribution can be observed by the pulsed electro-acoustic (PEA) measurement. No charge packets are observed to occur in polyethylene. Therefore a pulse excitation method, firstly proposed by Hozumi et al.[92], is employed to initiate a charge packet in polyethylene. The pulse excitation method is shown in Figure 4-4. A dc bias voltage is applied across the polyethylene film from the very beginning; once a quasi-stable distribution of space charge is achieved after several minutes, a pulse voltage with a width of 250 ms and large amplitude of several kilovolts is superimposed onto the dc voltage. The peak amplitude of the overall voltage is up to 15 kV. Due to the excitation of space charge by a large pulse voltage, a packet of positive charge carriers immediately forms at the anode and travels towards the cathode under the dc bias voltage. Hence the dynamics of

positive charge packets under the biased electric field can be observed in polyethylene. A difference of the acquired charge profiles after the pulse excitation from the quasi-stable distribution gives clearly a picture of the development of positive charge packets.

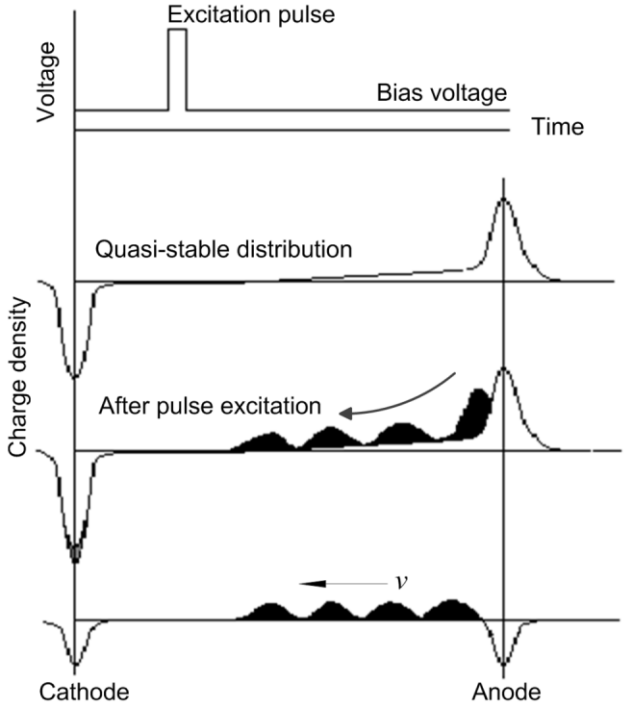


**Figure 4-4:** Schematic diagram of the pulse excitation method

### *4.2.2 Charge packets under low electric fields*

Measured space charge profiles under a bias dc field of 20 kVmm$^{-1}$ after pulse excitation are shown in Figure 4-5(a). This result does not demonstrate clearly the formation and movement of charge packets. Hence the quasi-stable distribution of space charge achieved at 300s since the application of the dc bias voltage but prior to the pulse excitation is subtracted from all of the acquired space charge profiles. Then the remaining charge profiles clearly show the development of a positive charge packet as shown in Figure 4-5(b). A small packet of positive charge carriers is formed at the anode and travels slowly into the bulk of polyethylene. The dynamics of the positive charge packet at a dc field of 50 kVmm$^{-1}$ is shown in Figure 4-6. The movement of positive charge packet in polyethylene is indicated by the arrow.

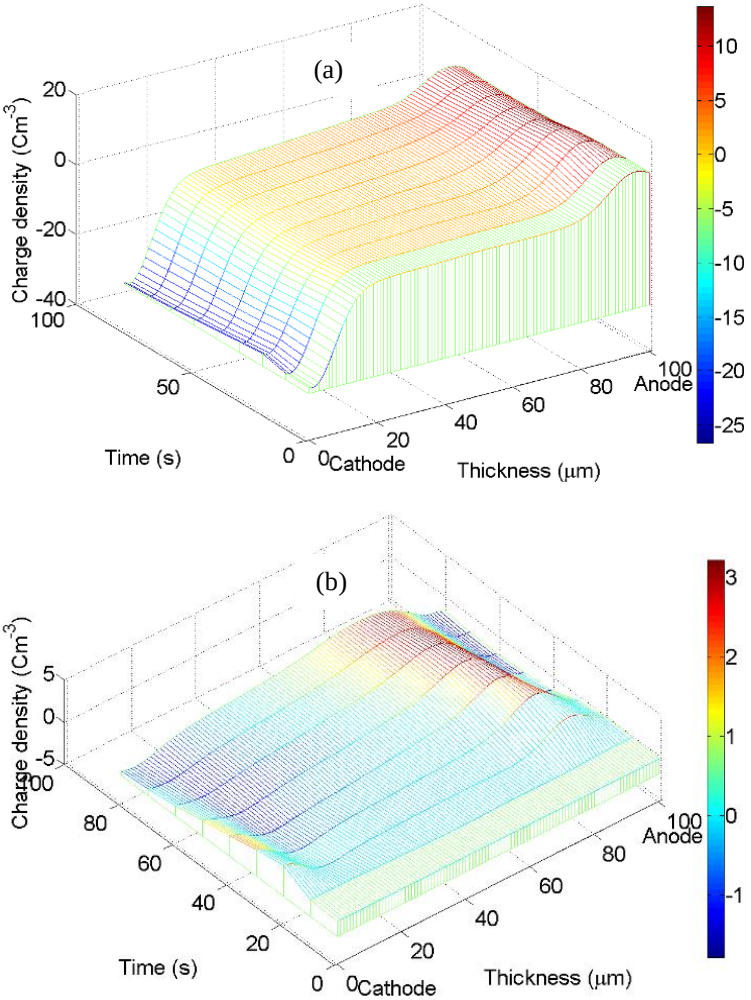


**Figure 4-5:** Space charge profiles after pulse excitation at 20 $kVmm^{-1}$: (a) unsubtracted; (b) subtracted.

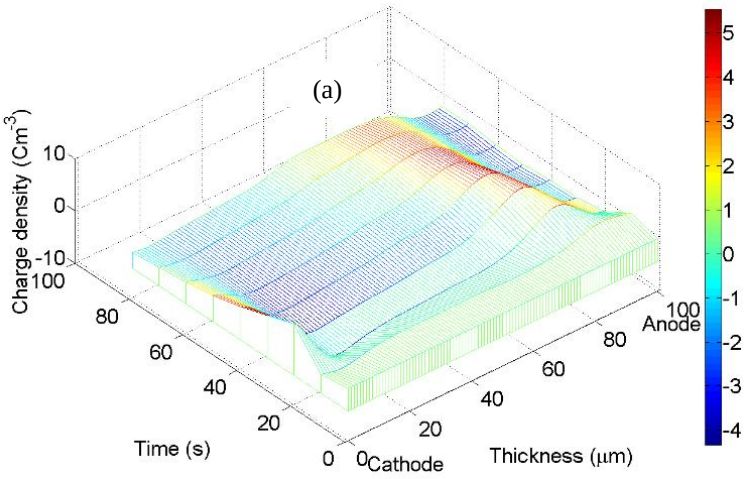

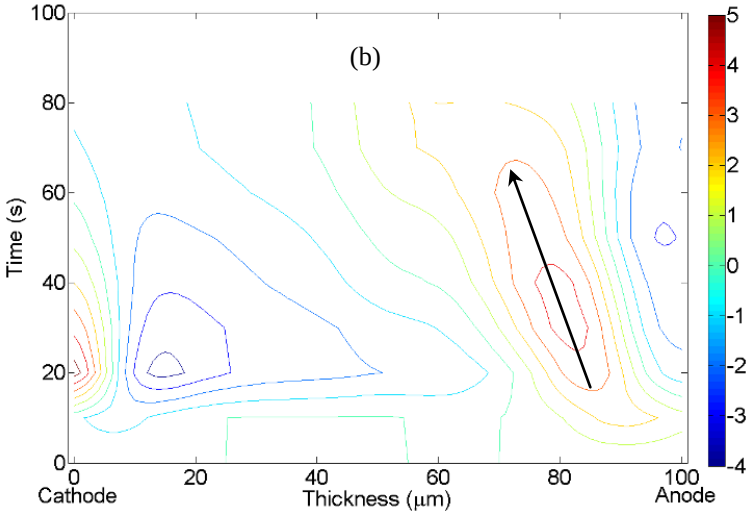


**Figure 4-6:** Subtracted charge profiles at 50 kVmm$^{-1}$: (a) 3D plot; (b) contour plot.

### *4.2.3 Velocity of charge carriers*

To characterize positive charge packets, it is preferable to evaluate the velocity of the packets. A two-dimensional contour plot is used to display the travel of the packet as shown in Figure 4-6(b) and hence the average velocity of the positive charge carriers under the applied dc field can be determined. Actually the velocity is averaged from more than 3 measurements. Moreover its dependence on the electric field can be determined from repeated tests under dc electric fields ranging from 10 to 70 kVmm$^{-1}$. The dependence of the velocity of positive charge carriers on the applied electric field is plotted in Figure 4-7. It is noticeable that the velocity of positive charge carriers does not constantly increase with electric field. The velocity starts to decrease gradually when the electric field exceeds 40 kVmm$^{-1}$; followed by a second rise at higher stress above 60 kVmm$^{-1}$. This type of field dependence was first observed in polyethylene [93]. It resembles the 'Gunn Effect' seen in semiconducting materials [94] and suggests that a negative differential mobility is involved in the behaviour of positive charge packets in polyethylene. The apparent mobility of positive charge carriers evaluated from the velocity curve is plotted in Figure 4-8. It shows that positive charge carriers in polyethylene have the mobility of the order of $10^{-15}$ - $10^{-14}$ m$^2$V$^{-1}$s$^{-1}$. The mobility tends to decrease when the field is increased. On the other hand, as shown in Figure 4-6(b), negative charge carriers seem to travel faster and reach the opposite electrode more quickly than positive species even though there is no formation of negative charge packets in polyethylene.

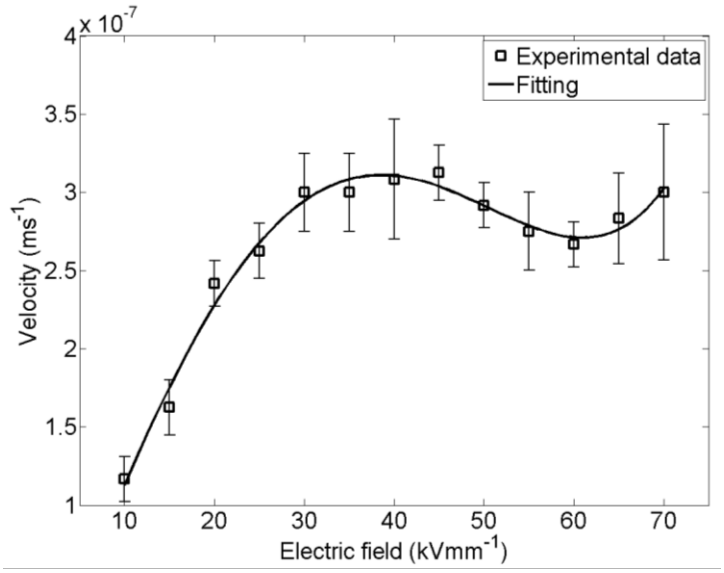


**Figure 4-7:** Velocity of positive charge carriers under low applied electric fields

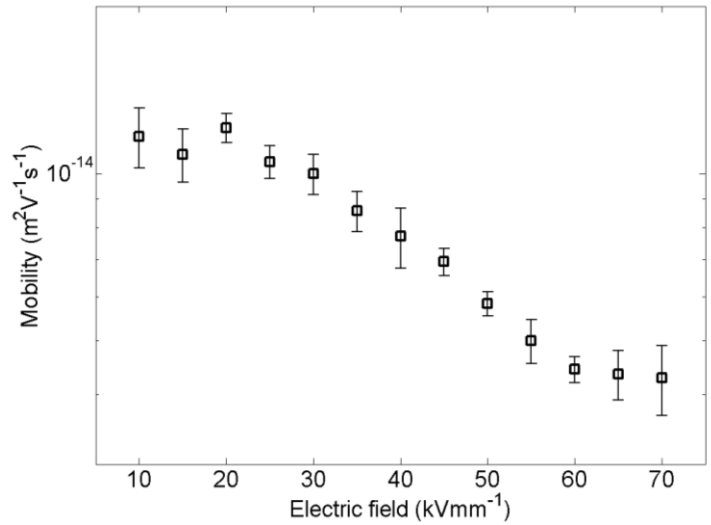


**Figure 4-8:** Mobility of positive charge carriers under low applied electric fields

### *4.2.4 Charge packets under high electric fields*

When the applied field is increased above 55 kVmm$^{-1}$, positive charge packets can be formed and observed in polyethylene without additional pulse excitation. The charge packets appear as soon as 15 seconds after the application of the dc voltage. Therefore a normal space charge measurement procedure can be performed to capture the dynamics of positive charge packets. To clearly present the characteristics of charge packets, subtraction from the original charge distribution at the 15 seconds instance prior to the appearance of the charge packet is performed. The subtracted charge

profiles in polyethylene at a dc field of 80 kVmm$^{-1}$ and 100 kVmm$^{-1}$ are shown in Figure 4-9. It is clearly observed that the positive charge packet formed at 100 kVmm$^{-1}$ travels slower than the one formed under an applied dc field of 80 kVmm$^{-1}$.

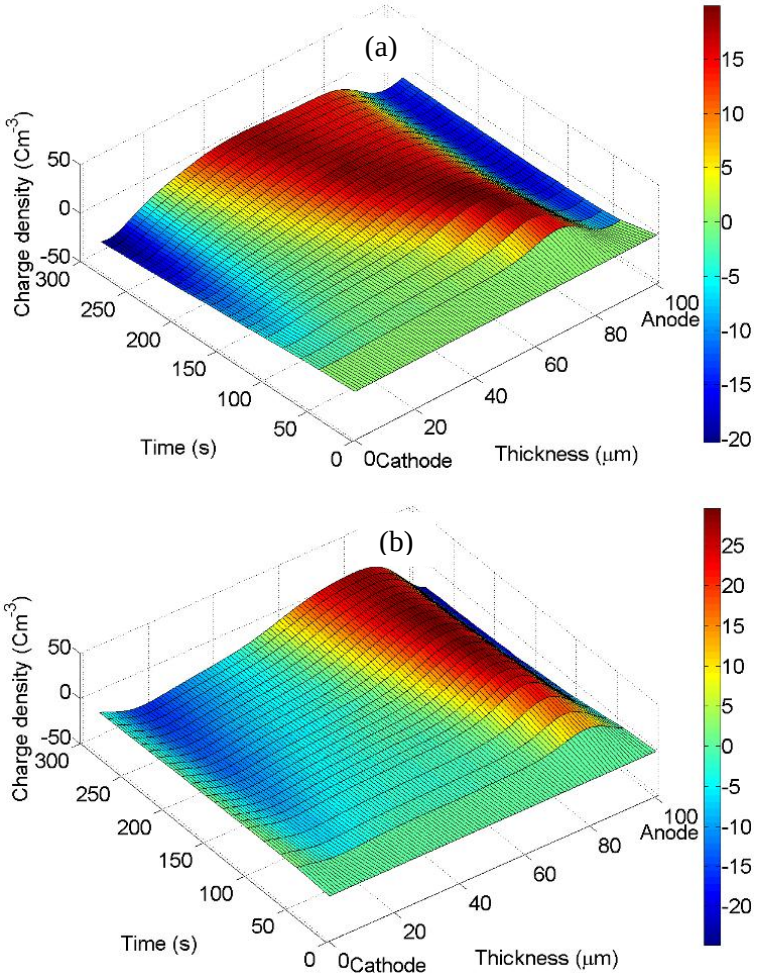


**Figure 4-9:** Subtracted charge profiles under high electric fields: (a) 80 kVmm$^{-1}$; (b) 100 kVmm$^{-1}$.

The velocity of positive charge carriers is also evaluated using the contour plot and its dependence on the electric field is shown in Figure 4-10. A reduction of velocity with increased fields is again observed. The velocity decrease until the breakdown strength of polyethylene is achieved as reported in [47]. But large variations occur around a field of 70 kVmm$^{-1}$, which is similar to the upturn shown in Figure 4-7. The mobility of positive charge carriers under high electric fields is plotted in Figure 4-11. It demonstrates an overall negative differential dependence on the electric field.

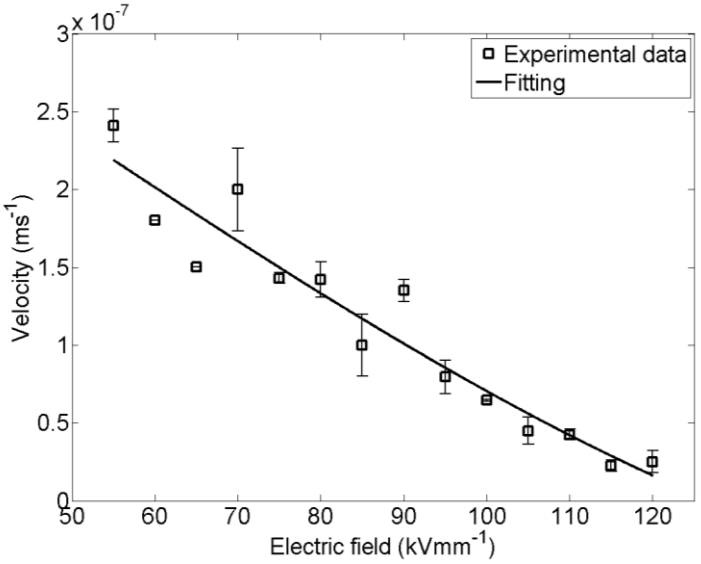


**Figure 4-10:** Velocity of positive charge carriers under high applied electric fields

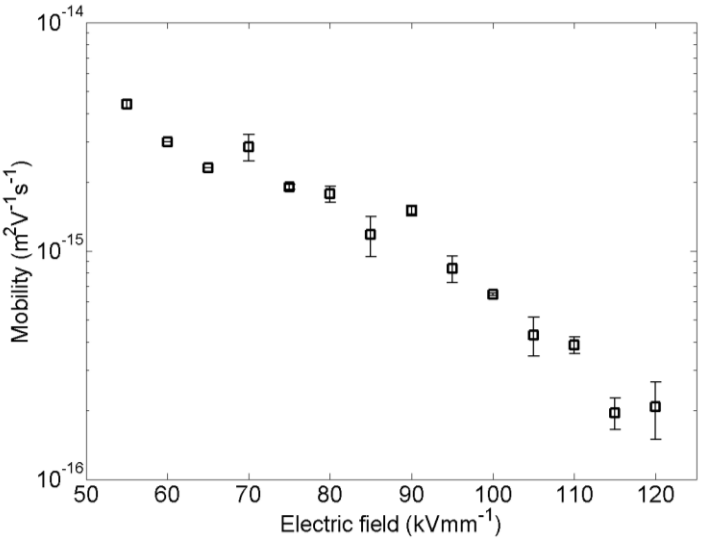


**Figure 4-11:** Mobility of positive charge carriers under high applied electric fields

## 4.3 Numerical modelling

### *4.3.1 Model description*

The bipolar charge transport model has been employed to simulate the dynamics of charge packets in polyethylene under dc electric fields. There are two essential points to be highlighted. Firstly, no ionization processes are considered in the model, electrons and holes are negative and positive charge carriers respectively. They are generated by the electronic injection at the contact between the electrode and the polymer. Secondly, the behaviours of electrons and holes are different. Experimental

results indicate that negative charge carriers move more quickly in the bulk than positive charge carriers. Thereafter electrons are presumed to travel with a large constant mobility in the simulation while the transport of holes is described by the experimental velocity curve obtained from the observed dynamics of positive charge packets. The current density due to the flow of mobile electrons is described as,

$$J_e = \mu_e n_e E \tag{4-1}$$

Where $\mu_e$ is mobility of mobile electrons; $n_e$ is the concentration of mobile electrons; $E$ is the local electric field.

The current density due to the flow of holes is expressed as,

$$J_h = v_h n_h \tag{4-2}$$

Where $v_h$ is the velocity of holes and it is obtained from experiments; $n_h$ is the concentration of mobile holes.

### *4.3.2 Simulated charge packets in polyethylene*

The experimental *V-E* curve in the low field region from 10 to 70 kVmm$^{-1}$ indicates that the velocity of positive charge carriers starts to decrease at the field around 40 kVmm$^{-1}$ and the velocity continues to decrease at higher fields. Furthermore, positive charge packets are also directly observed in polyethylene without any excitation method when the applied field exceeds 55 kVmm$^{-1}$ and they have lower drifting velocity at increased electric fields. Therefore there must be a close correlation between the reduction of velocity and the phenomenon of charge packets. Two typical field values, 20 kVmm$^{-1}$ in the positive differential region and 50 kVmm$^{-1}$ in the negative differential region, are applied across the polyethylene film with a thickness of 100 μm in the simulation. The dynamics of space charge is modelled using the asymmetric parameters for electrons and holes as detailed in Table 4-1.

Simulated space charge profiles under these two dc electric fields are shown in Figure 4-12. For a dc field of 20 kVmm$^{-1}$, electrons and holes are injected into the bulk of polyethylene and move towards the opposite electrodes. No charge packets are formed. In contrast, a positive charge packet forms at the anode and travels to the cathode for a field of 50 kVmm$^{-1}$. Furthermore, a second broad charge packet is generated at the anode once the first packet is absorbed at the cathode, which

reproduces the repetition of charge packets. This suggests that the decrease of the velocity with electric fields is crucial to the formation of charge packets.

**Table 4-1:** Parameters for the charge packet modelling

| Parameter | Value | Unit |
|---|---|---|
| Barrier height for injection | | |
| $w_{ei}$ (electrons) | 1.15 | eV |
| $w_{hi}$ (holes) | 1.14 | eV |
| Transport of carriers | | |
| $\mu_0$ (for electrons) | $2.5\times10^{-13}$ | $m^2V^{-1}s^{-1}$ |
| *Velocity of holes* | Experimental velocity | |
| Trap density | | |
| $N_{0et}$ (electrons) | 100 | $Cm^{-3}$ |
| $N_{0ht}$ (holes) | 10 | $Cm^{-3}$ |
| Trapping coefficients | | |
| $B_e$ (electrons) | $7\times10^{-3}$ | $s^{-1}$ |
| $B_h$ (holes) | $7\times10^{-5}$ | $s^{-1}$ |
| Recombination coefficients | | |
| $S_0$ trapped electron-trapped hole | $4\times10^{-3}$ | $m^3C^{-1}s^{-1}$ |
| $S_1$ mobile electron-trapped hole | $4\times10^{-3}$ | $m^3C^{-1}s^{-1}$ |
| $S_2$ trapped electron-mobile hole | $4\times10^{-3}$ | $m^3C^{-1}s^{-1}$ |
| $S_3$ mobile electron-mobile hole | 0 | $m^3C^{-1}s^{-1}$ |
| Permittivity of polyethylene | 2.3 | |
| Temperature | 295 | K |

For high electric fields, the dynamics of space charge in polyethylene under a dc field of 100 $kVmm^{-1}$ is modelled using the experimental velocity for positive charge carriers (holes). The simulated space charge profiles are shown in Figure 4-13. It is clearly observed that a large positive charge packet is generated at the anode and it increasingly grows when travelling into the bulk of polyethylene. This agrees with the experimental observation of positive charge packets in low density polyethylene under high electric fields greater than 100 $kVmm^{-1}$ [89]. The increase of the amplitude suggests a lower velocity in front of the charge packet where the field is continuously raised by the charge packet. In other words, the velocity of positive charge carriers (holes) continuously decreases under high electric fields.

The decrease of velocity of positive charge carriers with electric field or the negative differential mobility is confirmed to be important to the formation of positive charge packets in polyethylene by the simulation. However, this is not the only reason. The travelling charge packet also suggests the dominance of mobile charge carriers over the trapped charge carriers in the system, which indicates a low trapping rate in the region where a charge packet occurs. Hence the effect of trapping coefficient on the

formation of charge packets has been examined using the simulation. The simulated charge profiles in polyethylene at dc field of 50 kVmm$^{-1}$ in the case of various trapping coefficients are shown in Figure 4-14. The results show that positive charge packets cannot be formed in the case of a large trapping coefficient greater than $7\times10^{-3}$ for holes. A large trapping coefficient leads to more trapped holes and less mobile holes, which cannot raise significantly the electric field in the bulk of polyethylene and consequently ensure a lower velocity in front of the charge carriers. Therefore the charge packet cannot be observed. This suggests a correlation between the trapping characteristics and the formation of charge packets in polyethylene.

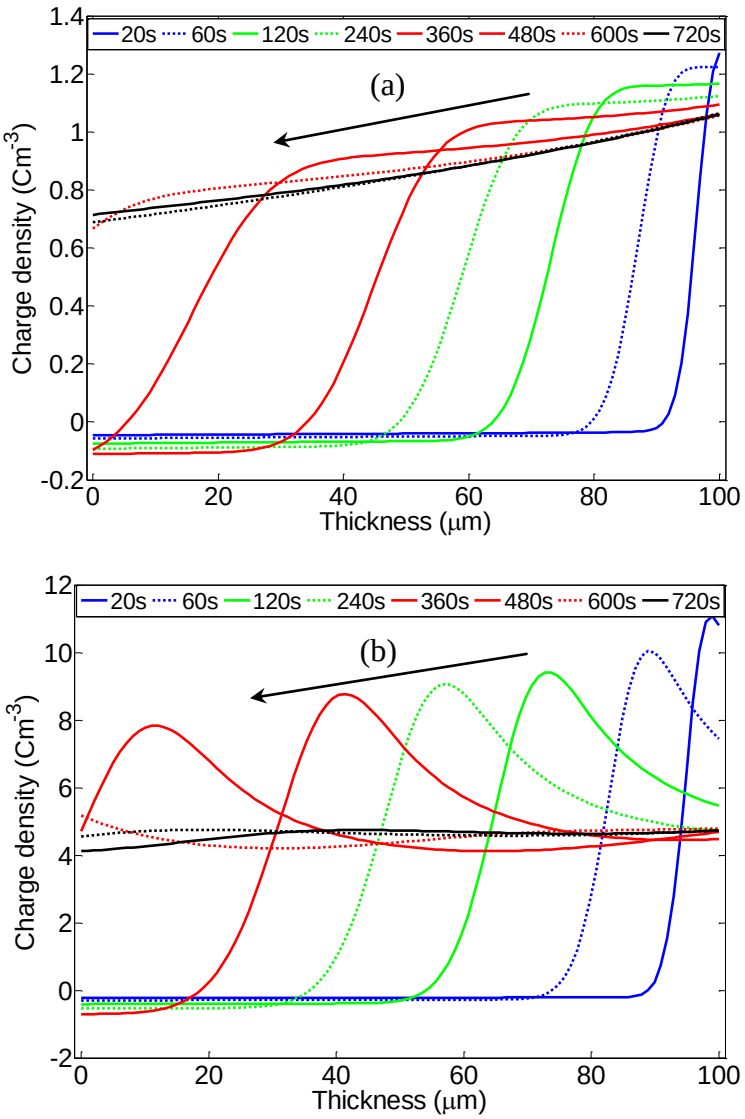


**Figure 4-12:** Simulated space charge profiles in polyethylene at low electric fields: (a) 20 kVmm$^{-1}$; (b) 50 kVmm$^{-1}$.

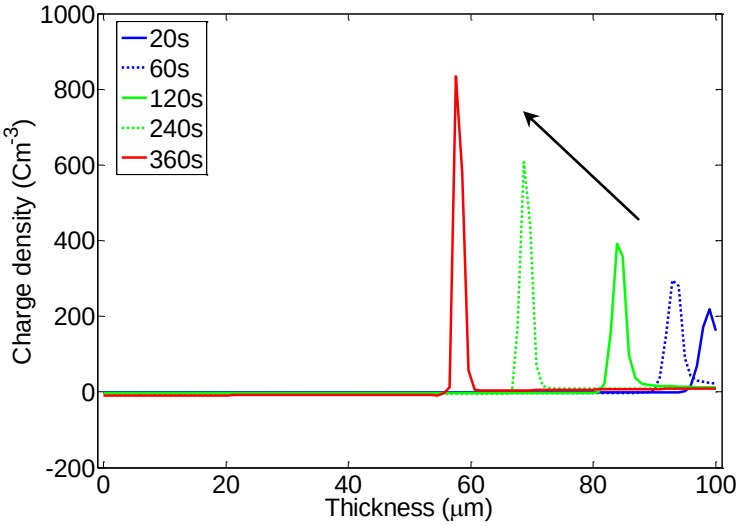


**Figure 4-13:** Simulated space charge profiles in polyethylene at a high electric field of 100 $kVmm^{-1}$

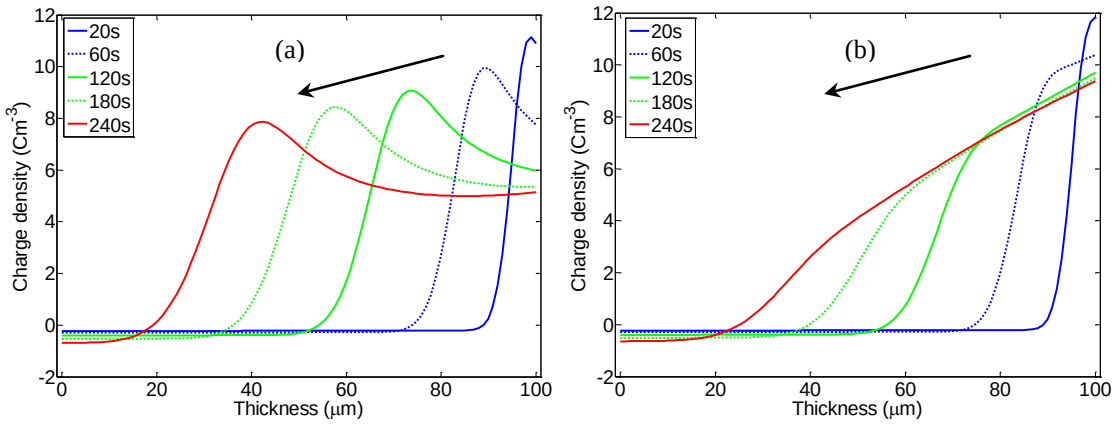


**Figure 4-14:** Simulated pace charge profile at various trapping coefficients under 50 $kVmm^{-1}$: (a) $7\times10^{-4}$; (b) $7\times10^{-3}$.

## 4.4 Discussion

Positive charge packets can only be observed in polyethylene under low electric field conditions with the additional requirement of excitation by a large pulse voltage. But they can be directly observed at high dc electric fields greater than 55 $kVmm^{-1}$ without additional excitation. This suggests that there is a dependence of the appearance of charge packets on the electric field. When further investigating the behaviours of positive charge packets under various electric fields, the occurrence of the charge packets demonstrates a close correlation with the reduction of velocity at increased electric fields. Therefore there must be an effect of the electric field on the

transport of positive charge carriers (holes). The reason why a higher electric field leads to slower transport of holes in polyethylene is not fully understood. A single crystal of polyethylene of lamella thickness has demonstrated high conductance [95]. The overall low mobility of holes is therefore predominantly constrained by holes transfer in the amorphous inter-lamella regions, which introduces more localized trapping energies [96]. The question would be how the electric field affects holes transfer through inter-lamella space. The low trapping coefficient required for generating the charge packets is also related to the electric field. If conduction due to holes transfer is trap-limited, the unfilled trapping centres region in the front of the charge packets would lead to low carriers mobility and the filled trapping centres region in the rear would lead to high mobility and this would be a reasonable hypothesis for the physics behind.

## 4.5 Summary

The dynamics of positive charge packets in polyethylene under dc electric fields has been observed using the pulsed electro-acoustic technique in experiments. The decrease of the velocity of positive charge carriers with electric field and the negative differential mobility have been found in polyethylene. The reduction of velocity has been proved to be crucial to the formation of positive charge packets in polyethylene by numeric simulation when the reduced velocity is introduced into the bipolar charge transport model to simulate the charge packets. A weak trapping dynamics is also found to be necessary for the formation of charge packets, which suggests that the trap-limited holes transport might account for the phenomenon of charge packets.

# Chapter 5 Dynamics of Space Charge under AC Electric Fields

The wide application of insulation materials under ac voltage systems raises a concern of the effect of space charge on the electrical performance and life expectation of the insulators under ac high electric fields. This chapter first reviews the existing research on space charge under ac stresses. Then the experimental investigation of space charge in polyethylene under applied ac sinusoidal voltages measured using a fast pulsed electro-acoustic system is reported. The effects of the applied voltage amplitude, ac frequency and dc offset voltage on the dynamics of space charge are discussed. In addition, the bipolar charge transport model is further developed to simulate the space charge behaviours subjected to ac voltages; the influences of voltage amplitude and ac frequency are discussed as well.

## 5.1 Space charge in polyethylene under ac electric stress

Considerable efforts have been made to examine space charge characteristics in polymeric insulation materials under dc voltages using the pulsed electro-acoustic (PEA) technique while space charge behaviour under ac voltages has not been fully investigated. There are two possible reasons for the limited research on ac space

charge: first, the quite small quantity of charge density (even down to zero at high frequency) under applied ac fields is assumed to be much less problematic than that for an applied dc field [97-99] and hence attracts less research attention; second, the measurement of space charge under ac stress cannot easily be undertaken using the existing measurement equipment as it requires faster data acquisition and accurate synchronization with the ac supply in order to identify the phase related space charge. The accumulation of space charge in the vicinity of electrodes for an applied ac field of 18 $kVmm^{-1}$ at 50 Hz has been observed in XLPE [100]. Charge is also found in LDPE subjected to an applied ac field of 95.6 $kVmm^{-1}$ at a low frequency of 0.2 Hz [49]. Residual charge in LDPE for an applied 50 Hz ac field of 20 $kVmm^{-1}$ has also been reported [48]. These results reveal that ac space charge is closely related to applied frequency and the resultant field. Detailed information about the charge build-up and trapping characteristics cannot be easily determined due to the frequently reversing field and the asymmetric properties of positive and negative charge carriers. Moreover, the combination of capacitive charge, induced charge at the electrodes and space charge in the bulk of polymers inevitably complicate the analysis local to the electrodes. The long term effect of ac voltage on space charge formation in polyethylene has been demonstrated by Chen et al [101]. As a majority of polymeric insulation systems are under ac stresses, it is necessary to understand space charge behaviour under ac electric fields and its influence on long term performance.

### *5.1.1 Measurement system for space charge under ac voltages*

A pulsed electro-acoustic (PEA) system equipped with a fast high voltage pulse generator has been developed in order to acquire the dynamics of space charge in polymers under ac voltages. There are two essential components for the measurement system: a 2 kHz HV pulse generator and a high performance digital signal averager "Eclipse" which has a maximum sampling frequency of 2 $GSs^{-1}$. The 2 kHz HV pulse generator allows detection of space charge under ac voltages with arbitrary waveforms having frequencies up to 100 Hz. The Eclipse signal averager has a large memory which allows capture the details of fast time-varying signals. A schematic diagram of the ac space charge test system is illustrated in Figure 5-1. AC voltage is applied across the polymeric film using a high voltage amplifier; the fast HV pulse generator is used to stimulate charge layers in the polymer and trigger the Eclipse signal averager simultaneously. The output of PEA setup is acquired by Eclipse and stored in its

memory then transferred into a PC for subsequent processing. In the current system, the Eclipse is not required to be synchronized with ac voltage sources, a data processing program has been developed to distinguish the phase resolved PEA signals and resultant space charge profiles at specific phase angles in a voltage cycle.

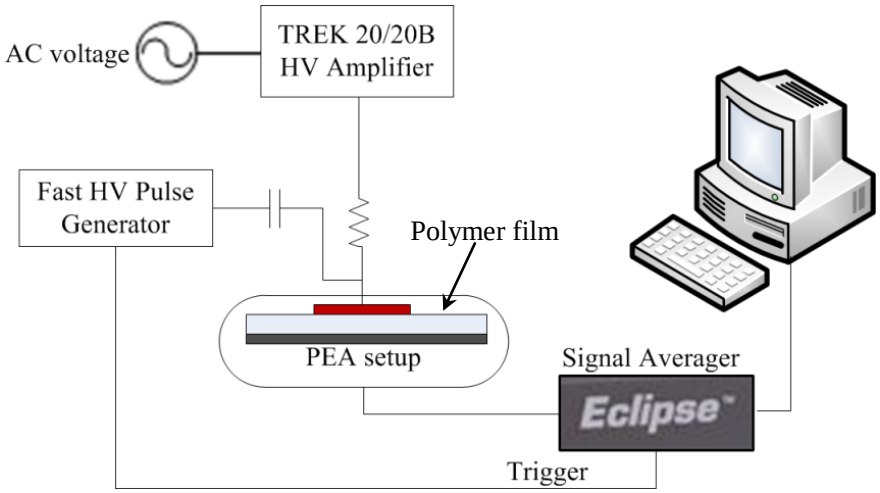


**Figure 5-1:** Schematic diagram of ac space charge measurement system

The measured signal is stored in a binary file which contains large amounts of data series. A user-defined program has been developed to readout these data series and remove any noise due to the environment. As no synchronization procedure is undertaken, the corresponding phase angle of specific PEA signal in each ac voltage cycle has to be determined. The Hilbert transform is a suitable tool for the analysis of time-varying signals which contains the phase angle information [50]. In practice, the denoised PEA signals in each ac voltage cycle are firstly combined into a matrix. This matrix contains time-varying signals $u(t)$ and it has an Hilbert transform $H\{u(t)\}$ ,

$$H\{u(t)\} = \frac{1}{\pi}\int_{-\infty}^{+\infty}\frac{u(\tau)}{t-\tau}d\tau \tag{5-1}$$

An analytic signal $\psi(t)$ which contains the phase information can be obtained from the Hilbert transform,

$$\psi(t) = u(t) + jH\{u(t)\} \tag{5-2}$$

The phase angle $\varphi(t)$ of the time-varying signal can be calculated as,

$$\phi(t) = \arctan\frac{H\{u(t)\}}{u(t)} \tag{5-3}$$

In experiments, 20 charge profiles are acquired in each ac voltage cycle, which results in a series of phase angles determined every 18°. As no synchronization is

applied with ac voltage, the phase angle of each charge profile relies on the initial phase angle of the first data point. Once the measured PEA signals are denoised and their phase angles are determined, then a deconvolution method is employed to determine the space charge density. The distribution of local electric field in the bulk of polymer film is also evaluated.

### *5.1.2 Space charge under ac voltages*

In experiments, the top electrode in the PEA setup is a semiconducting carbon-loaded polymer (Semicon) which is prepared from carbon-loaded polyethylene pellets by hot pressing at 150 ℃; the bottom electrode is flat Aluminium (Al). The test samples are nominally additive free fresh LDPE films with a thickness of 100 ± 5 μm, supplied by GoodFellow Ltd. All the measurements are undertaken at room temperature.

The space charge measurement is taken immediately on the application of a sinusoidal voltage and at every hour until it has experienced 8 hours of ac stressing. During the polarization process, the ac voltage is switched off and reapplied quickly, which allows a short interval to detect the residual electric charge in polyethylene at the stressing time of every hour. When the sample has been polarized for 8 hours, the voltage is permanently removed and the decay of space charge is recorded. The experimental voltage protocol is shown in Figure 5-2. The polarization period when the voltage is on is called “volts on” while it is referred to as “volts off” otherwise. Space charge measurements have been undertaken for polyethylene samples subjected to ac sinusoidal voltages with various amplitudes and ac frequencies. Space charge distributions at volts on, volts off and during the decay process have been determined.

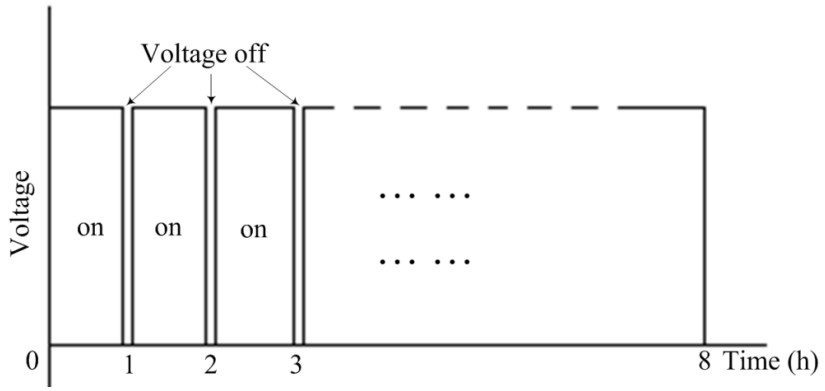


**Figure 5-2:** Experimental voltage protocol for ac space charge measurement

**(1) Charge build up under the volts on condition**

A sinusoidal voltage with a peak value of 3 kV was applied across a 100 μm LDPE film, which results into an r.m.s field of 21.2 $kVmm^{-1}$. Space charge measurements were carried out at frequencies of 0.1 Hz, 1 Hz, 10 Hz and 50 Hz. Space charge results obtained at volts on, volts off conditions and during the decay processes were evaluated. Space charge distributions in LDPE film undergoing 8 hours of ac stressing under peak voltage of 3 kV at the frequency ranging from 0.1 Hz to 50 Hz are shown in Figure 5-3. The figure presents charge profiles at various phase angles in a voltage cycle. It is seen that at a low frequency of 0.1 or 1 Hz, the space charge peaks at the electrodes are narrow and have large amplitudes while they are broad and have small amplitudes at 10 Hz and 50 Hz. This is attributed to the sampling frequency of the acquisition device. The PEA signals are acquired with a sampling frequency of 2 $GSs^{-1}$ at 0.1 and 1 Hz while they are detected with a sampling frequency of 1 $GSs^{-1}$ at 10 and 50 Hz. The results show that charge accumulation in the bulk of polyethylene is around zero compared to the significant amount of charge at the electrodes. This indicates a low level of charge accumulation in polyethylene under ac voltages. The phase angle measurement indicates significant changes to the quantity and the polarity of charge densities at the electrodes rather than in the bulk of the polyethylene. There is no significant influence of bulk charge on the charge densities at the electrodes, which suggests a peak charge density at the electrodes appearing at around 90° and 270° in an ac voltage cycle, corresponding to conditions for peak applied stress.

In order to examine the effect of ac field strength on space charge dynamics, the measurements were repeated for sinusoidal voltages with a peak voltage of 6 kV, which results in an r.m.s field of 42.4 $kVmm^{-1}$. Space charge distributions in polyethylene subjected to 8 hours of ac stressing are shown in Figure 5-4. The peaks at the electrodes are significantly increased. It is noticeable that a small amount of heterocharge is found near the top electrode at a low frequency of 0.1 Hz while this is not observed under a peak voltage of 3 kV. In contrast, no heterocharge is observed at 50 Hz.

The evolution of charge profiles at the phase angle of 90° with stressing time is shown in Figure 5-5 and 5-6. There is no significant change in the charge profiles over the entire stressing time. It is noted that charge profiles under the volts on condition show a slight displacement during the ac stressing period. This is due to ambient

temperature variations which lead to thermal expansion of polyethylene film sample during such a long stressing period.

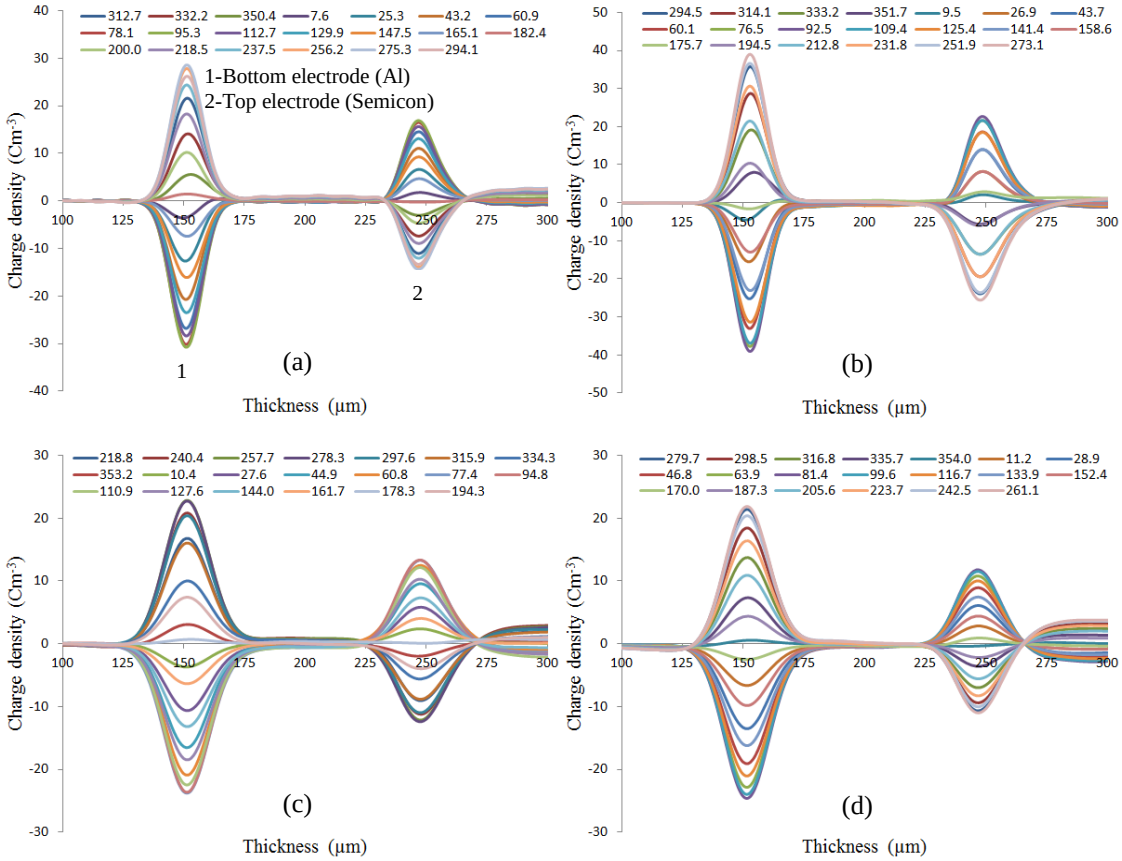


**Figure 5-3:** Space charge profiles in LDPE under ac voltages (3 kV) at 8 hours of stressing: (a) 0.1Hz; (b) 1 Hz; (c) 10 Hz; (d) 50 Hz.

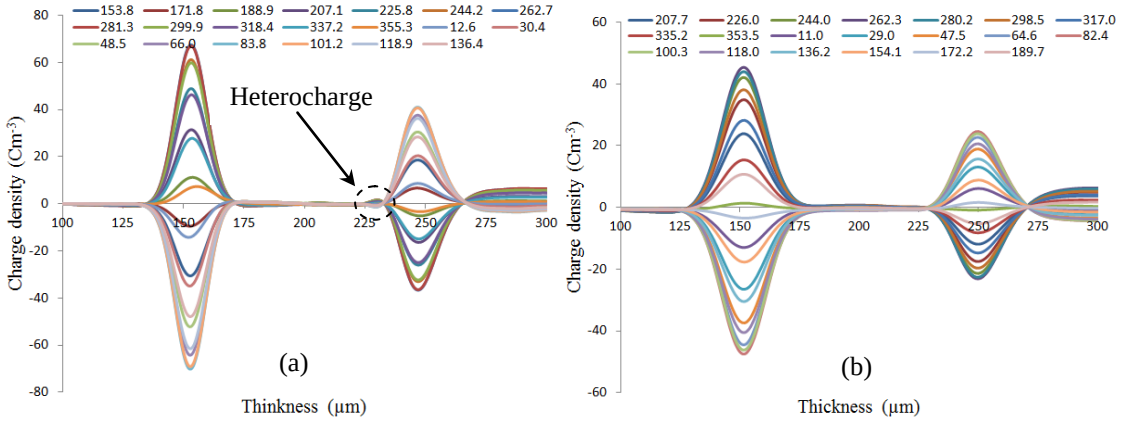


**Figure 5-4:** Space charge profiles in LDPE under ac voltages (6 kV) at 8 hours of stressing: (a) 0.1 Hz; (b) 50 Hz.

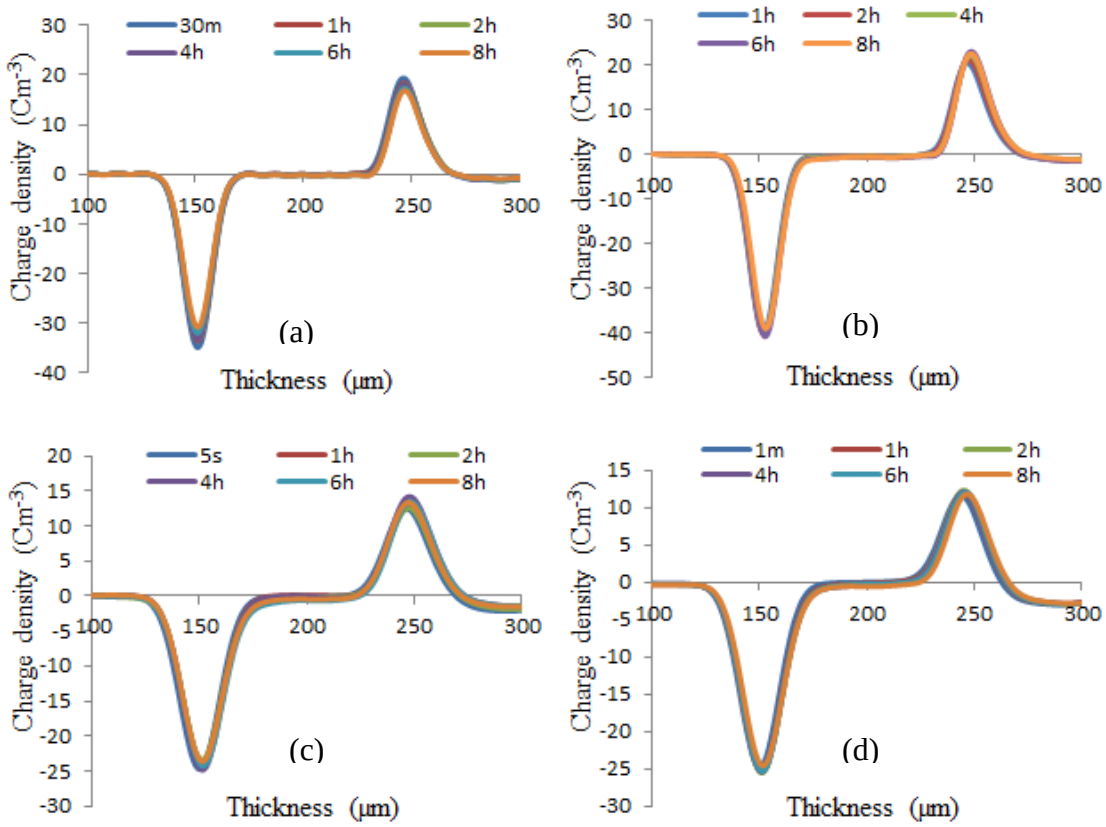


**Figure 5-5:** Evolution of space charge under ac voltages (3 kV): (a) 0.1 Hz; (b) 1 Hz; (c) 10 Hz; (d) 50 Hz.

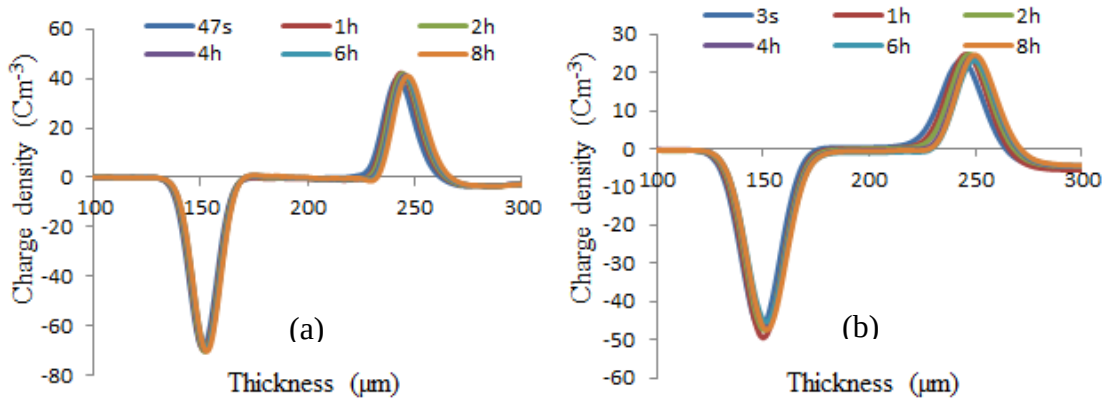


**Figure 5-6:** Evolution of space charge under ac voltages (6 kV): (a) 0.1 Hz; (b) 50 Hz.

### (2) Charge behaviour under the volts off condition

The volts off tests are conducted to further examine the residual charge in the bulk. The charge distribution in polyethylene when the voltage is removed for a short interval every hour is shown in Figure 5-7 and 5-8. For a peak voltage of 3 kV, a small quantity of positive charge is observed at the Al electrode and negative charge near the

semicon electrode at low frequencies between 0.1 Hz and 10 Hz while this does not appear at 50 Hz. The quantity of this charge is significantly increased for a peak voltage of 6 kV, but only negative charge appears at the semicon electrode at 50 Hz. The semicon electrode has been found to produce a lower barrier height for charge carrier injection into polymers [102]. Hence the constantly negative charge near the top electrode may be due to the higher injection efficiency of electrons than holes from the semicon electrode, while the constantly positive charge near the bottom electrode suggests a higher injection efficiency of holes from Aluminium.

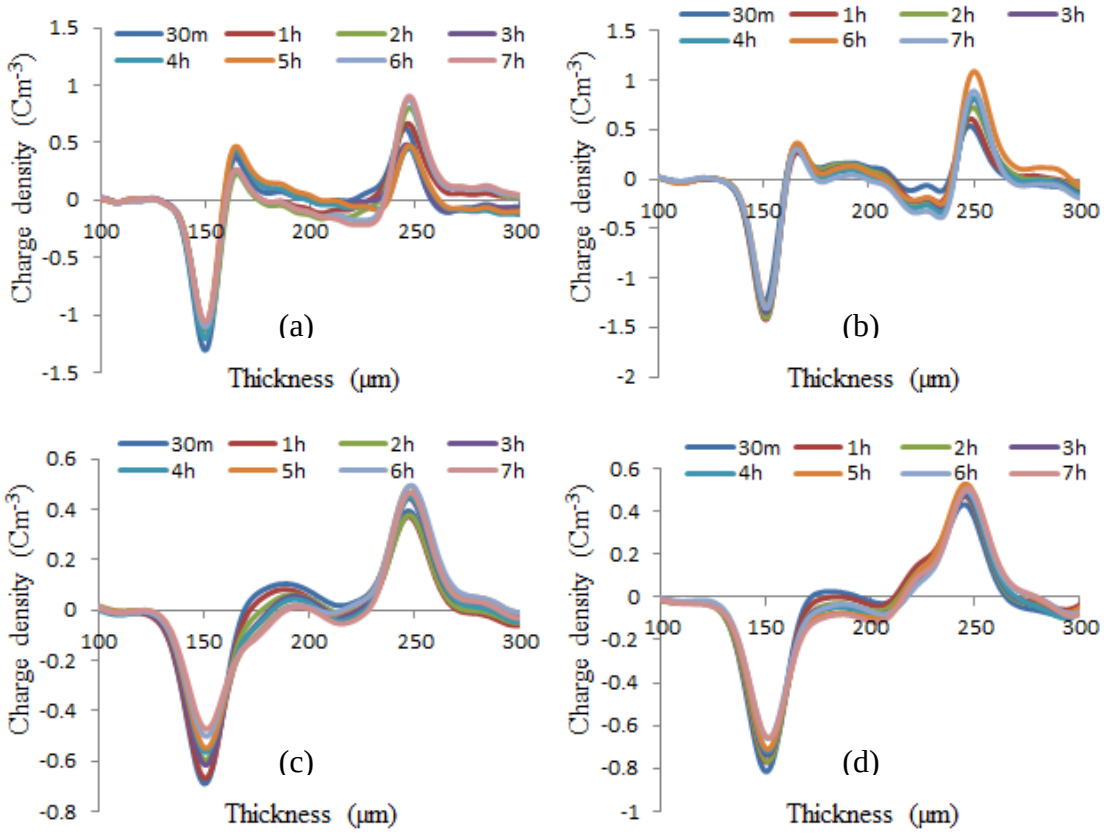


**Figure 5-7:** Space charge profiles in LDPE at volts off condition (3 kV): (a) 0.1 Hz; (b) 1 Hz; (c) 10 Hz; (d) 50 Hz.

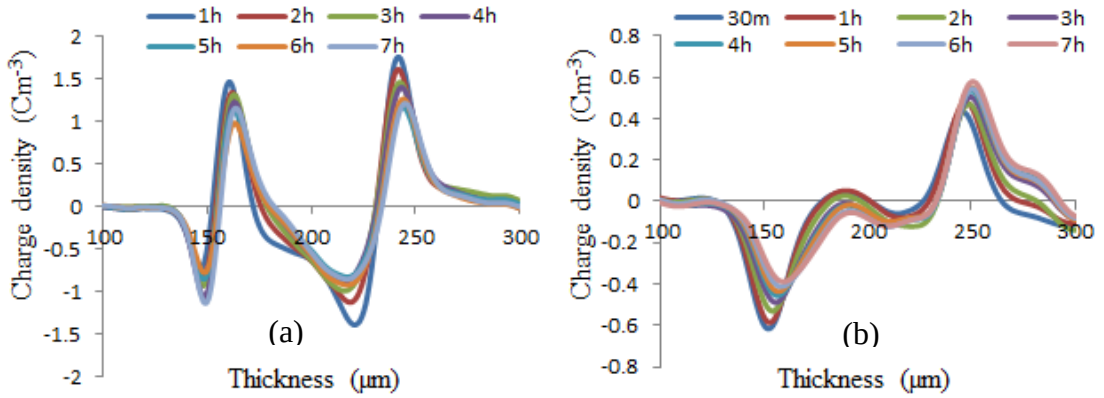


**Figure 5-8:** Space charge profiles in LDPE at volts off condition (6 kV): (a) 0.1 Hz; (b) 50 Hz.

The volts off test gives an indication of space charge which may be trapped in deep trapping sites and cannot escape easily. It cannot present the fast dynamics of charge carriers immediately after removal of the applied voltage. Hence a decay test is undertaken to detect the relaxation of space charge after the voltage is removed. The decay of space charge in polyethylene after 8 hours of ac stressing under a peak voltage of 3 kV and 6 kV are shown in Figure 5-9 and 5-10. After ac stressing at 50 Hz, as less charge is injected into the polymer, its decay appears to be very slow. While for stressing at 0.1 Hz, relatively more charge is injected into the bulk of polymer, the decay is fast over the first minute followed by a subsequent slower decay. The slow relaxation of space charge after ac stressing indicates the influence of ac stressing on the trapping characteristics of electrical charge carriers in polymers and consequently the electrical response of polymeric insulation materials.

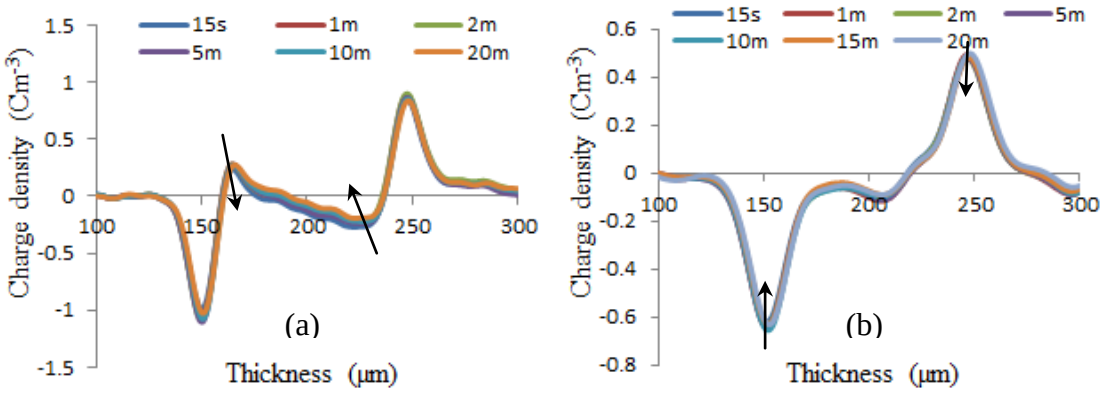


**Figure 5-9:** Decay of space charge in LDPE after 8 hours of ac stressing (3 kV): (a) 0.1 Hz; (b) 50 Hz.

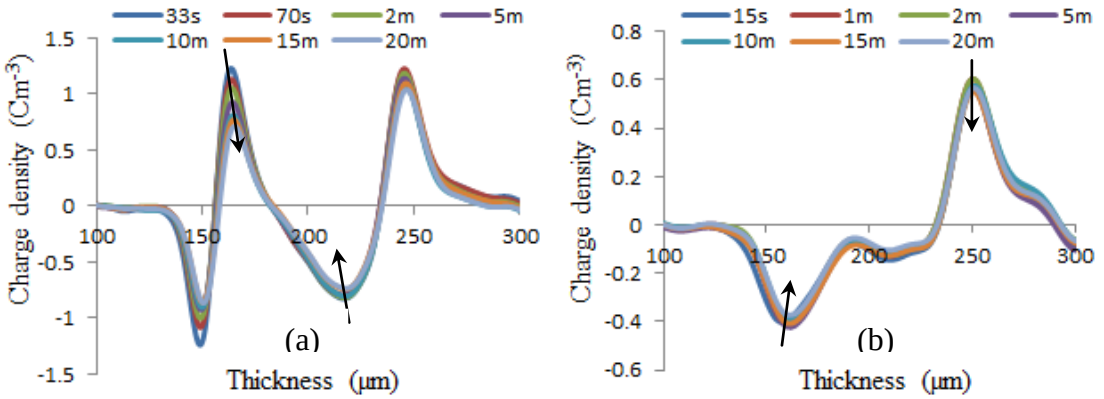


**Figure 5-10:** Decay of space charge in LDPE after 8 hours of ac stressing (6 kV): (a) 0.1 Hz; (b) 50 Hz.

**(3) Space charge under combined ac and dc voltages**

As discussed previously, the quantity of space charge in polyethylene under ac voltages is very small. This leads to slight distortion of electric fields in the polymer, which is less significant than under dc conditions. However, in the situation of an ac voltage with a dc offset involved as in the converter transformers, the behaviour of space charge and its influence on the electrical performance of insulators is not yet known. Therefore an experimental investigation of space charge in polyethylene under combined ac and dc voltages has been undertaken. In the experiment, additive free low density polyethylene films with a thickness of 100 μm are used as test samples. The fast ac space charge measurement system is employed for all tests. A 50 Hz sinusoidal voltage with a dc offset is generated using a signal generator, and then the combined voltage is amplified by the HV amplifier and applied across the polyethylene film mounted in the PEA setup. Space charge measurements are subsequently conducted at a room temperature of around 22℃.

The first task is to examine the effect of combined voltages on the threshold field for space charge in polyethylene at room temperature. Previous research indicates that the threshold for space charge in LDPE is around 10 $kVmm^{-1}$ [29]. But the actual threshold for space charge depends on the dielectric materials, the electrode materials and the temperature. At a room temperature of 22℃, the PEA measurement shows a very small quantity of charge and a slow decay in LDPE film after experiencing an applied dc field of 8 $kVmm^{-1}$ (dc 800 V) for 2 hours as shown in Figure 5-11(a). The residual charge in LDPE at volts off condition after experiencing the applied 50 Hz ac sinusoidal voltage with a peak value of 3 kV for 2 hours is shown in Figure 5-11(b), which also shows a small quantity. Under the combination of the 50 Hz ac voltage of 3 kV and the dc offset of 800 V, the space charge profiles in an ac cycle at 2 hours of stressing is shown in Figure 5-11(c). It shows a distribution of negative charge in the bulk of polyethylene. Once the combined voltages are permanently removed, the decay of charge is recorded and shown in Figure 5-11(d). The negative charge dominates the whole bulk of polyethylene. The quantity of charge in the bulk is much higher (up to 2 $Cm^{-3}$), compared to that found under pure dc or ac voltages. This suggests that the combination of ac and dc voltages may change the threshold for space charge accumulation in polymers.

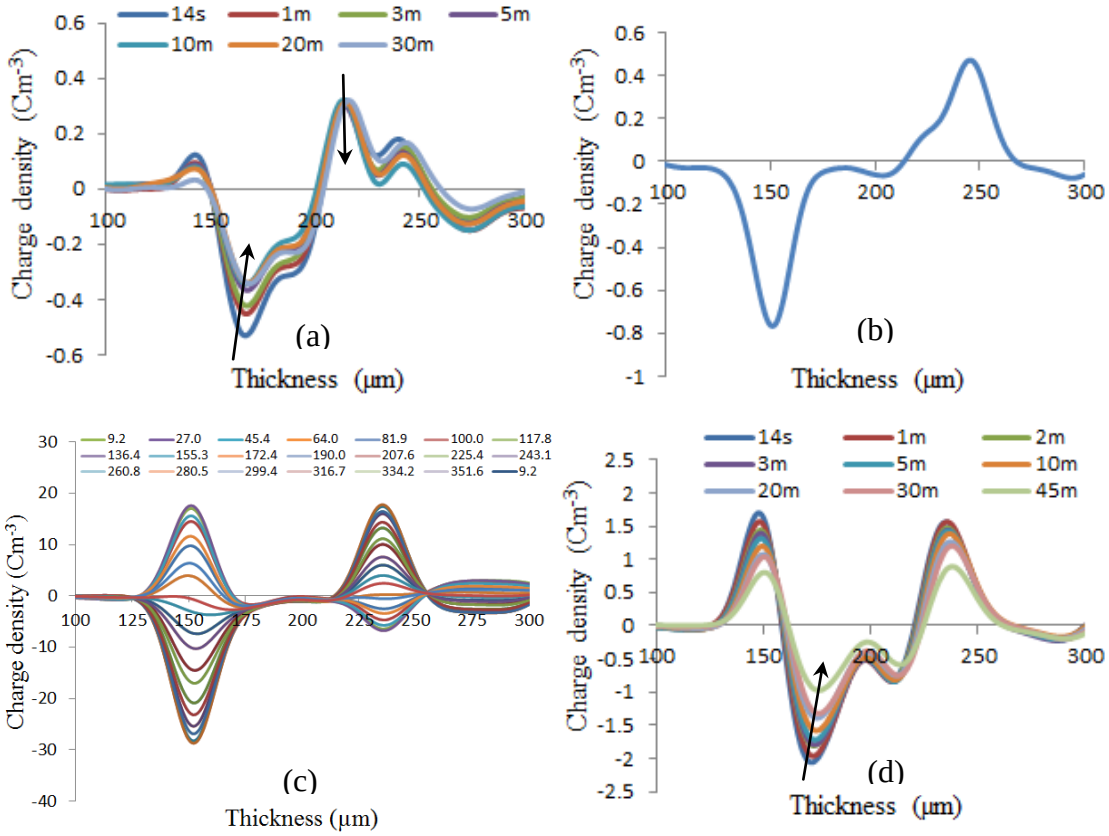


**Figure 5-11:** Space charge profiles in LDPE under various conditions: (a) charge decay after 2 hours of stressing under dc 800 V; (b) volts off charge profile at 2 hours of stressing under 50 Hz ac 3 kV; (c) volts on profiles at 2 hours of stressing under 50 Hz ac 3 kV with a dc offset 800V; (d) charge decay after 2 hours of stressing under combined voltages.

This experiment has been repeated on the 100 μm LDPE films aged by ultraviolet irradiation for 17 days. The decay of space charge in aged LDPE after 2 hours of stressing under a dc field of 8 kVmm$^{-1}$ (dc 800 V) is shown in Figure 5-12(a). Both positive and negative charges exist in the bulk. The quantity of charge density is much larger than that in the virgin polyethylene, which indicates that the space charge threshold could be lowered due to the aging process. Actually a pure 50 Hz sinusoidal voltage of 3 kV can only raise a small quantity of 0.1 Cm$^{-3}$ in the bulk of aged LDPE film. For the combination of the 50 Hz ac voltage of 3 kV and a dc voltage of 800 V, the decay of space charge in the aged polyethylene after 2 hours of stressing is shown in Figure 5-12(b). It shows that the quantity of charge density has been increased to the maximum of 2.5 Cm$^{-3}$. This increase is consistent with the experimental observation in the virgin polyethylene.

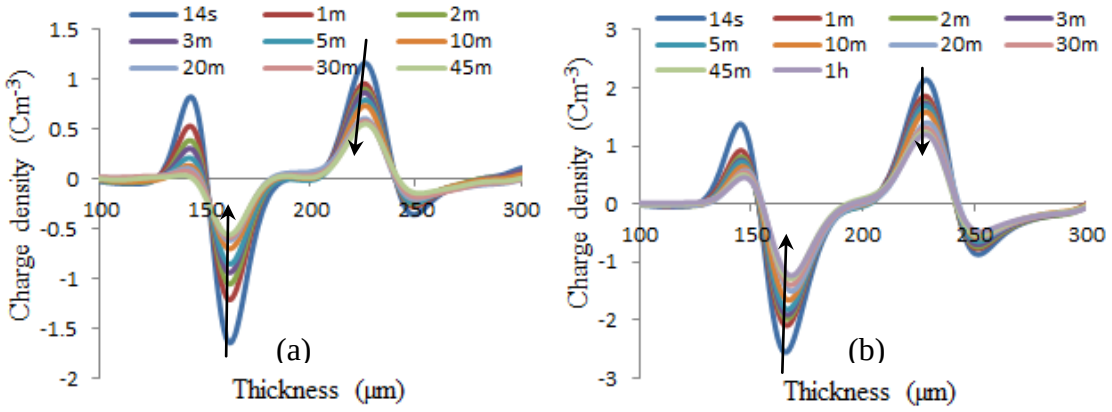


**Figure 5-12:** Decay of space charge in UV aged LDPE after experiencing the electric stressing of 2 hours: (a) pure dc 800 V; (b) combined 50 Hz ac 3 kV and dc 800 V.

A dc voltage of 2 kV has been combined with a 50 Hz ac sinusoidal voltage with various peak values and applied across the 100 μm virgin LDPE films. Space charge measurements are then undertaken and the relaxation of charge in polyethylene after 2 hours of stressing under the combined voltages is shown in Figure 5-13. The quantity of charge and its decay after the stressing under the combined dc 2 kV and ac 1 kV voltage are almost the same as that stressed under a pure dc voltage of 2 kV as shown in Figure 5-13(a-1) and (b-1). When the ac voltage peak is increased to 2 kV, the quantity of charge is slightly reduced by 0.5 $Cm^{-3}$ as shown in Figure 5-13(c-1). For a higher peak voltage of 3 kV, the charge density in polyethylene has been increased to a maximum of 3 $Cm^{-3}$ as shown in Figure 5-13(d-1). The quantity of charge goes to a value of 6 $Cm^{-3}$ at the peak voltage of 4 kV as shown in Figure 5-13(e-1).

The amount of total charge in polyethylene is calculated by integrating the absolute value of net charge, positive charge and negative charge over the thickness of polyethylene film (between the positions of electrodes) as described below.

$$Q = \int_0^d |\rho| S dx \tag{5-4}$$

Where $\rho$ is the charge density; $S$ is the area of the interface of polymer/electrode; $dx$ is the spatial resolution of output signal and $d$ is the thickness of the specimen.

The decay of the total charge, positive charge and negative charge is shown in Figure 5-13 as well. The quantity of charge at the beginning of the decay shows no big change when the peak of ac voltage is less than 2 kV; while the total charge increases greatly once the peak of ac voltage exceeds 2 kV compared with the amount of total charge in polyethylene stressed under the pure dc voltage of 2 kV.

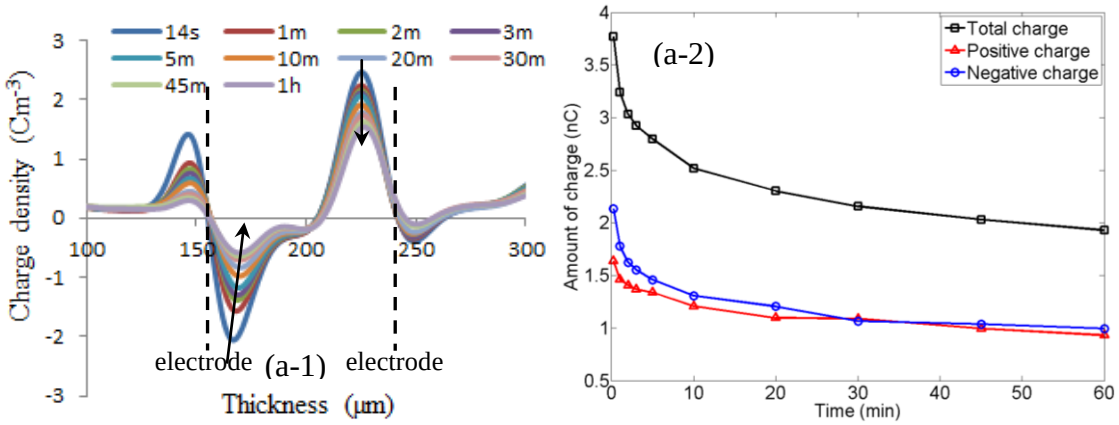
14s
1m
2m
3m
5m
10m
20m
30m
45m
1h
Charge density (Cm-3)
electrode
(a-1)
electrode
Thickness (μm)
(a-2)
Total charge
Positive charge
Negative charge
Amount of charge (nC)
Time (min)

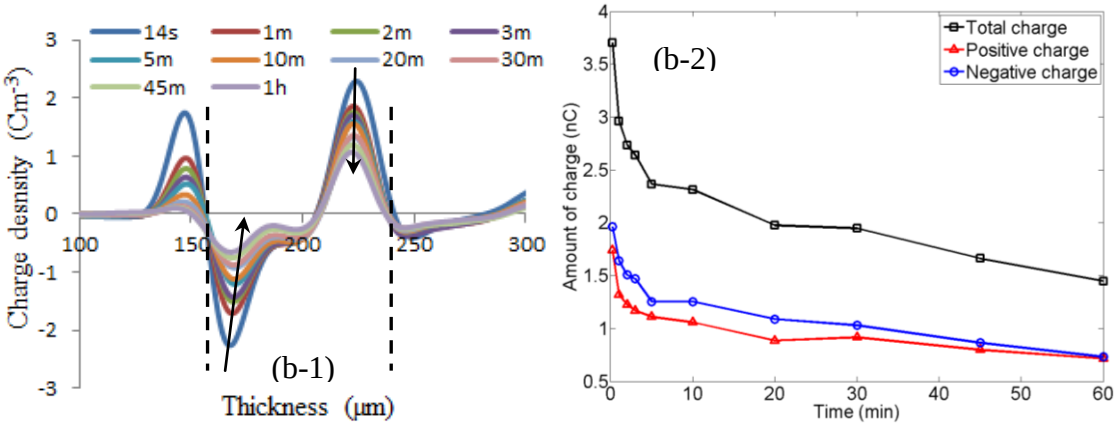
14s
1m
2m
3m
5m
10m
20m
30m
45m
1h
Charge desnsity (Cm-3)
(b-1)
Thickness (μm)
(b-2)
Total charge
Positive charge
Negative charge
Amount of charge (nC)
Time (min)

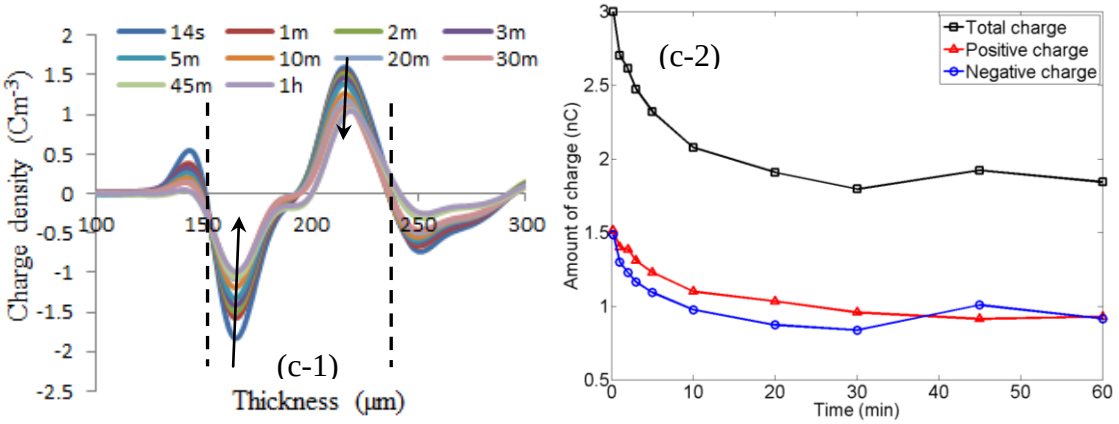
14s
1m
2m
3m
5m
10m
20m
30m
45m
1h
Charge density (Cm-3)
(c-1)
Thickness (μm)
(c-2)
Total charge
Positive charge
Negative charge
Amount of charge (nC)
Time (min)

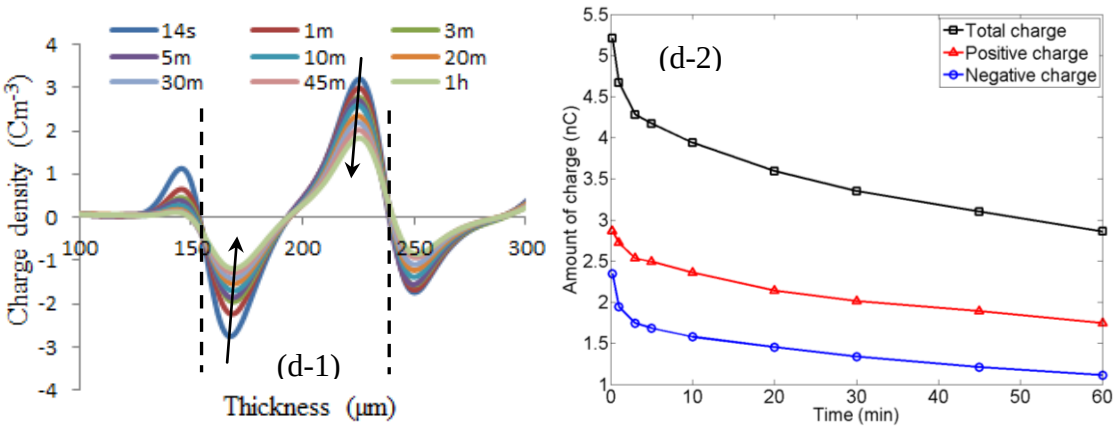
14s
1m
3m
5m
10m
20m
30m
45m
1h
Charge density (Cm-3)
(d-1)
Thickness (μm)
(d-2)
Total charge
Positive charge
Negative charge
Amount of charge (nC)
Time (min)

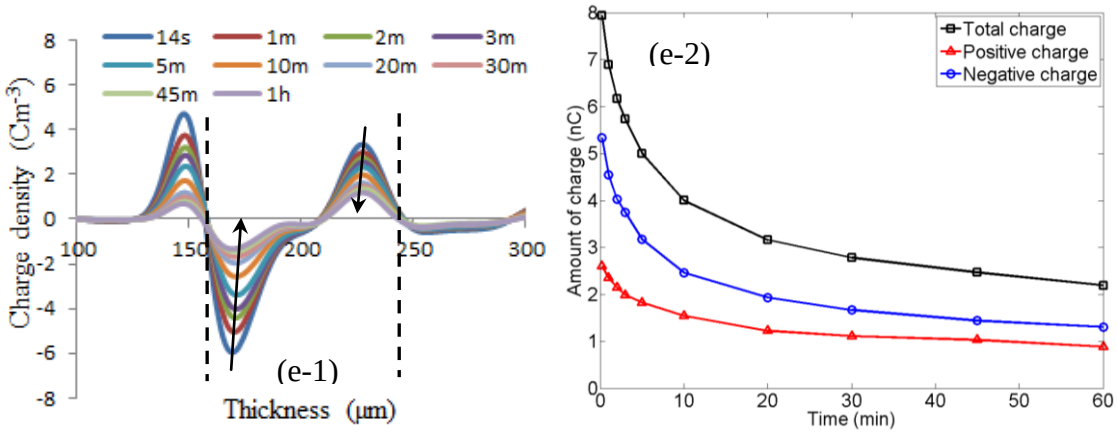


**Figure 5-13:** Charge decay after 2 hours of stressing under various combined voltages: (a-1) dc 2 kV; (b-1) dc 2 kV + ac 1 kV; (c-1) dc 2 kV + ac 2 kV; (d-1) dc 2 kV + ac 3 kV; (e-1) dc 2 kV + ac 4 kV; (a-2),(b-2),(c-2),(d-2),(e-2) corresponding decay of total amount of charge.

## 5.2 Modelling of space charge under ac electric stress

Compared with the experiments, numerical modelling provides an alternative approach of investigating charge injection and trapping in the bulk of polymers without considering any capacitive and image charges especially at the interface of polymer/electrode, which makes the analysis easier. Hence the bipolar charge transport model which is developed to simulate the dynamics of space charge under dc conditions has been improved further to facilitate the simulation of space charge in polyethylene under variable frequency and amplitude ac fields.

### *5.2.1 Model description*

A polyethylene film of 100 μm thick is subjected to an ac sinusoidal voltage in the simulation. The applied voltage $V$ is described as,

$$V = V_p \sin(2\pi ft) \tag{5-5}$$

Where $V_p$ is the peak voltage; $f$ is the ac frequency; $t$ is the stressing time.

The symmetric parameters for electrons and holes are employed in the simulation of space charge under ac voltages for a simplified analysis. These parameters are given in Table 5-1. The transport of electrons and holes is described by power-law mobility. Firstly a dc voltage $V_d$=3.54 kV is set to be a reference voltage compared with an equal r.m.s value of a sinusoidal voltage which has a peak value of $V_p$=5 kV. Space charge

within a polyethylene film of 100 μm under a dc voltage of 3.54 kV is simulated using the same parameters. The simulated evolution of space charge is shown in Figure 5-14.

**Table 5-1:** Parameters for ac space charge modelling

| Parameter | Value | Unit |
|---|---|---|
| Barrier height for injection | | |
| $w_{ei}$ (electrons) | 1.1 | eV |
| $w_{hi}$ (holes) | 1.1 | eV |
| Power law mobility | | |
| $\mu_0$ | $4.5\times10^{-16}$ | $m^2V^{-1}s^{-1}$ |
| $n$ | 1.165 | |
| Trap density | | |
| $N_{0et}$ (electrons) | 100 | $Cm^{-3}$ |
| $N_{0ht}$ (holes) | 100 | $Cm^{-3}$ |
| Trapping coefficients | | |
| $B_e$ (electrons) | $7\times10^{-3}$ | $s^{-1}$ |
| $B_h$ (holes) | $7\times10^{-3}$ | $s^{-1}$ |
| Recombination coefficients | | |
| $S_0$ trapped electron-trapped hole | $4\times10^{-3}$ | $m^3C^{-1}s^{-1}$ |
| $S_1$ mobile electron-trapped hole | $4\times10^{-3}$ | $m^3C^{-1}s^{-1}$ |
| $S_2$ trapped electron-mobile hole | $4\times10^{-3}$ | $m^3C^{-1}s^{-1}$ |
| $S_3$ mobile electron-mobile hole | 0 | $m^3C^{-1}s^{-1}$ |
| Permittivity of polyethylene $\varepsilon_r$ | 2.3 | |

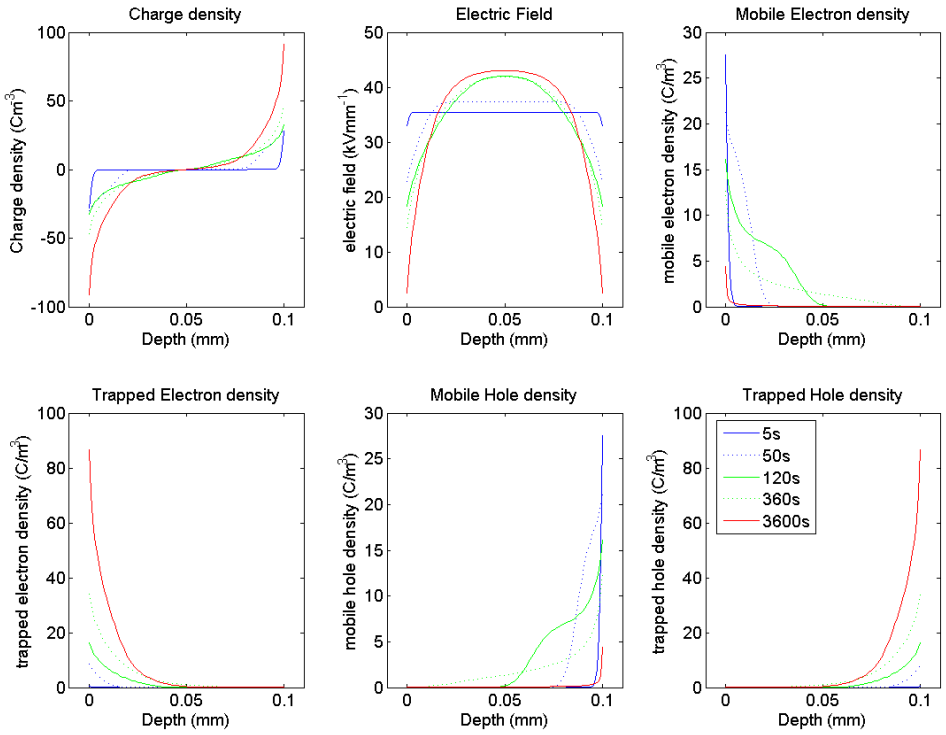


**Figure 5-14:** Simulation of space charge evolution in polyethylene under a dc field of 35.4 $kVmm^{-1}$

### *5.2.2 Simulated space charge under ac voltages*

#### (1) The dependence of space charge on ac frequency

The unique property of ac voltage is the frequently reversing polarity that leads to reversing stress across the sample and considerably affects the charge injection and build-up in dielectrics. The real effect of ac frequency on space charge behaviour needs to be examined. The first task is the simulation of space charge in polyethylene under applied sinusoidal voltage with a peak value of 5 kV at various ac frequencies.

The evolution of space charge in a 100 μm polyethylene film under ac voltage ($V_p$=5 kV) with the frequency ranging from 0.01 Hz to 70 Hz has been simulated. Charge profiles for applied frequencies below 10 Hz are normally determined after simulating the equivalent 3600s stressing while those above 10 Hz are after simulating 600s stressing time as considerable computation is required at higher frequencies. The simulated charge profiles at various phase angles in a voltage cycle are given in Figure 5-15 and 5-16. Space charge mainly accumulates in the vicinity of the electrodes with a quite small quantity in the bulk even after undergoing a stressing time of 3600s. The electric field in the bulk of polyethylene is slightly altered compared to the dc condition shown in Figure 5-14. This suggests that more attention has to be paid to the charge at the interface of polymer/electrode in respect with ageing of polymers under ac stresses. Furthermore, the charge distribution is phase dependent. The maximum charge density does not always appear at 90 ° and 270 ° where the peak of applied field comes. At lower frequencies of 0.01 Hz, the peak density occurs at 90 ° and 270 ° while it shifts to 140 ° and 324 ° for a frequency of 50 Hz. This agrees with the experimental observation by S. S. Bamji et al. [48]. The total amount of charge is also phase related as shown in Figure 5-17. The maximum value occurs at the zero crossing points 0 °, 180 ° and 360 ° while the minimum goes to 90 °, 270 ° of the applied voltage. When the frequency increases, the amount of charge is greatly reduced. The reduction is due to limited charge injection over the very short injection duration at higher frequencies and the alternating injection of opposite charges. It is noticed that heterocharge is formed near the electrodes at 0.01 Hz, which is also observed at 0.1 Hz in experiments described previously. The heterocharge is also observed in XLPE at an ac r.m.s field of 28.7 $kVmm^{-1}$ of 0.02 Hz by X Wang et al. [52].

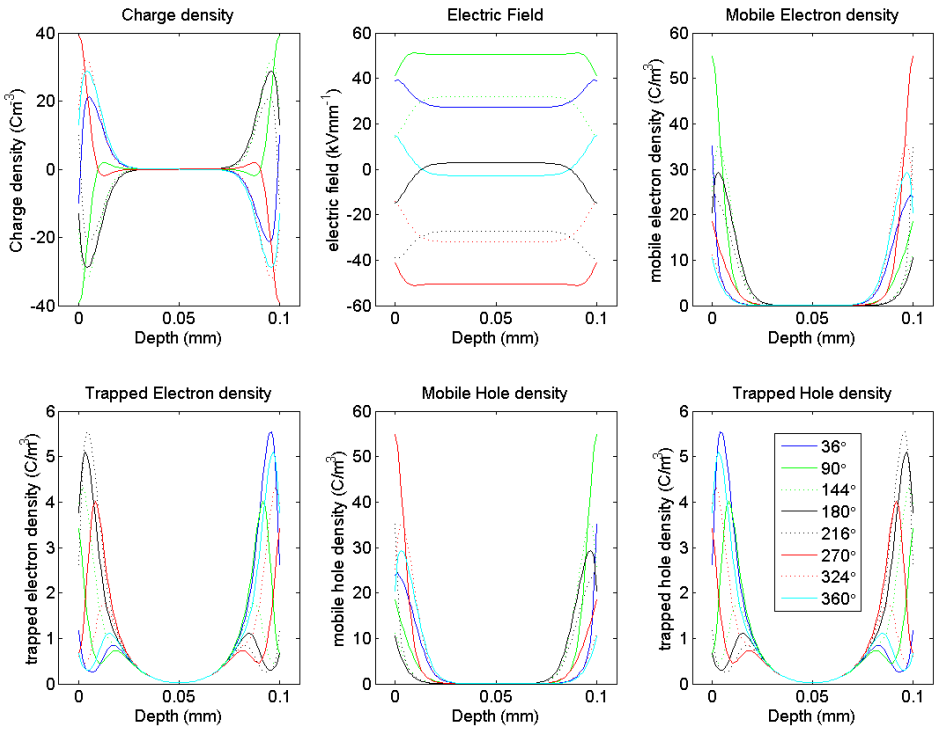


**Figure 5-15:** Simulated space charge in polyethylene per cycle of 5kV 0.01Hz ac voltage

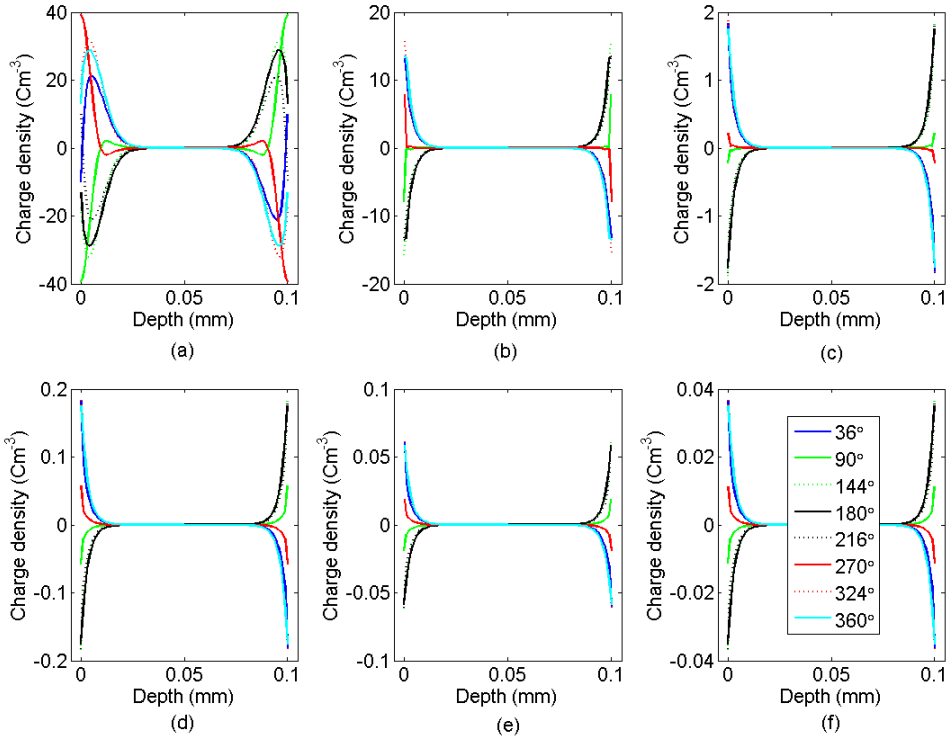


**Figure 5-16:** Simulated space charge in polyethylene per cycle at various frequencies under 5kV ac voltage

(a) 0.01 Hz; (b) 0.1 Hz; (c) 1 Hz; (d) 10 Hz; (e) 30 Hz; (f) 50 Hz.

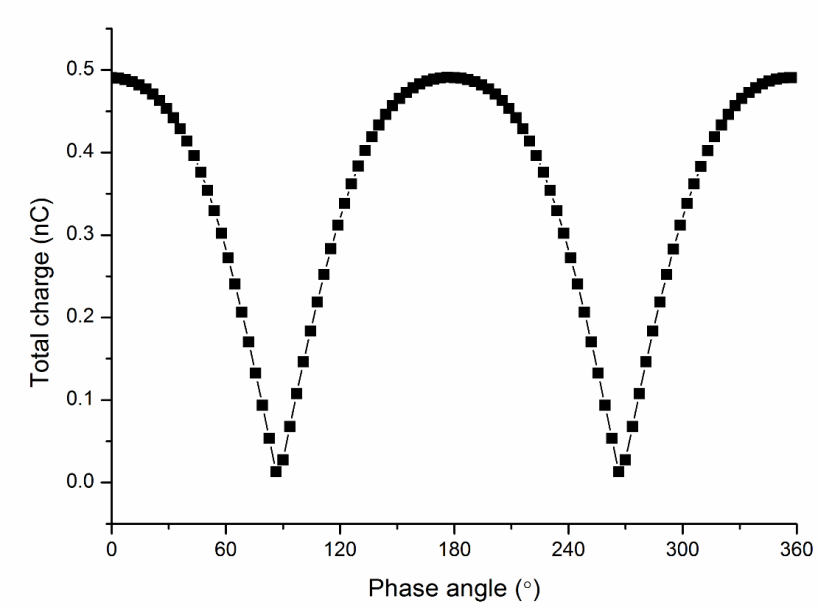


**Figure 5-17:** Total amount of charge per cycle of 5 kV 1 Hz ac voltage

To further investigate the behaviour of space charge, the total amount of net charge, mobile and trapped negative charge (electrons) within the specimen at the stressing time of 3600s are calculated by integrating the charge density over the thickness.

$$Q = \int_V \rho dV = \int_0^d \rho(x) S dx \tag{5-6}$$

Where $\rho$ is the charge density; $d$ is the thickness of specimen; $S$ is the area of interface of electrode/specimen.

The dependence of the amount of charge on the ac frequency is plotted in Figure 5-18(a). The amount of net charge, mobile and trapped electrons decrease rapidly when the frequency increases from 0.01 Hz to 0.1 Hz, followed by a gradual decrease when the frequency is above 0.1 Hz and reduction to zero above 10 Hz. The absolute total charge amount after dc stressing of 3600s at 3.54 kV is around 63.7 nC while the value at an ac voltage with a frequency of 0.01 Hz is less than 30 nC. Even though the quantity of space charge is very low under ac voltages, it can still penetrate into the bulk if undergoing plenty of stressing time. There is a fair quantity of positive/negative charge in the bulk even though the measurable net charge is very low. This is illustrated in Figure 5-18(b) which shows the amount of charge at the end of 36 cycles of ac stressing at different frequencies. Charges can reach the middle of the bulk at 0.01 Hz after an ac stressing time of 3600s. But the penetration depth seems to decrease with

increased frequency as shown in Figure 5-19. The maximum charge density tends to shift from 80 °at 0.01 Hz to 144 °at 50 Hz as shown in Figure 5-20. This is attributed to the limited injection of charge carriers at higher frequency leading to a very slow reversal of the polarity of space charge.

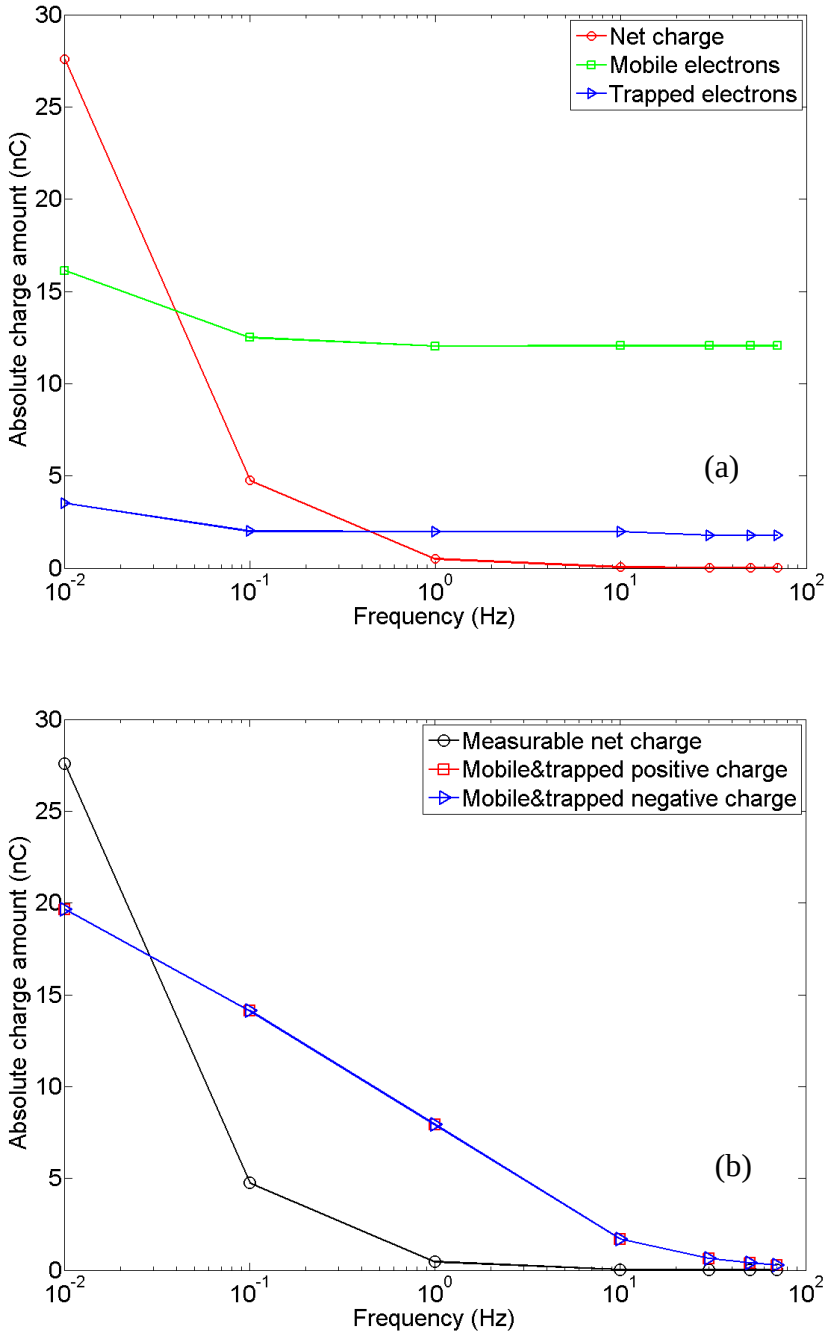


**Figure 5-18:** The dependence of charge amount on ac frequency (5 kV)
(a) amount of charge at the end of ac stressing for 3600s; (b) amount of charge at the end of ac stressing for 36 cycles.

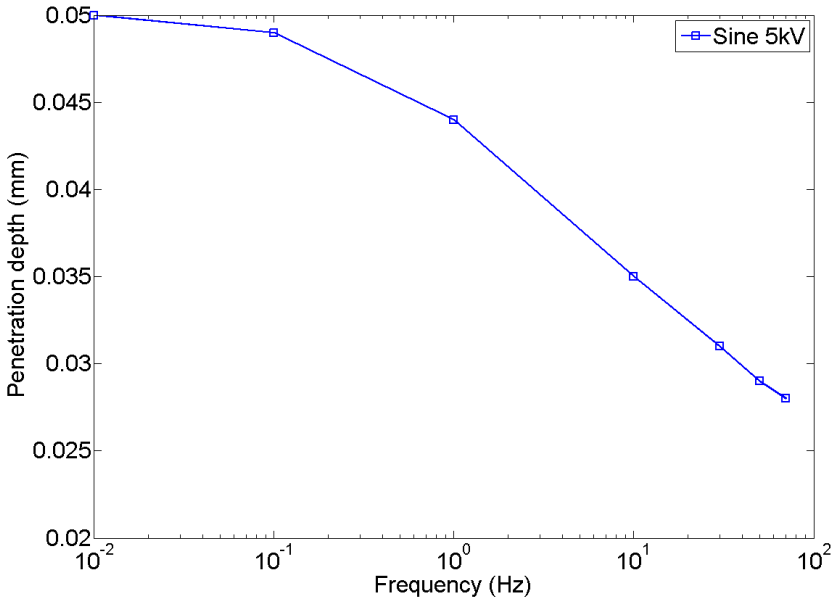


**Figure 5-19:** Penetration depth into the bulk under ac voltage (5 kV) at various frequencies

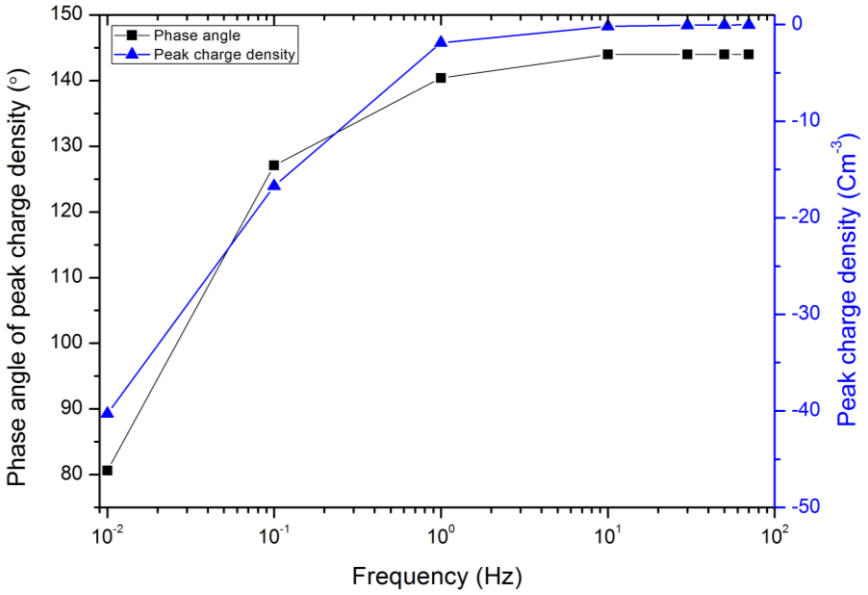


**Figure 5-20:** Peak charge density under ac voltage (5 kV) at various frequencies

### (2) The dependence of space charge on electric field

In addition to frequency, the other concern is the effect of electric field on space charge under ac conditions. Here the frequency is fixed at 10 Hz and 50 Hz while peak voltage is increased from 2 kV to 10 kV resulting in a peak field increasing from 20 $kVmm^{-1}$ to 100 $kVmm^{-1}$. The simulated space charge profiles at the phase angle of 90° in a sinusoidal voltage cycle with a frequency of 10 Hz and 50 Hz and varying electric fields ranging from 20 $kVmm^{-1}$ to 100 $kVmm^{-1}$ are shown in Figure 5-21 and 5-22. It is

seen that the quantity of space charge increases with the applied electric field, and that charge can move further into the bulk even though the quantity of charge is very low at 50 Hz. Mobile charge density is quite larger than the trapped charge density, which might be a result of the small trapping coefficients used in the simulation. Due to less accumulation of space charge at 10 Hz or 50 Hz, the electric field is slightly distorted. The dependence of the amount of total charge at the end of stressing for 600s on the applied electric field is shown in Figure 5-23. The total charge increases with applied field rapidly especially when the field is above 80 kVmm$^{-1}$.

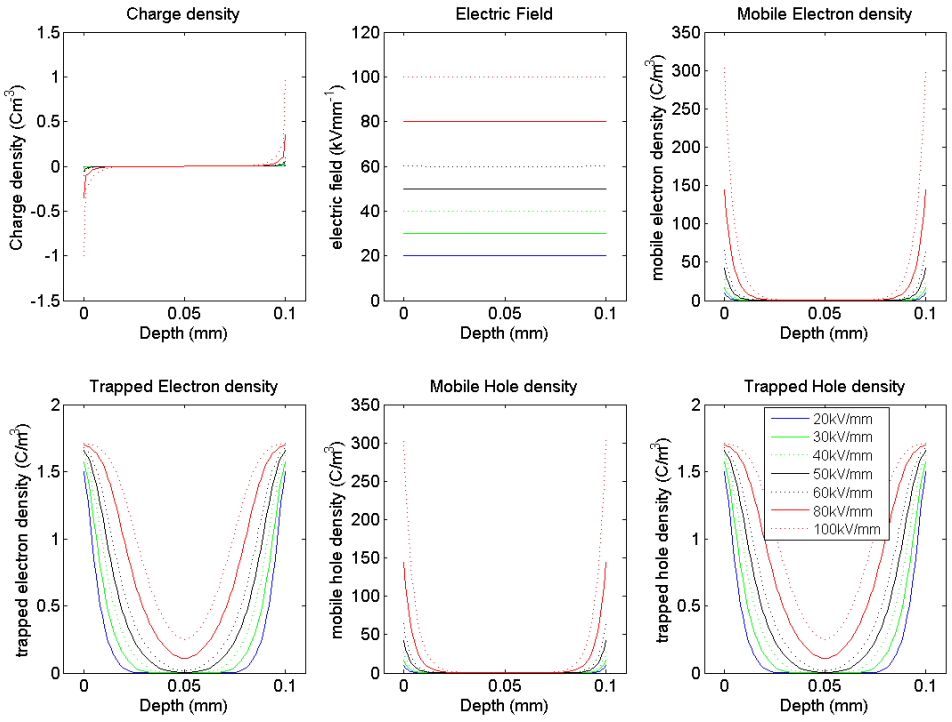


**Figure 5-21:** Space charge profiles at 90 °under various electric fields (10 Hz)

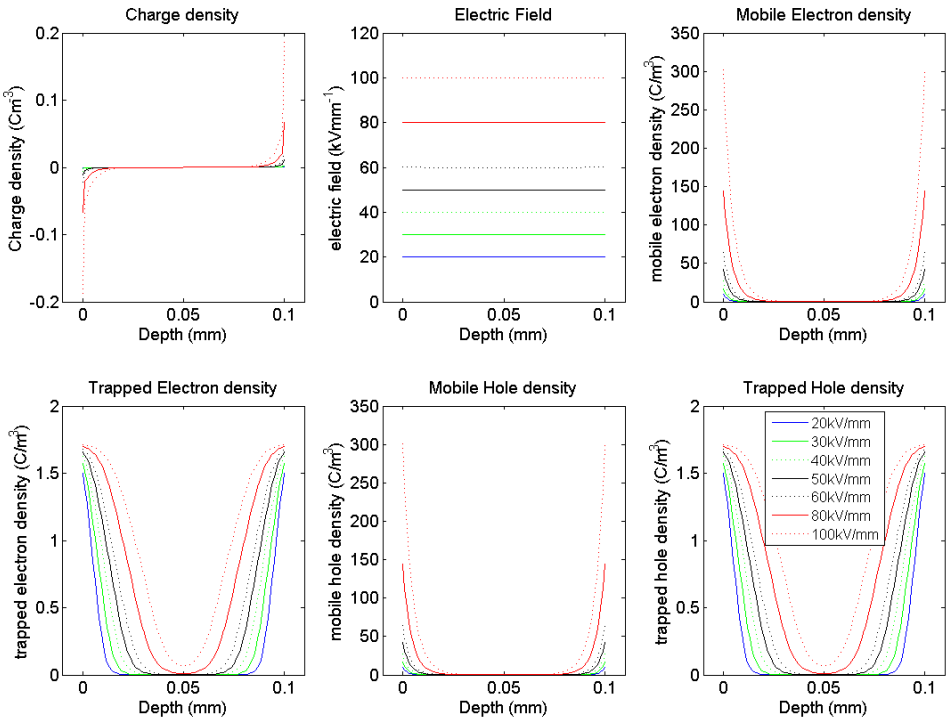


**Figure 5-22:** Space charge profiles at 90 °under various electric fields (50 Hz)

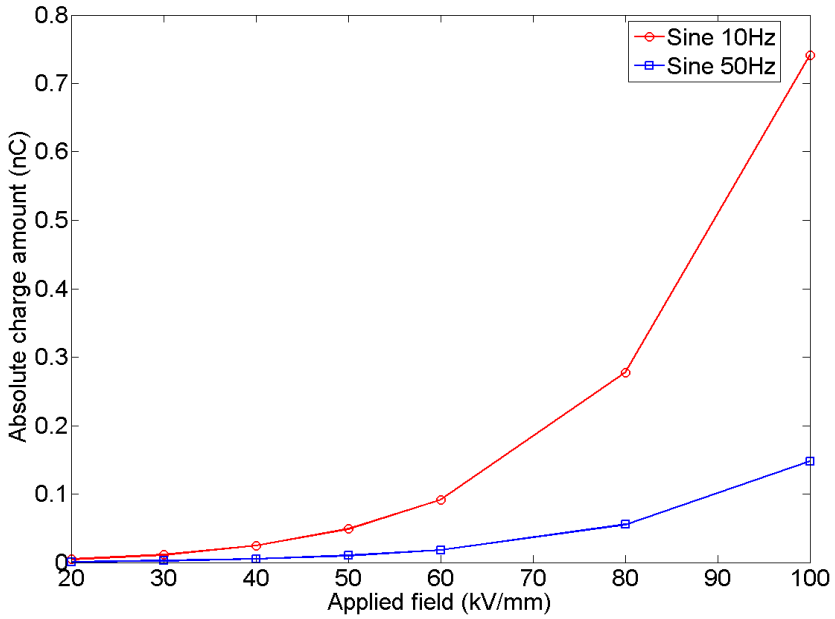


**Figure 5-23:** Total amount of charge vs. applied electric field

### *5.2.3 Current density under ac voltages*

The current density under ac voltages has also been examined using the simulation. The current density per cycle of ac voltage with a peak value of 5 kV at 50 Hz is shown in Figure 5-24(a). It shows that the total current density is a sinusoidal

waveform leading the applied voltage by 90 °, which indicates that the displacement component dominates the total current density. The displacement and conduction current densities are both plotted in Figure 5-24(b). The amplitude of the displacement current density is larger than the conduction current density and shows a 90 ° lead over the ac voltage while the conduction current is synchronized with the ac supply. The pattern of the conduction current is more close to the injection current density at the electrodes. Actually the conduction current density at 0.01 Hz presents peaks prior to 90 ° which is similar to the dissipation current in XLPE under ac fields [103].

When increasing the frequency, the total current density rises linearly with ac frequency as shown in Figure 5-25(a) because of the derivative of the time-dependent electric field. The conduction current density, however, decreases with frequency due to the reduced quantity of mobile charges. The increase of peak voltage, i.e. the applied field also enhances the current density. Total current density increases linearly with applied field as shown in Figure 5-26(a), which is consistent with the dependence of the displacement current on the electric field. However, the conduction current increases nonlinearly and shows a sharp increase when the field is above 80 kVmm$^{-1}$. This suggests a close correlation with the current injection at the electrodes. Actually the log scale of conduction current density as a function of square root of electric field $E^{1/2}$ closely matches with the Schottky law as shown in Figure 5-26(b).

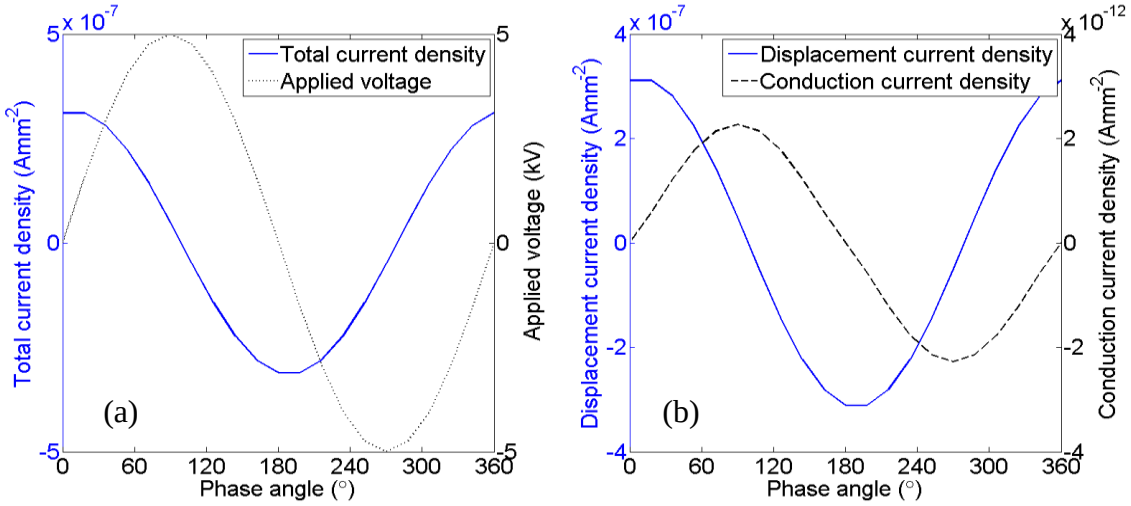


**Figure 5-24:** Current density per cycle of 5kV 50Hz ac voltage

(a) Total current density: (b) Displacement and conduction current density

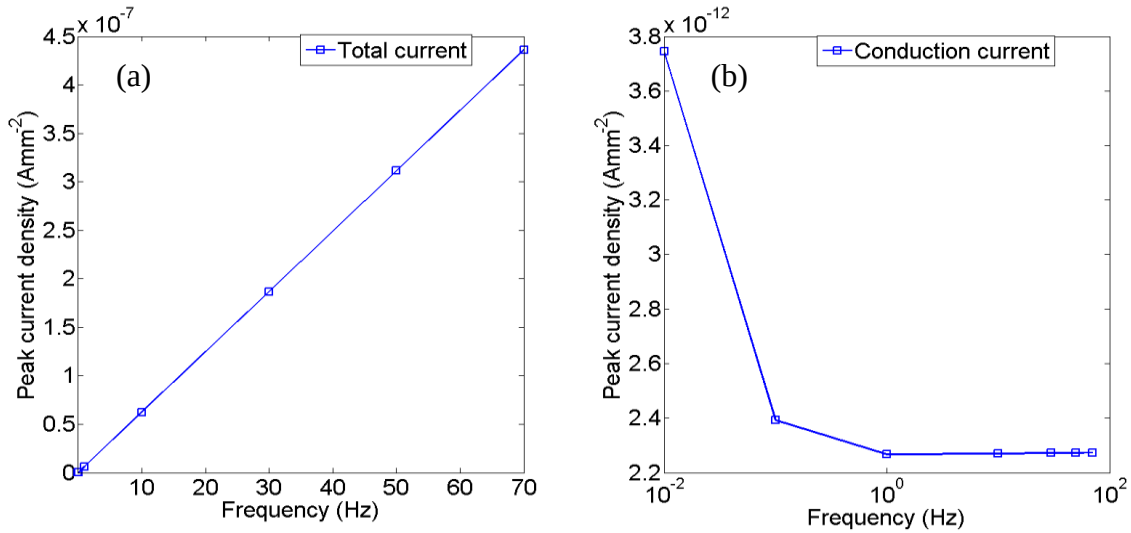


**Figure 5-25:** Current density under ac voltage (5 kV) vs. ac frequency

(a) Total current density: (b) Conduction current density

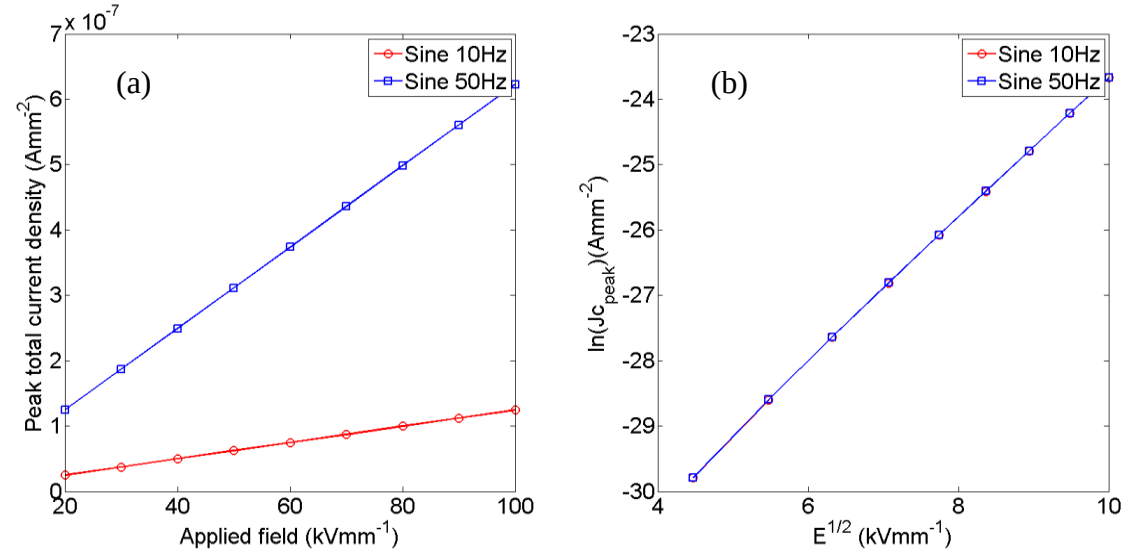


**Figure 5-26:** Peak of current density per cycle of ac voltage vs. applied field

(a) Total current density; (b) Conduction current density

## 5.3 Discussion

The dynamics of space charge in polyethylene under ac voltages has been investigated through experiments and numerical modelling. The experiments and simulation both show low quantities of charge accumulation in the bulk of polyethylene at the power frequency of 50 Hz even for an applied peak field of 60 kVmm$^{-1}$. This indicates a slight electric field distortion in the polymeric insulation under ac conditions. However the presence of heterocharge in the vicinity of electrodes observed

both in experiments and simulation may raise the electric field at the interface of polymer/electrode. Consequently this enhanced electric field at the interface combined with its frequently reserving polarity will lead to the much more recombination of opposite polarity charge carriers and could lead to significant electroluminescence. The enhanced field stress and electroluminescence at the interface may accelerate the ageing of polymeric insulation materials in the region, which may result into the premature failure of the cable insulation. The combination of ac and dc voltages may raise a concern of the effect of space charge on the electrical performance of insulators in the converter transformers as experiments show an obvious enhancement of space charge accumulation in polyethylene under the combined voltages.

On the other hand, the frequently reversing polarity of applied field makes the extraction of charge carriers from the electrodes much easier as charge carriers are not required to travel across the polymer to be extracted from the opposite electrode. This results into less charge carriers injected into the polymer other than intense recombination. Hence the residual charge existing in the polymer might be those deeply trapped charge carriers which cannot easily be detrapped through extraction or recombination processes. The slow relaxation of space charge along with the low quantity of charge accumulation under ac voltages are therefore linked with the charge carriers trapped in deep trapping sites under ac voltages.

The space charge measurement only gives the net charge density across the polymer under ac voltages. However the simulation provides an insight into the individual contribution of mobile and trapped charge carriers during the polarization and the depolarization process. The net charge in the polymeric insulation material may be very low but the density of mobile or trapped charge carriers might be relatively high, which could also affect the electrical performance of polymers under ac stresses. The symmetric parameters of electrons and holes involved in the simulation may not be representative of the practical situation in the polymer. Therefore further investigation into the dynamics of space charge under ac voltages needs to be undertaken considering the unique properties of holes and electrons.

## 5.4 Summary

The behaviour of space charge in polyethylene subjected to ac electric fields has been investigated by experiments. Even though the quantity of space charge is very small under ac conditions, lowering the ac frequency or increasing the applied field can definitely increase the amount of space charge in polyethylene. Charge carriers are able to travel through the polymer after experiencing enough time of ac stressing even at the power frequency of 50 Hz. But care has to be taken for the interfacial effect of space charge in polymers as relative more charge accumulates at the interface of polymer/electrode under ac voltages. The combination of ac and dc voltages has been found to be able to enhance the accumulation of space charge in polyethylene and reduce the threshold. The characteristics of space charge and current densities in polymers under ac stresses has been reproduced and understood using the numeric simulation, the effects of ac frequency and applied field have been revealed as well.

# Chapter 6 Modelling of Electroluminescence in Polymers

The charge dynamics in polyethylene subjected to ac electric fields have revealed that space charge tends to accumulate adjacent to the interface between the electrode and polymers rather than into the bulk of polymers. This highlights the need to study the interfacial effect of space charge under ac stresses. Interfacial behaviour can be observed experimentally by measurement of electroluminescence in polymers. This chapter first summarizes the existing research of electroluminescence in polymers. Then the characteristics of electroluminescence in polyethylene subjected to ac voltages are investigated by numeric simulation using the further developed bipolar charge transport model. The effects of voltage waveform, amplitude and ac frequency as well as physical parameters on the resultant electroluminescence are discussed.

## 6.1 Electroluminescence in polymers

Electroluminescence (EL) is the light emission originated from the energy dissipation process of molecules excited by accelerated electrons or by recombination of opposite polarity charge carriers in dielectrics [104, 105]. This optical emission provides a probe of the degradation process and has been linked with the early aging of

polymers subjected to electric fields [106, 107]. Extensive research has been undertaken to understand the characteristics of EL under dc and ac conditions. Experimental results have shown that EL under dc stresses is closely related to charge transport in insulation materials based on measured *I-V* curves [107]. With the assistance of charge mapping techniques in solid dielectrics, the charge injection, transport and trapping dynamics could be examined more clearly. Hence the investigation into the correlation between EL and space charge has been pursued [108, 109]. EL emission is normally observed in polyethylene at high fields of over 200 $kVmm^{-1}$ in the needle-plane or needle-needle electrode arrangement [110]. However EL at low fields of 15 $kVmm^{-1}$ is also reported in polyethylene sandwiched between two planar electrodes [111], which reveals that the recombination of opposite charge carriers in dielectrics is not the only origin for EL, since the charge injection from a metal into the conduction band or valance band of a polymer at such low fields is practically impossible due to the large potential barrier at the interface of metal/polymer. Therefore a mechanism of EL emission at the metal/polymer interface taking account into the surface states has been proposed [112]. Detailed investigation of EL under dc and ac fields has been implemented by G Teyssedre et al [107]. The EL emission at dc and ac conditions are discussed and the results show that the charge transport process in the bulk of polymer is responsible for the EL emission under dc voltages and the onset field of EL is the threshold for the excitation mechanism of the remarkable conduction current value; while the interfacial effect related to the charge injection determines the EL emission under ac voltages. The onset field of EL under ac conditions is lower than that under dc conditions. The typical phase resolved electroluminescence under ac voltage is shown in Figure 6-1. The dependence of EL on the applied field is given in Figure 6-2.

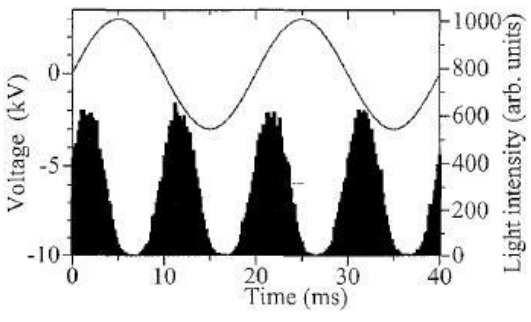


**Figure 6-1:** Electroluminescence in PTFE under ac voltages [112].

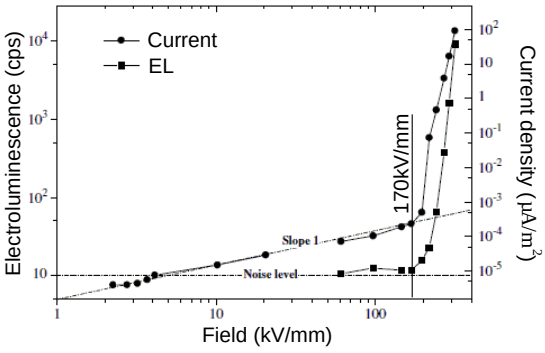


**Figure 6-2:** Current density and EL in PEI vs. field [107].

## 6.2 Numeric model

Electroluminescence is closely related with space charge in terms of the source of charge carriers. Under ac electric fields, the simulation of space charge has shown that charge carriers cannot easily penetrate into the bulk of polyethylene under the effects of charge trapping and frequently reversing of applied field. The injected charge carriers mostly accumulate in the vicinity of the electrodes and they could be neutralized by injected opposite charge carriers when the applied field reverses. The frequently reserving field consequently leads to intense recombination of opposite charge carriers and energy dissipation in the form of light emission, i.e., electroluminescence (EL). A bipolar charge model proposed by Lewin et al. considers that charge carriers are injected and trapped in a micrometre-region near the electrodes which plays a significant role in the resultant light emission process [113]. EL intensity is evaluated from the injection current at the electrodes and trapped charge in the local region without taking into account the charge transport process in the bulk. It presents reasonable electroluminescence results. However, space charge travelling across the polyethylene film under ac voltages has been observed in experiments described previously. Hence the contribution of charge transport along with the charge injection and trapping to the electroluminescence needs to be examined. The bipolar charge transport model has therefore been developed to simulate electroluminescence in polymers under ac voltages.

In the simulation, an ac voltage is applied across a thin film of polyethylene with a thickness of 100 μm, which is the same thickness of additive free low density polyethylene used in the experimental measurement of electroluminescence. The numerical modelling program remains almost the same as that used for simulating space charge under ac stresses. The transport of electrons and holes is described using the power-law mobility. Essential parameters related to the injection of charge carriers, transport of charge carriers, the trapping dynamics and the recombination behaviours are adjusted to achieve reasonable electroluminescence under ac stresses. The electroluminescence created by the recombination of opposite charge carriers under ac stresses is described as,

$$\mathrm{EL} \propto \mathrm{TRR} = S_0 n_{ht} n_{et} + S_1 n_{ht} n_{e\mu} + S_2 n_{et} n_{h\mu} + S_3 n_{h\mu} n_{e\mu} \qquad (6\text{-}1)$$

Where TRR is the total recombination rate of electrons and holes; $S_i$ are the recombination coefficients; $n_{e\mu}$, $n_{et}$, $n_{h\mu}$ and $n_{ht}$ are the density of mobile electrons, trapped electrons, mobile holes and trapped holes respectively. The parameterization in the simulation of electroluminescence in polyethylene under ac voltages is given in Table 6-1. The feature of the parameterization is that relative large injection rate, large trapping density and trapping coefficients are required to supply large amount of charge accumulation in the system for the intense recombination process under ac conditions. This indicates more significantly interfacial effect of space charge under ac conditions than that indicated by the ac space charge modelling. Symmetric parameters for electrons and holes are employed under all types of applied voltages, sinusoidal, triangular and square waveforms.

**Table 6-1:** Parameterization for the EL simulation under ac voltages

| Parameter | Value | Unit |
|---|---|---|
| Barrier height for injection | | |
| $w_{ei}$ (electrons) | 0.87 | eV |
| $w_{hi}$ (holes) | 0.87 | eV |
| Power-law mobility | | |
| $\mu_0$ | $1.5\times10^{-16}$ | $m^2V^{-1}s^{-1}$ |
| $n$ | 1.165 | |
| Trap density | | |
| $N_{0et}$ (electrons) | $2\times10^{4}$ | $Cm^{-3}$ |
| $N_{0ht}$ (holes) | $2\times10^{4}$ | $Cm^{-3}$ |
| Trapping coefficients | | |
| $B_e$ (electrons) | 600 | $s^{-1}$ |
| $B_h$ (holes) | 600 | $s^{-1}$ |
| Recombination coefficients | | |
| $S_0$ trapped electron-trapped hole | 0 | $m^3C^{-1}s^{-1}$ |
| $S_1$ mobile electron-trapped hole | 0.4 | $m^3C^{-1}s^{-1}$ |
| $S_2$ trapped electron-mobile hole | 0.4 | $m^3C^{-1}s^{-1}$ |
| $S_3$ mobile electron-mobile hole | $4\times10^{-3}$ | $m^3C^{-1}s^{-1}$ |

## 6.3 Electroluminescence under an applied ac sinusoidal voltage

The first task is to investigate the electroluminescence due to recombination of bipolar charge carriers in polyethylene on the application of a sinusoidal ac voltage as shown in Figure 6-3. The recombination of opposite polarity charge carriers in polyethylene of 100 μm under sinusoidal voltages of 50 Hz with various peak voltages ranging from 5 kV to 9 kV has been investigated by simulation; and the total recombination rate under sinusoidal voltages with a peak voltage of 6 kV at various frequencies ranging from 10 Hz to 90 Hz have also been considered.

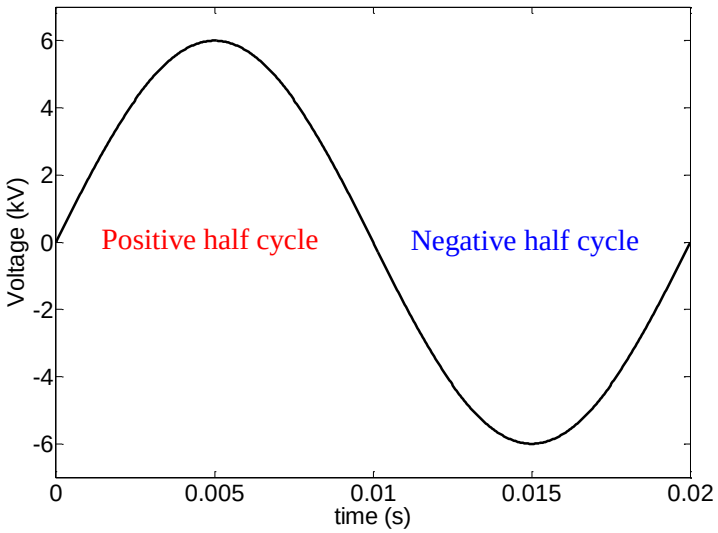


**Figure 6-3:** Applied sinusoidal voltage waveform in the EL simulation

Under an ac applied field, the charge recombination seems to be closely related to charge injection which depends on the field strength at the electrodes. The injection field at the electrodes is shown in Figure 6-4. The electric field at the electrodes has been distorted from a sinusoidal waveform and the peak field comes at an earlier phase angle of 66.2°. The field value is lower than the applied peak field of 60 $kVmm^{-1}$. The reduction is caused by homocharge accumulation in the vicinity of electrodes. On the other hand, there also exists a large amount of heterocharge near the electrodes which otherwise enhances the electric field and leads to phase lead over the applied voltage. Such distorted injection fields accordingly creates a peak of injection current density prior to the voltage peak as shown in Figure 6-5.

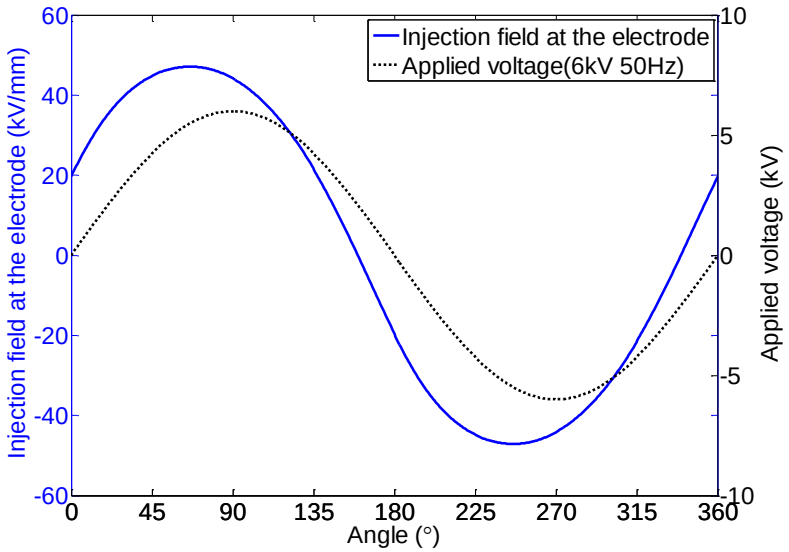


**Figure 6-4:** Injection field per cycle of sinusoidal voltage (6 kV 50 Hz)

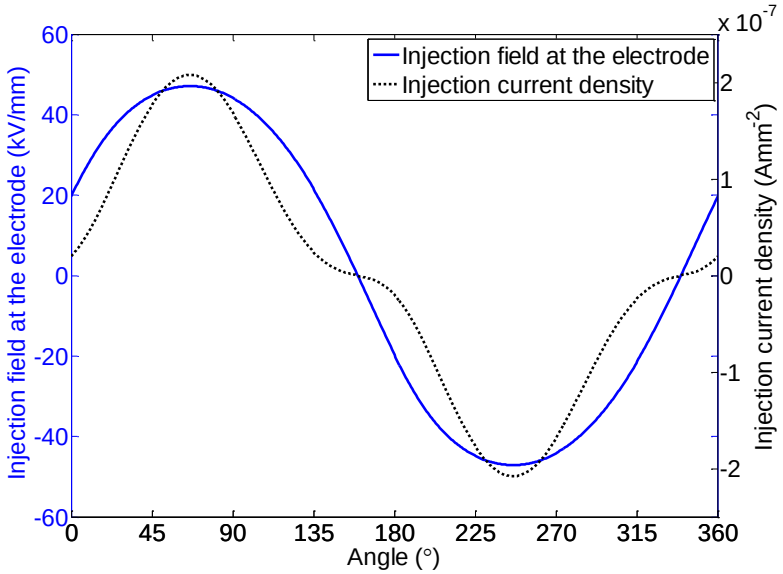


**Figure 6-5:** Injection current density per cycle of sinusoidal voltage (6 kV 50 Hz)

The conduction current density in the bulk of polyethylene has also been investigated as the density of charge carriers is not only related to charge injection at the interface but also to the conduction process in the bulk. The pattern of conduction current density in a voltage cycle resembles the injection current density as shown in Figure 6-6. It also shows a phase lead over the applied voltage. But the conduction current density is in the order of $10^{-13}$ Amm$^{-2}$ much lower than the injection current density of $10^{-7}$ Amm$^{-2}$ due to less mobile charge carriers available in the system.

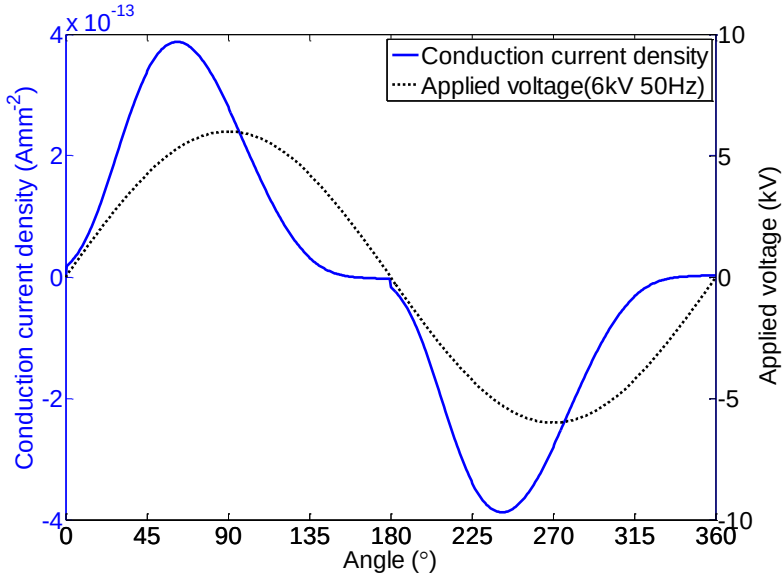


**Figure 6-6:** Conduction current density per cycle of sinusoidal voltage (6 kV 50 Hz)

The total recombination rate (TRR) that represents the electroluminescence (EL) is plotted in Figure 6-7. TRR presents a peak value in the first and third quarter of sinusoidal voltage; they are both prior to the peak voltage in the half cycle. The first peak occurs at 54° leading over the sinusoidal voltage. In the positive half cycle, the increasingly injected holes from the electrode in the first quarter encounter the residual electrons, which lead to the first peak of recombination rate; when the voltage enters into the negative half cycle, the remaining holes will encounter more injected electrons in the third quarter and hence creates the second peak in the negative half cycle.

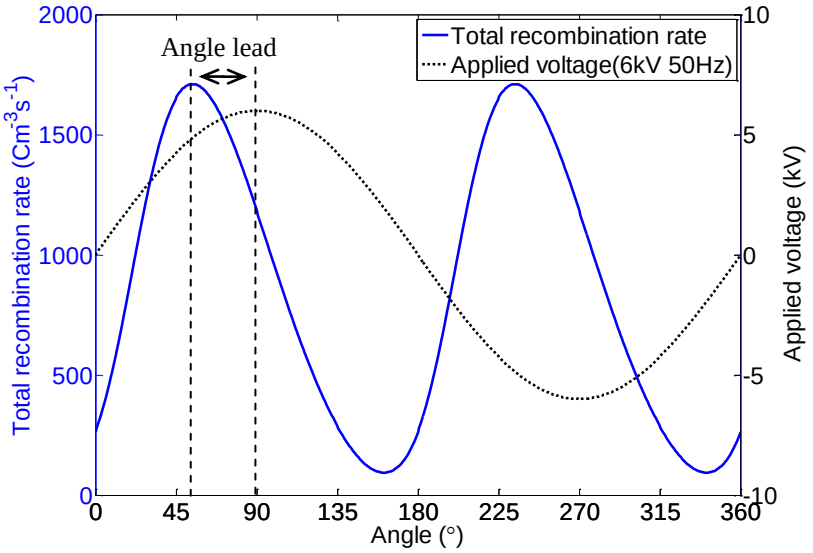


**Figure 6-7:** Total recombination rate per cycle of sinusoidal voltage (6 kV 50 Hz)

The specific contribution of charge carriers to the total recombination rate has also been examined. The densities of mobile/trapped electrons and mobile/trapped holes at the interface of electrode/polymer in a voltage cycle are plotted in Figure 6-8 and Figure 6-9 respectively. Due to the large trapping coefficient of 600, there are much more trapped charge carriers than mobile species in the system. Mobile electrons and trapped holes both demonstrate a maximum density prior to 90˚ in the positive half cycle and hence the recombination between these two species leads to the first peak of TRR. Similarly the maximum density of mobile holes and trapped electrons in the negative half cycle determines the second peak of TRR. The contribution of the recombination between mobile electrons and mobile holes is much less due to the lower density of those two species and the small recombination coefficient for these two. The recombination between trapped electrons and trapped holes is not considered.

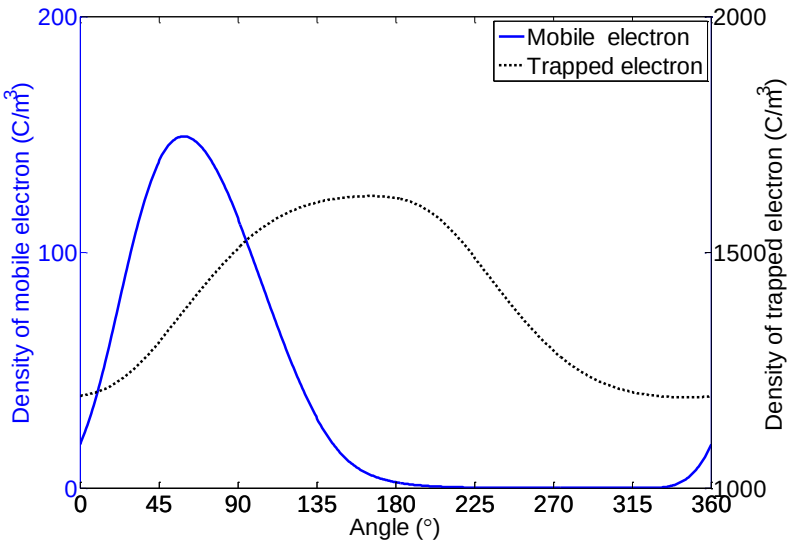


**Figure 6-8:** Density of mobile and trapped electrons per cycle of sinusoidal voltage (6 kV 50 Hz)

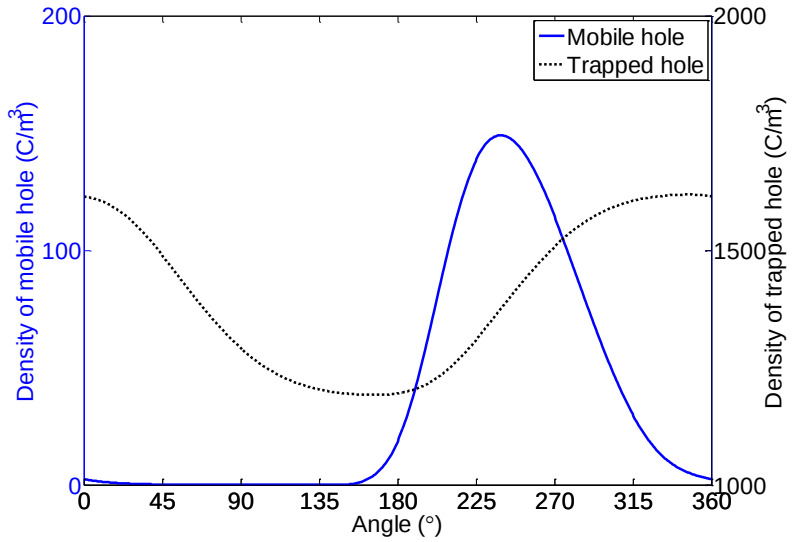


**Figure 6-9:** Density of mobile and trapped holes per cycle of sinusoidal voltage (6 kV 50Hz)

In terms of time dependence, the recombination rate basically presents a transient increase until a saturation level is achieved as shown in Figure 6-10. The saturation level is higher than zero, which is due to the non-zero density of either mobile or trapped charge carriers, leading to a large recombination rate.

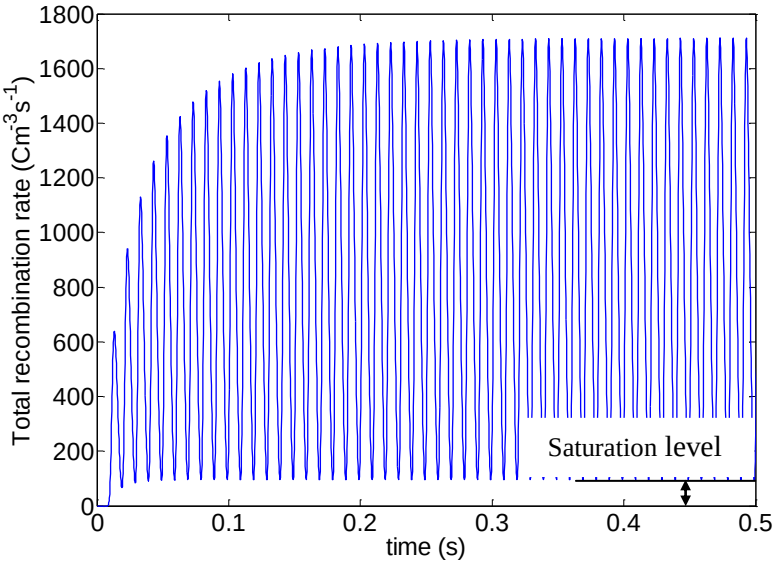


**Figure 6-10:** Evolution of TRR with time under sinusoidal voltage (6 kV 50 Hz)

### *6.3.1 Influence of peak voltage on EL*

The effect of applied voltage on the electroluminescence due to recombination of bipolar charge carriers in polymers has been examined in the simulation. Sinusoidal voltages of 50 Hz with peak voltages ranging from 5 kV to 9 kV are applied across the polyethylene film of 100 μm; the total recombination rate or EL is simulated and the results are shown in Figure 6-11. To simplify the analysis, the saturation level is subtracted from the simulated total recombination rate so that the recombination rate in different conditions can be compared on the same graph. It is seen that TRR rises with the increase of applied voltage, and that higher voltage leads to a larger phase lead over the applied voltage. This is highlighted in Figure 6-12 which shows that the higher the applied voltage is, the earlier the maximum TRR occurs. The peak value of TRR increases linearly with the applied peak voltage as shown in Figure 6-13. A fit of the simulated total recombination rate to the experimental measurement of electroluminescence in polyethylene under a sinusoidal voltage of 50 Hz with the peak value of 6 kV is shown in Figure 6-14. It shows that the simulation reproduces the phase resolved electroluminescence but the simulation presents two identical peaks in a voltage cycle while the experiment shows a reduced second peak in the negative half cycle and the two peaks are not perfectly symmetric. The equal peaks in the simulation are produced by the symmetric parameters for electrons and holes and symmetric charge injection at the electrodes. However, the contact between the polyethylene film and the two electrodes might not be identical in the experiment, which leads to different

characteristics of charge carriers at the interface especially for the barrier height of charge injection. The different properties of the interfaces affect the consequent charge injection and recombination process. Hence there could be an attenuated light emission.

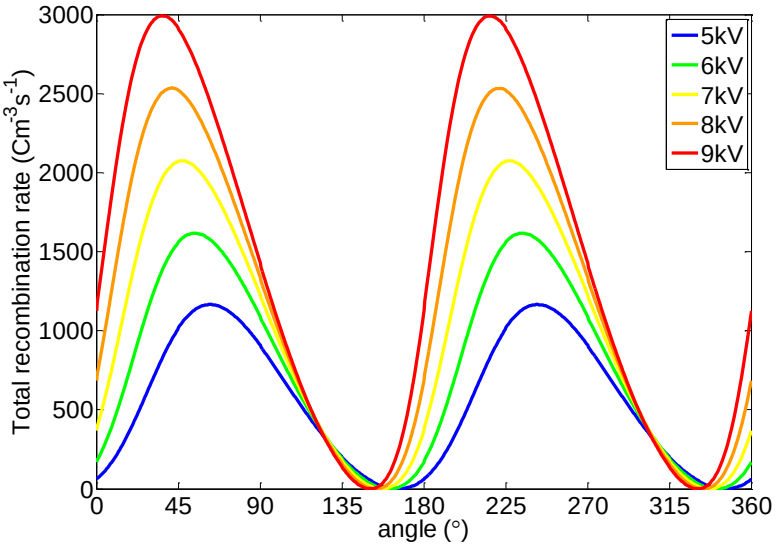


**Figure 6-11:** Total recombination rate at various sinusoidal voltages

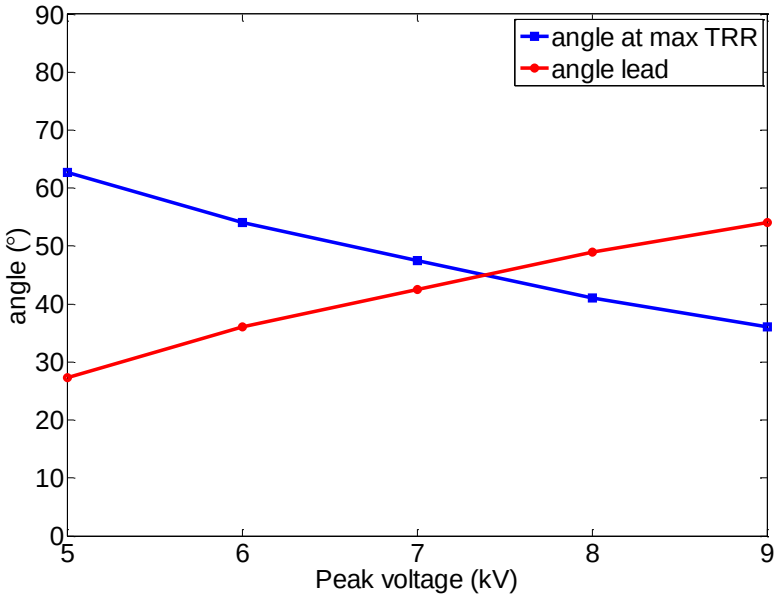


**Figure 6-12:** Phase angle of max TRR vs. applied sinusoidal voltage (50 Hz)

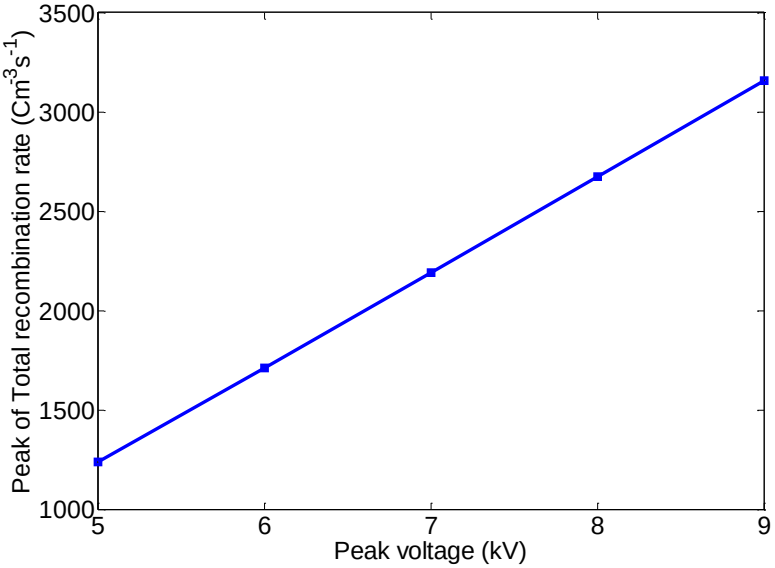


**Figure 6-13:** Peak value of TRR vs. applied peak voltage at 50 Hz

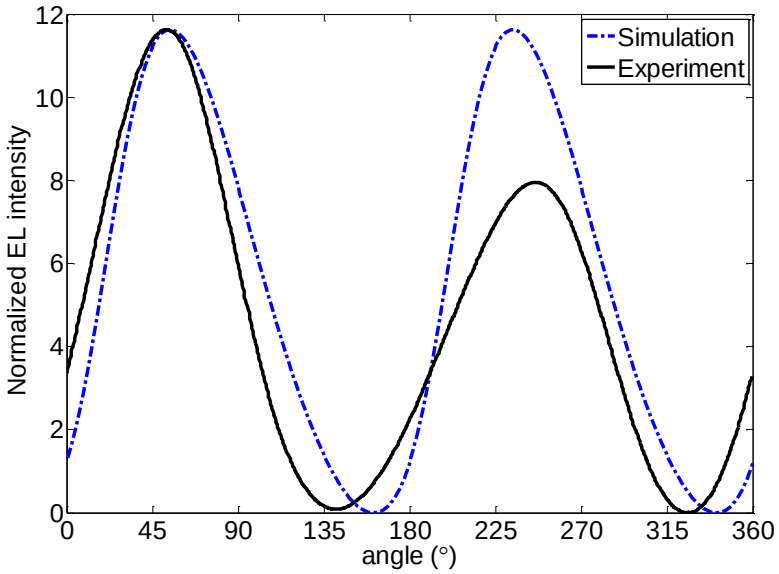


**Figure 6-14:** Simulated TRR and experimental EL in PE under sinusoidal voltages (6 kV 50 Hz)

### *6.3.2 Influence of ac frequency on EL*

The effect of ac frequency on the electroluminescence has been examined using the simulation. The total recombination rate in polyethylene under ac sinusoidal voltages with a peak value of 6 kV at various frequencies ranging from 10 Hz to 90 Hz is simulated and the TRR subtracted from the saturation level are shown in Figure 6-15. Higher frequency leads to more interaction of opposite charge carriers and creates

intense recombination process and eventually increased EL intensity. The amplitude of TRR increases nonlinearly with ac frequency as shown in Figure 6-16. On the other hand, the increase of ac frequency leads to the shift of maximum TRR to larger phase angles as shown in Figure 6-17. This might result from reduced injection current density at higher frequencies, which consequently generates insufficient heterocharge to enhance the injection current density at the electrodes.

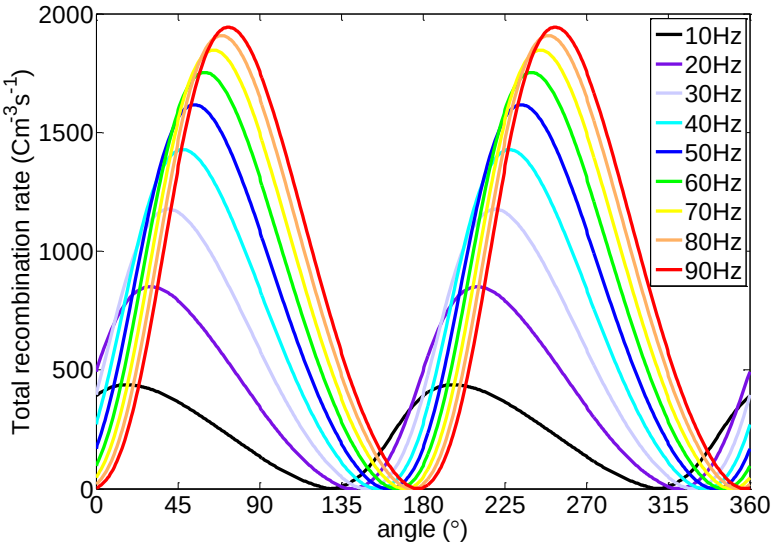


**Figure 6-15:** Total recombination rate under sinusoidal voltages of various frequencies

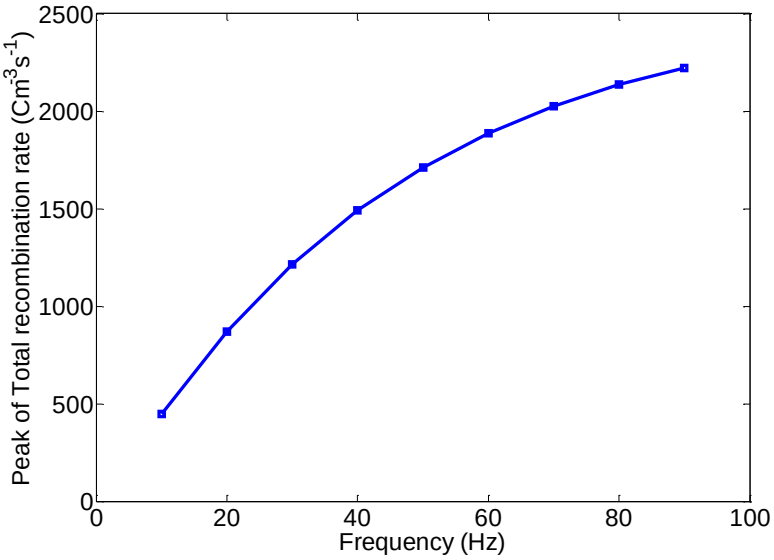


**Figure 6-16:** Peak value of TRR under sinusoidal voltages of various frequencies

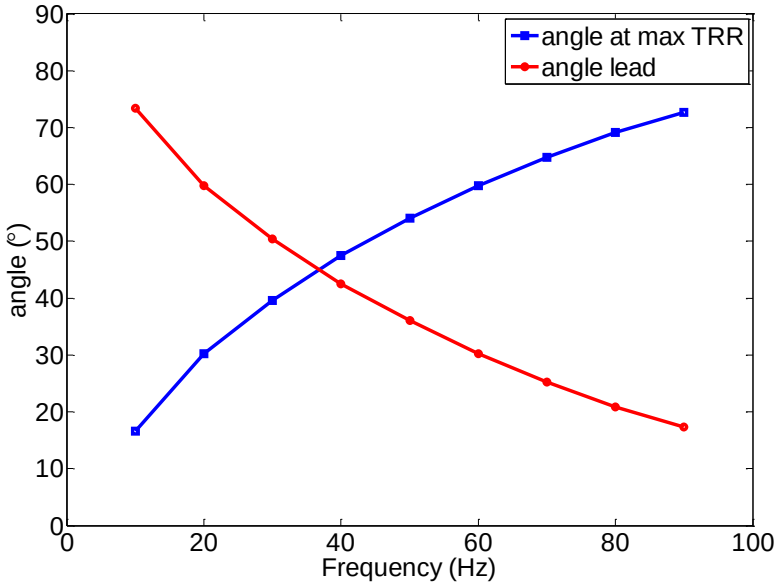


**Figure 6-17:** Phase angle of max TRR under sinusoidal voltages at various frequencies

## 6.4 Electroluminescence under an applied ac triangular voltage

Total recombination rate (TRR) in polyethylene under ac triangular voltages has been simulated to examine how the ac waveform affects the electroluminescence. An ac triangular voltage with a peak voltage of 6 kV is used in the simulation (Figure 6-18). The total recombination rate under ac triangular voltages of 50 Hz with various peak values ranging from 6 kV to 8 kV have been simulated. The TRR subtracted from the saturation level under triangular voltages is shown in Figure 6-19. TRR demonstrates totally different pattern from that under sinusoidal voltages. The peak value of TRR does not come earlier than that of applied voltage but seems to appear around 90° when applied voltage is below 7 kV. The peak shifts to a lower phase angle less than 90° for a peak voltage of 8 kV as shown in Figure 6-20. The magnitude of the TRR increases with applied voltage.

A comparison of simulated TRR with experimental EL in polyethylene under an ac triangular voltage of 50 Hz with a peak value of 6 kV is shown in Figure 6-21. It shows that TRR lags behind the measured EL in the phase angle of the first peak while the second peaks appear at the same phase angles. However the simulation does not match the asymmetric pattern of the experimental EL result.

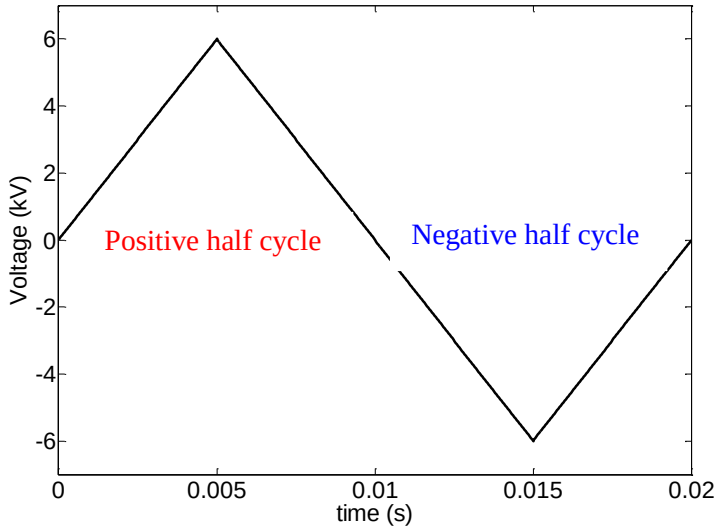


**Figure 6-18:** Applied triangular voltage for the EL simulation (6 kV 50 Hz)

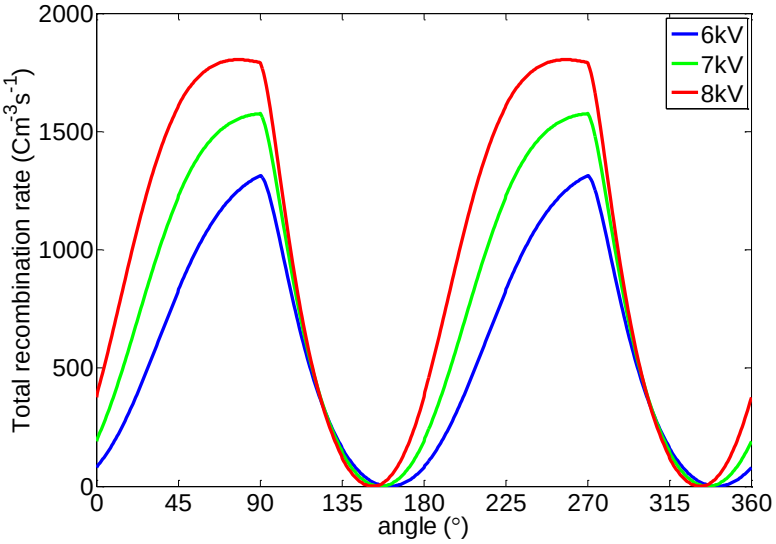


**Figure 6-19:** Total recombination rate under various triangular voltages (50 Hz)

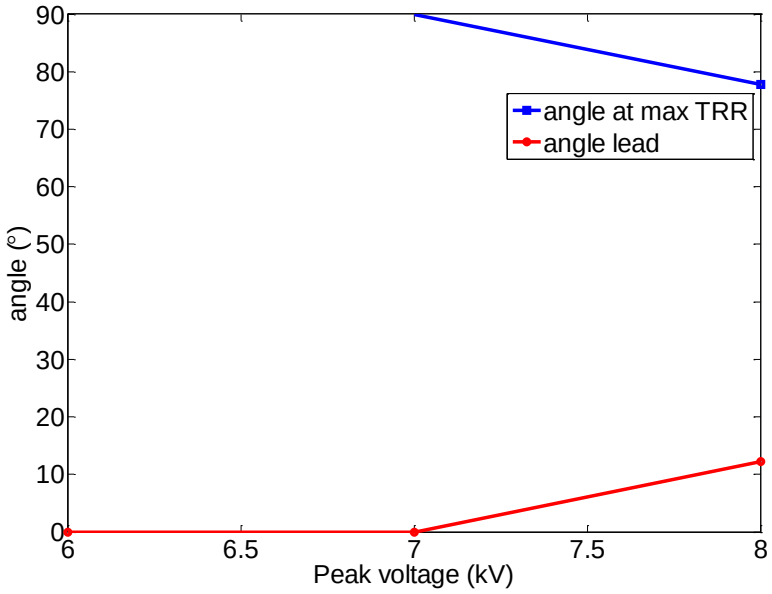


**Figure 6-20:** Phase angle of max TRR vs. applied triangular voltages (50 Hz)

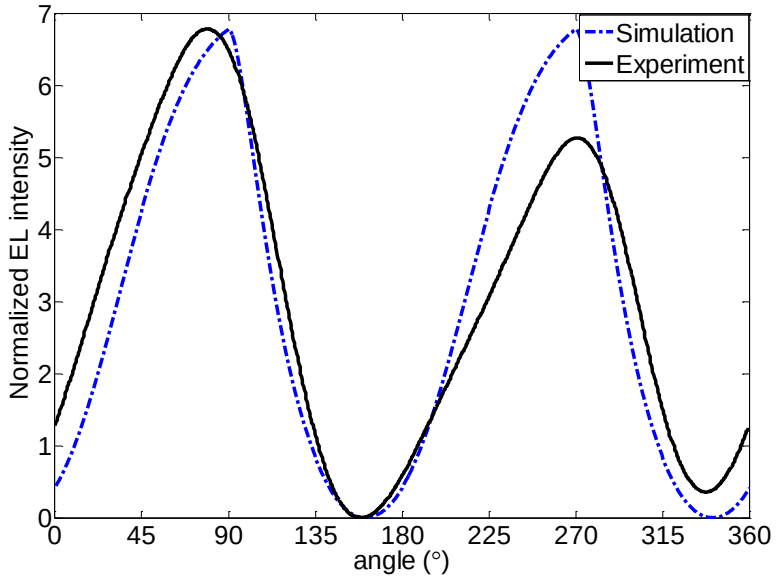


**Figure 6-21:** Simulated TRR and experimental EL in PE under triangular voltage (6 kV 50 Hz)

## 6.5 Electroluminescence under an applied ac square voltage

Electroluminescence due to recombination of bipolar charge carriers in polyethylene under ac square voltages of 50 Hz with peak voltages of 6 kV, 7 kV and 8 kV has been simulated. The waveform of square voltage is shown in Figure 6-22. The simulated TRR under square voltages shows the first peak at lower phase angles around 20° than that under sinusoidal or triangle voltages as shown in Figure 6-23. The rise to

the maximum TRR is also quicker. However the change in phase shift is not as significant as that under sinusoidal voltages when increasing the applied voltage as indicated in Figure 6-24. A comparison of simulated TRR to the experimental EL in polyethylene under an ac square voltage of 50 Hz with the peak value of 6 kV is shown in Figure 6-25. Both the simulation and experiment show a fast rising to the maximum and rapid falling with a tail in each half voltage cycle.

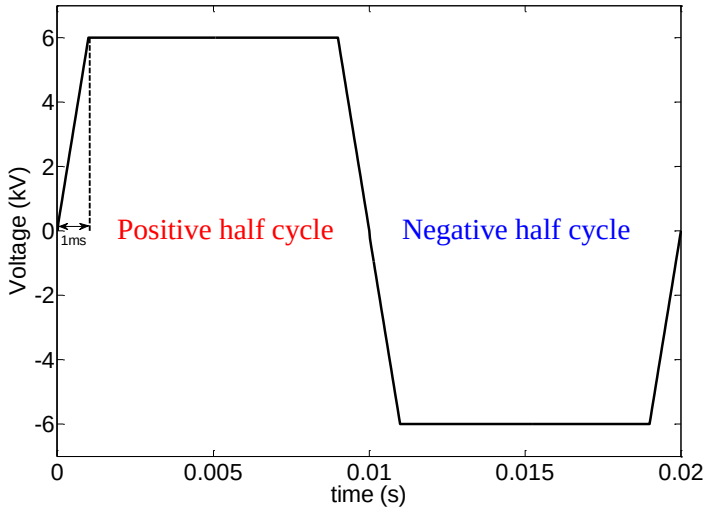


**Figure 6-22:** Applied square voltage for the EL simulation (6 kV 50 Hz)

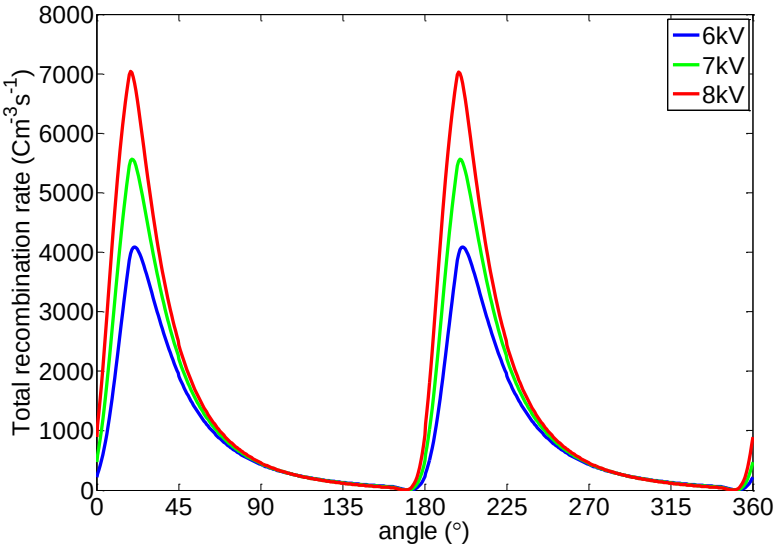


**Figure 6-23:** Total recombination rate under various square voltages (50 Hz)

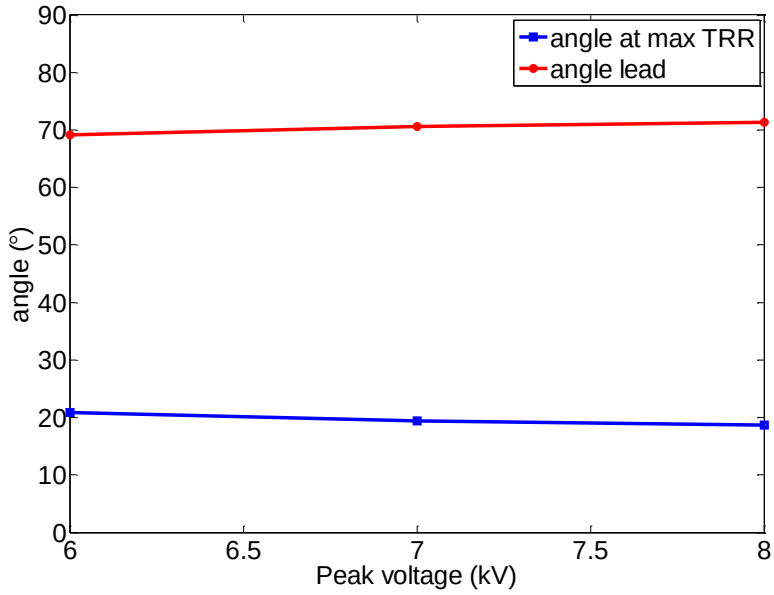


**Figure 6-24:** Phase angle of max TRR vs. applied square voltages (50 Hz)

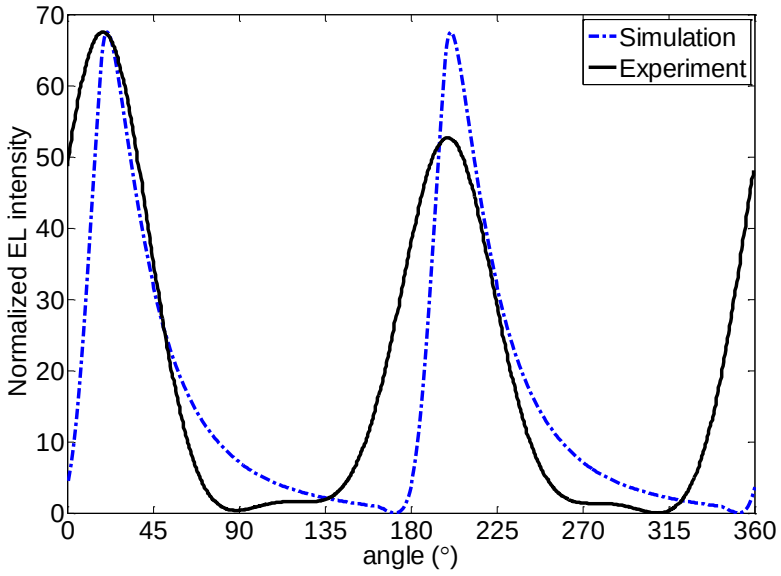


**Figure 6-25:** Simulated TRR and experimental EL in PE under square voltages (6 kV 50 Hz)

## 6.6 Influence of parameters on electroluminescence

Initial simulation of electroluminescence due to recombination of bipolar charge carriers in polymers under ac stress indicates that EL is closely related to the dynamic behaviour of charge carriers. This behaviour depends on the injection current density at the electrode/polymer interface, the trapping characteristics and the recombination probability of charge carriers in polymers. Therefore the effects of the essential three parameters, injection barrier height for carriers, trapping coefficient and the

recombination coefficient on the TRR or EL in polyethylene under a sinusoidal voltage of 50 Hz with a peak value 6 kV have been investigated using the simulation.

### *6.6.1 Influence of injection current density on EL*

The injection current density depends greatly on the potential barrier height at the electrodes according to the Schottky law where a low injection barrier height normally leads to a large injection current. The total recombination rate under a sinusoidal voltage of 50 Hz with a peak voltage of 6 kV in the case of different injection barrier heights $w_i$ has been simulated and the simulation results are shown in Figure 6-26. It reveals that TRR at larger injection current densities (or lower injection barrier heights $w_{ei}$) has a larger magnitude. Furthermore, the increased injection current densities at lower barrier heights lead to the leading of the peak of TRR in each half cycle.

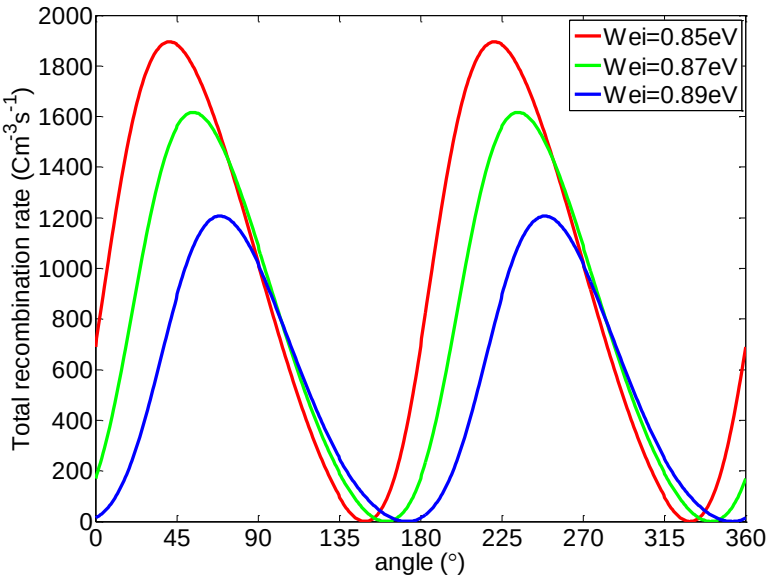


**Figure 6-26:** TRR at different injection barrier heights under sinusoidal voltage (6 kV 50 Hz)

### *6.6.2 Influence of charge trapping on EL*

The trapping coefficient which defines the trapping rate for mobile charge carriers also has an important effect on the charge dynamics and hence charge recombination. The total recombination rate (TRR) for the injection barrier height of 0.87 eV at various trapping coefficients $B_e$=400, 600, 800 at sinusoidal voltage of 50 Hz with peak voltage of 6 kV is shown in Figure 6-27. It is seen that a larger trapping

coefficient leads to more trapped charge carriers resulting into a larger value of TRR and shifting of the peak value to smaller phase angles.

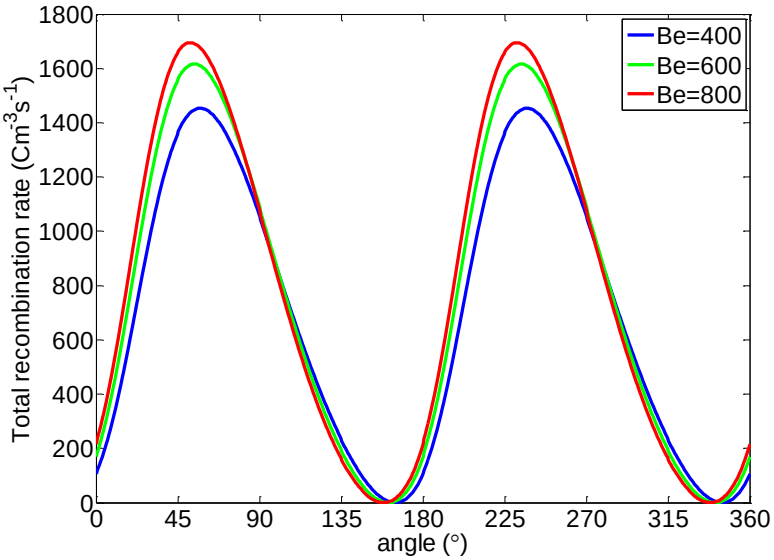


**Figure 6-27:** TRR at different trapping coefficients under sinusoidal voltage (6 kV 50 Hz)

### *6.6.3 Influence of recombination coefficient on EL*

The contribution of recombination between different charge pairs to the electroluminescence has been examined in the simulation, which shows that the mobile-trapped charge pairs play a dominant role in the electroluminescence rather than the mobile-mobile or the trapped-trapped opposite charge pairs. Hence the current recombination coefficients $S_i$ in Table 6-1 have been increased and reduced by one order of magnitude to investigate their effects on the resultant electroluminescence. The total recombination rate at different recombination coefficients $S_i$ under sinusoidal voltages of 50 Hz with a peak voltage of 6 kV is shown in Figure 6-28. The increase of recombination coefficient directly increases the magnitude of TRR. The phase lead over the applied voltage is increased as well.

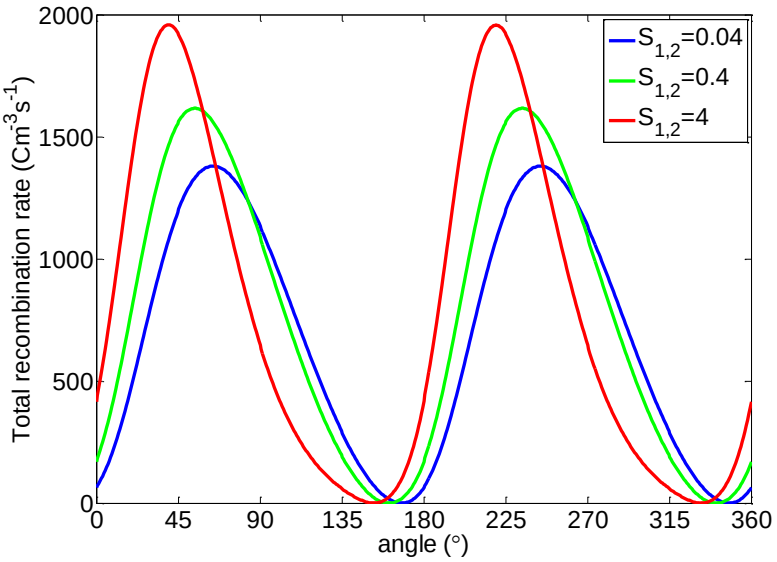


**Figure 6-28:** TRR at different recombination coefficients under sinusoidal voltage (6 kV 50 Hz)

## 6.7 Discussion

Simulation and experiments both present two peaks of recombination rate or electroluminescence at earlier phase angles prior to 90˚ and 270˚, the angle of applied peak voltage. The presence of such early peaks is related with the phase lead of injection current density over the applied voltage which depends on the distorted electric field at the electrodes. The distortion of electric fields at the electrodes is determined by the accumulated space charge near the electrode. The heterocharge which enhances the electric fields at the electrodes has been confirmed to contribute the phase leading over the applied voltage. Furthermore, the simulation has achieved reasonable fit with the experimental electroluminescence in polyethylene subjected to different waveform of ac voltages, which indicates that the charge transport model is capable of describing the behaviours the charge carriers related with the electroluminescence.

In terms of the voltage waveform, for an equal peak voltage and same ac frequency, TRR under a square voltage presents the largest amplitude and the phase lead over the applied voltage followed by that under a sinusoidal voltage and then that experiencing a triangular voltage as shown in Figure 6-29. This is because the largest r.m.s electric field is applied across the specimen under square wave voltages when the parameterization remains the same in the simulation.

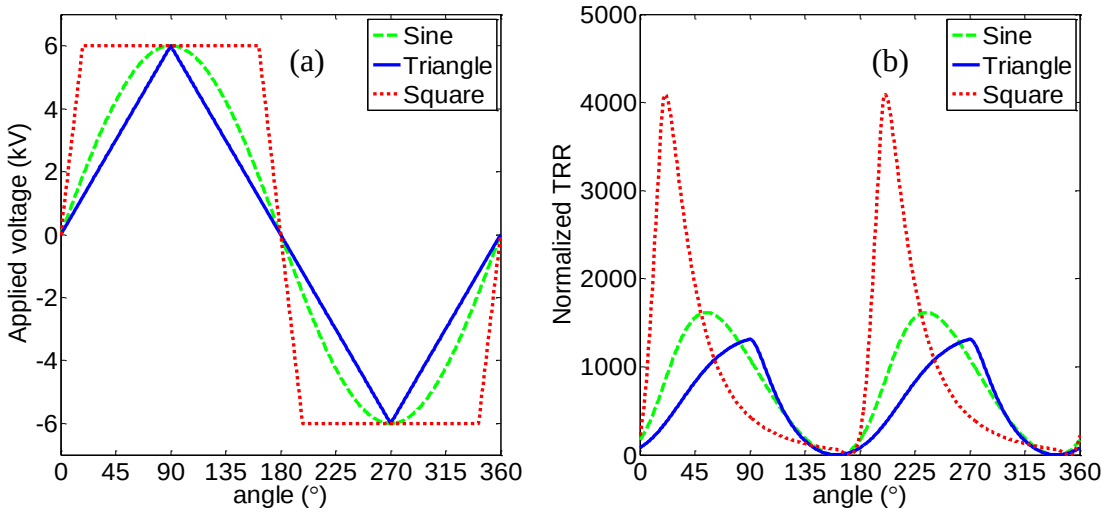


**Figure 6-29:** TRR under different waveforms of applied voltage

(a) Applied voltages; (b) Simulated TRR.

## 6.8 Summary

Electroluminescence in polyethylene under three types of ac voltages, sinusoidal, triangular and square voltages has been simulated using the bipolar charge transport model. Simulated EL presents two peaks in the 1$^{st}$ and 3$^{rd}$ quarter per cycle of applied voltage and shows a reasonable match with experimental results. The correlation between the injection current density and the electroluminescence has been confirmed. The contribution of charge dynamics to EL is understood by simulation as well. More importantly, the influence of essential parameters related to the charge injection, trapping and recombination on the resultant electroluminescence has been revealed.

# Chapter 7 Conclusions and Future Work

## 7.1 Conclusions

This report concentrates on the research into space charge in polyethylene under various electric stresses. The research work has been accomplished by implementing numerical modelling of the behaviour of space charge in polyethylene under dc and ac voltages and experimental measurement of space charge in additive free polyethylene. The characteristics of electroluminescence due to space charge are also investigated in polymeric insulation materials. Based on this fundamental work, several conclusions can be drawn.

A bipolar charge transport model, which involves bipolar charge carrier injection at the contact of dielectric/electrodes, charge transport with trapping and recombination has been developed to simulate the dynamics of space charge in polyethylene subjected to electric fields. The simulation with symmetric parameterization for positive charge (holes) and negative charge (electrons) has reproduced the basic behaviours of space charge and the evolution in polyethylene under the dc volts on condition. A fit of simulation result with experimental measurement has been achieved by optimizing the

parameters in the model. More importantly the influence of essential parameters related to the properties of material on the behaviour of space charge has been revealed through the simulation, which indicates that the charge injection at the electrodes, charge transportation and trapping in the bulk of polyethylene play significant roles in the development of space charge. The electronic conduction mechanism in polyethylene and its effect on space charge behaviours are examined using a simulation model that has field dependent mobility. Power-law mobility seems to be a suitable field-dependent mobility for the simulation of space charge in polyethylene.

The decay of space charge in polyethylene after the removal of an applied voltage is normally expected to reveal some useful information of trapped charge carriers and trapping characteristics correlated with the physical/chemical structure of polymers. The decay of space charge simulated using the bipolar charge transport model shows an overall slow relaxation process, which is attributed by the non-detrapping of trapped charge carriers in the model. Furthermore, the bipolar charge transport model is modified to simulate the space charge behaviours in the corona charged polyethylene films and the contribution of space charge in the bulk and surface charge to the surface potential decay of corona charged specimen. The simulation reproduces the crossover of the surface potential decay, where the surface potential decays faster at higher initial potentials and suggests that there is a large contribution of surface charge to the overall surface potential decay.

The velocity of positive charge carriers in polyethylene has been evaluated from the experimental observation of positive charge packets in polyethylene under dc electric fields. The decrease of velocity with electric fields which results into a negative differential mobility is firstly observed. By incorporating the experimental velocity result into the bipolar charge transport model, it is found that the formation of charge packets depends on the electric fields which can lead to a reduced velocity of charge carriers at increased electric field. A weak trapping coefficient for positive charge carriers is equally necessary for the formation of charge packets.

A fast pulsed electro-acoustic system along with data processing program for testing space charge in polymers under ac voltages has been developed. It is capable of detection of space charge under ac voltages with arbitrary waveforms of frequency up

to 100 Hz. Space charge in low density polyethylene under ac sinusoidal voltages of variable amplitudes and frequencies has been measured. The results show that space charge distributions under ac voltages are phase-dependent. A very small quantity of charge is observed in the bulk of polyethylene at the power frequency of 50 Hz even after experiencing an r.m.s field of 42.4 $kVmm^{-1}$ for 8 hours rather than the significant amount of charge at the electrodes. The residual charge in the bulk of polyethylene is very low, i.e., less than 1.5 $Cm^{-3}$. Noticeably heterocharge is observed in the vicinity of the electrodes under ac voltages of 50 Hz and low frequencies. The numerical modelling of space charge under ac voltages also shows that a small quantity of phase-dependent charge mostly accumulates in the vicinity of electrodes instead of moving into the polymer bulk and that the accumulation of space charge can be significantly suppressed by increasing the ac frequency. Noticeably heterocharge occurs near the electrodes especially at low frequency in the simulation, which indicates that the interfacial effect of space charge under ac stress should be fully considered. Due to less charge accumulation in the polymer bulk, the total current density is dominated by the displacement current density under ac stresses. However the combination of ac and dc voltages has been found to be able to lower the threshold of space charge accumulation in polyethylene and increase the amount of charge.

Electroluminescence (EL) under ac electric fields is simulated using the bipolar charge transport model. EL is modelled by the recombination of opposite polarity charge carriers accumulated in polyethylene. The simulated EL reproduces the peaks in the $1^{st}$ and $3^{rd}$ quarter of ac sinusoidal, triangular and square voltages observed from experiments. EL under square voltages presents the earliest peaks among these three types of voltages followed by sinusoidal voltages and triangular voltages. These peaks lead over the applied voltage in phase and this phase lead tends to decrease when increasing ac frequency or lowering the voltage amplitude. Moreover, the injection of charge carriers at the interface of polymer/electrode and trapping characteristics of charge carriers in the bulk both play important roles in the resultant EL intensity. These show a strong correlation between space charge and electroluminescence in polymers.

## 7.2 Future work

The bipolar charge transport model has been employed to implement the simulation work throughout the thesis. The simulation results are able to present the

basic behaviours of space charge and its evolution trend in polyethylene subjected to electric fields. This model may be applied to other solid dielectrics if they are additive free. However, more specifically, when applying this model to reproduce the space charge distribution which can be compared with experiments in polyethylene; it requires the changing of parameters in the model to achieve this objective. The change of injection barrier height for electronic charge carriers from dc to ac condition probably suggests that the electrode/polyethylene interface might behave differently and leads to changed injection rate of charge carriers. In terms of the electroluminescence, the simulation involves relatively large injection rate, large trapping coefficients and trapping density compared with the parameters used for the dc and ac space charge modelling to achieve the comparable results with experimental observations. This suggests more contribution of charge injection and trapping to the resultant electroluminescence originated by the recombination of charge carriers. The bipolar charge transport model can reflect the distinct influence of the parameters on different physical processes, such as dc space charge, ac space charge and electroluminescence, but it has its own limitation of describing the different physical processes using the same set of parameters. This indicates that the physical process of space charge or electroluminescence may be more complicated than what the bipolar charge transport model can describe. Other factors or physical processes may have to be incorporated for a better simulation. For the simulation of space charge under ac stress, care has to be taken for the spatial resolution of the discretization approach in the numerical computation as space charge mostly accumulates in the region close to the electrodes. Actually when looking into the simulated space charge in 100 μm polyethylene film at power frequency of 50 Hz, the penetration depth of space charge into the bulk is around 25 μm much larger than the spatial resolution of 1 μm used in the simulation. The current spatial resolution is small enough to resolve the space charge nearby the interface of electrode/polyethylene. However, a nonlinear discretization approach may be used to achieve more details of space charge accumulation nearby the electrodes in the future work.

In the bipolar charge transport model, more concern has been focused on the charge generation and transport process during the build-up and relaxation of space charge in polyethylene under various electric fields. The specific trapping and detrapping characteristics are not yet considered. The exact trapping characteristics

could be far more complicated, which depends on the distribution of trapping energy levels and detrapping mechanism that are closely related to the physical/chemical defects existing in the polymer structure. The correlation between the trapping characteristics and the accumulation of space charge is of great importance for understanding the origin of charge carriers and their influence on the performance of polymeric insulation materials under electric stress. These trapping /detrapping characteristics of charge carriers, which determines the behaviours of space charge under dc or ac electric fields is not yet well understood and investigated adequately. Therefore a new description of the trapping process of charge carriers at the specific energy levels in the band gap of polymers needs to be proposed based on the experimental inspection of the relaxation of trapped charges. New simulations of space charge involving trapping energy need to be developed.

In terms of properties of charge carriers, almost identical properties for positive and negative charges are assumed in the modelling of space charge. However, in reality, electrons and holes are expected to have unique drift mobility and trapping characteristics in the semi-crystalline polyethylene; and the charge carrier injection at the interface of polymer/electrode is not always same as it depends on the materials and the surface states. Hence the distinct properties of positive and negative charge carriers have to be determined and incorporated into future theoretical analysis.

# References


[1] C. A. Harper, *Modern Plastics Handbook*. New York: McGraw-Hill, 1999.

[2] M. Yoshinao and K. Mamoru, "Development History of HVDC Extruded Cable with Nanocomposite Material," in *8th International Conference on Properties and applications of Dielectric Materials*, 2006, pp. 460-463.

[3] B. Venkatesulu and M. J. Thomas, "Erosion resistance of alumina-filled silicone rubber nanocomposites," *IEEE Transactions on Dielectrics and Electrical Insulation*, vol. 17, pp. 615-624, 2010.

[4] A. Ram, *Fundamentals of Polymer Engineering*. New York: Plenum Press, 1997.

[5] W. T. Shugg, "Overview of our heritage [dielectric materials]," in *Electrical Electronics Insulation Conference and Electrical Manufacturing & Coil Winding Conference*, 1993, pp. 191-194.

[6] D. Kind and H. Karner, *High Voltage Insulation Technology*. Brawnschweig: Friedr. Vieweg & Sohn, 1985.

[7] A. J. Peacock, *Handbook of Polyethylene: Structures, Properties and Applications*. New York: Marcel Dekker, Inc., 2000.

[8] J. B. Birks, *Modern Dielectric Materials*. London: Heywood & Company Ltd, 1960.

[9] J. F. Hall, "History and bibliography of polymeric insulators for outdoor applications," *IEEE Transactions on Power Delivery*, vol. 8, pp. 376-385, 1993.

[10] J. E. Mark, *Polymer data handbook*: Oxford University Press, 1999.

[11] "Characteristics properties of silicone rubber compounds," *Shin-Etsu Silicone Ltd.*, pp. 1-16, 2005.

[12] D. K. Das-Gupta, "Polyethylene: structure, morphology, molecular motion and dielectric behavior," *IEEE Electrical Insulation Magazine*, vol. 10, pp. 5-15, 1994.

[13] T. J. Lewis, "Polyethylene under electrical stress," *IEEE Transactions on Dielectrics and Electrical Insulation*, vol. 9, pp. 717-729, 2002.

[14] D. B. Malpass, *Introduction to Industrial Polyethylene: Properties, Catalysts, and Processes*: John Wiley & Sons, 2010.

[15] P. Argaut, H. Auclair, and E. Favrie, "Development of 500 kV low density polyethylene insulated cable," in *3rd International Conference on Power Cables and Accessories 10kV - 500kV*, 1993, pp. 77-81.

[16] W. J. Plate, T. H. Ling, and J. F. Nuccio, "Reassessment of Polyethylene Power Cable," *IEEE Transactions on Power Apparatus and Systems*, vol. 82, pp. 990-1002, 1963.

[17] G. F. Moore, *Electric Cables Handbook*. Oxford: Wiley-Blackwell, 1997.

[18] B. A. B. P. Ltd, "XLPE Compounds for Extra High Voltage Cables," 2010.

[19] R. Vogelsang, O. Sekula, H. Nyffenegger, and W. Weissenberg, "Long-term experiences with XLPE cable systems up to 550 kV," in *KONFERENCA SLOVENSKIH ELEKTROENERGETIKOV CIGRE SC B1* Kranjska Gora, 2009.
[20] M. Salah Khalil, "International research and development trends and problems of HVDC cables with polymeric insulation," *IEEE Electrical Insulation Magazine,* vol. 13, pp. 35-47, 1997.
[21] R. M. Eichhorn, "Treeing in Solid Extruded Electrical Insulation," *IEEE Transactions on Electrical Insulation* vol. EI-12, pp. 2-18, 1977.
[22] G. Chen and C. Tham, "Electrical treeing characteristics in XLPE power cable insulation in frequency range between 20 and 500 Hz," *IEEE Transactions on Dielectrics and Electrical Insulation,* vol. 16, pp. 179-188, 2009.
[23] L. A. Dissado and J. C. Forthergill, *Electrical Degradation and Breakdown in Polymers*. London: IET, 1992.
[24] N. Shimizu, N. Nagura, T. Suzuki, and A. Tanida, "Electroluminescence and degradation in PE caused by electron impact," in *2003 Annual Report of Conference on Electrical Insulation and Dielectric Phenomena* 2003, pp. 361-364.
[25] Z.-H. Fan, T. Takahashi, J. Suzuki, H. Miyata, S. Iemura, T. Itoh, T. Nakiri, and N. Shimizu, "Relation between electroluminescence and degradation in XLPE," *IEEE Transactions on Dielectrics and Electrical Insulation,* vol. 8, pp. 91-96, 2001.
[26] A. R. Blythe, *Electrical properties of polymers*, 2nd ed. Cambridge, Eng. ; New York: Cambridge University Press, 1979.
[27] P. Morin, J. Lewiner, C. Alquié, and T. Ditchi, "Space Charge in Solid Dielectrics," in *The Dielectrics Society*, Leicester, 1998.
[28] Y. Murooka and K. Hidaka, "Theoretical studies on nanosecond surface discharge phenomena observed using Lichtenberg figure method," *Electrical Engineering (Archiv fur Elektrotechnik),* vol. 74, pp. 163-173, 1990.
[29] G. C. Montanari, G. Mazzanti, F. Palmieri, A. Motori, G. Perego, and S. Serra, "Space-charge trapping and conduction in LDPE, HDPE and XLPE," *Journal of Physics D: Applied Physics,* vol. 34, p. 2902, 2001.
[30] K. C. Kao, *Dielectric phenomena in solids: with emphasis on physical concepts of electronic processes*. San Diego: Elsevier Academic Press, 2004.
[31] K. S. Suh, K. Jung Hoe, L. Seung Hyung, P. Jung Ki, and T. Takada, "Effects of sample preparation conditions and short chains on space charge formation in LDPE," *IEEE Transactions on Dielectrics and Electrical Insulation,* vol. 3, pp. 153-160, 1996.
[32] N. Hussin and G. Chen, "Space charge accumulation and conductivity of crosslinking byproducts soaked LDPE," in *2010 Annual Report Conference on Electrical Insulation and Dielectric Phenomena (CEIDP)*, 2010, pp. 1-4.
[33] W. Qi, G. Chen, and A. S. Alghamdi, "Influence of nanofillers on electrical characteristics of epoxy resins insulation," in *10th IEEE International Conference on Solid Dielectrics (ICSD)* 2010, pp. 1-4.
[34] M. A. Grado-Caffaro and M. Grado-Caffaro, "Electrical conductance from the Fowler-Nordheim tunneling," *Optik - International Journal for Light and Electron Optics*, vol. 116, pp. 299-300, 2005.
[35] G. G. Raju, *Dielectrics in electric fields*. New York: Marcel Dekker, 2003.
[36] J. G. Simmons, "Poole-Frenkel Effect and Schottky Effect in Metal-Insulator-Metal Systems," *Physical Review,* vol. 155, p. 657, 1967.
[37] N. F. Mott and R. W. Gurney, *Electronic processes in ionic crystals*, 2nd ed. New York: Dover Publications, 1964.

[38] L. A. Dissado, G. Mazzanti, and G. C. Montanari, "The role of trapped space charges in the electrical aging of insulating materials," *IEEE Transactions on Dielectrics and Electrical Insulation,* vol. 4, pp. 496-506, 1997.

[39] Y. Zhang, J. Lewiner, C. Alquie, and N. Hampton, "Evidence of strong correlation between space-charge buildup and breakdown in cable insulation," *IEEE Transactions on Dielectrics and Electrical Insulation,* vol. 3, pp. 778-783, 1996.

[40] T. Hori, K. Kaneko, T. Mizutani, and M. Ishioka, "Effects of electrodes on space charge in low-density polyethylene," in *Proceedings of the 7th International Conference on Properties and Applications of Dielectric Materials* 2003, pp. 855-858 vol.3.

[41] G. Chen, "Interfaces and Space Charge in Polymeric Insulating Materials," in *MRS 2005 Fall Meeting*, Boston, 2005.

[42] E. Kanegae, Y. Ohki, T. Tanaka, Y. Sekiguchi, Y. Murata, and C. C. Reddy, "Space Charge Behavior in Multi-layered Dielectrics with LDPE and LDPE/MgO Nanocomposites," in *Proceedings of 2010 International Conference on Solid Dielectrics (ICSD)*, Potsdam, Germany, 2010, pp. 196-199.

[43] X. Wang, M. Zheng, Xi Chen, Z. Peng, K. Wu, S. Liu, J. Peng, and S. Chen, "The Effect of Temperature Gradient on Space Charge Accumulation at SR/XLPE Interface under DC Stress," in *Proceedings of 2010 International Conference on Solid Dielectrics (ICSD)*, Potsdam, Germany, 2010, pp. 340-343.

[44] M. Fu and G. Chen, "Space charge measurement in polymer insulated power cables using flat ground electrode PEA system," *IEE Proceedings of Science, Measurement and Technology,* vol. 150, pp. 89-96, 2003.

[45] N. Hozumi, H. Suzuki, T. Okamoto, K. Watanabe, and A. Watanabe, "Direct observation of time-dependent space charge profiles in XLPE cable under high electric fields," *IEEE Transactions on Dielectrics and Electrical Insulation,* vol. 1, pp. 1068-1076, 1994.

[46] W. Choo, G. Chen, and S. G. Swingler, "Space charge accumulation under effects of temperature gradient and applied voltage reversal on solid dielectric DC cable," in *IEEE 9th International Conference on the Properties and Applications of Dielectric Materials (ICPADM)*, 2009, pp. 946-949.

[47] K. Matsui, Y. Tanaka, T. Takada, T. Fukao, K. Fukunaga, T. Maeno, and J. M. Alison, "Space charge behavior in low density polyethylene at pre-breakdown," *IEEE Transactions on Dielectrics and Electrical Insulation,* vol. 12, pp. 406-415, 2005.

[48] S. Bamji, M. Abou Dakka, and A. Bulinski, "Phase-resolved pulsed electro-acoustic technique to detect space charge in solid dielectrics subjected to AC voltage," *IEEE Transactions on Dielectrics and Electrical Insulation,* vol. 14, pp. 77-82, Feb 2007.

[49] A. See, J. C. Fothergill, L. A. Dissado, and J. M. Alison, "Measurement of space-charge distributions in solid insulators under rapidly varying voltage using the high-voltage, high-speed pulsed electro-acoustic (PEA) apparatus," *Measurement Science and Technology,* vol. 12, p. 1227, 2001.

[50] C. Thomas, G. Teyssedre, and C. Laurent, "A New Method for Space Charge Measurements Under Periodic Stress of Arbitrary Waveform by the Pulsed Electro-Acoustic Method," *IEEE Transactions on Dielectrics and Electrical Insulation* vol. 15, pp. 554-559, 2008.

[51] Z. Xu, J. Zhao, and G. Chen, "An Improved Pulsed Electroacoutic System for Space Charge Measurement under AC Conditions," in *Proceedings of 2010*

*IEEE International Conference on Solid Dielectrics (ICSD)*, Potsdam, Germany, 2010, pp. 398-401.

[52] X. Wang, N. Yoshimura, Y. Tanaka, K. Murata, and T. Takada, "Space charge characteristics in cross-linking polyethylene under electrical stress from dc to power frequency," *Journal of Physics D: Applied Physics*, vol. 31, p. 2057, 1998.

[53] Z. Xu and G. Chen, "Space Charge Behaviour at LDPE Interface under AC Electric Stress," in *The 6th International Space Charge Conference*, Tour, 2006.

[54] N. Ando and F. Numajiri, "Experimental Investigation of Space Charge in XLPE Cable Using Dust Figure," *IEEE Transactions on Electrical Insulation* vol. EI-14, pp. 36-42, 1979.

[55] M. S. Khalil and B. S. Hansen, "Investigation of space charge in low-density polyethylene using a field probe technique," *IEEE Transactions on Electrical Insulation* vol. 23, pp. 441-445, 1988.

[56] R. E. Collins, "Analysis of spatial distribution of charges and dipoles in electrets by a transient heating technique," *Journal of Applied Physics*, vol. 47, pp. 4804-4808, 1976.

[57] T. Pawlowski, R. J. Fleming, and S. B. Lang, "LIMM study of space charge in crosslinked polyethylene," *IEEE Transactions on Dielectrics and Electrical Insulation*, vol. 13, pp. 1023-1029, Oct 2006.

[58] Y. Suzuoki, H. Muto, T. Mizutani, and M. Ieda, "Investigation of Space Charge in High-Density Polyethylene Using Thermal-Pulse Response," *Japanese Journal of Applied Physics*, vol. 24, p. 604, 1985.

[59] S. Agnel, P. Notingher, Jr., and A. Toureille, "Space charge measurements under applied DC field by the thermal step method," in *2000 Annual Report of Conference on Electrical Insulation and Dielectric Phenomena*, 2000, pp. 166-170 vol. 1.

[60] N. H. Ahmed and N. N. Srinivas, "Review of space charge measurements in dielectrics," *IEEE Transactions on Dielectrics and Electrical Insulation*, vol. 4, pp. 644-656, 1997.

[61] R. J. Fleming, "Space charge in polymers, particularly polyethylene," *Brazilian Journal of Physics*, vol. 29, pp. 280-294, 1999.

[62] R. J. Fleming, "Space charge profile measurement techniques: recent advances and future directions," *IEEE Transactions on Dielectrics and Electrical Insulation*, vol. 12, pp. 967-978, 2005.

[63] J. Lewiner, "Evolution of Experimental Techniques for the Study of the Electrical Properties of Insulating Materials," *IEEE Transactions on Electrical Insulation*, vol. EI-21, pp. 351-360, 1986.

[64] Y. Li and T. Takada, "Progress in space charge measurement of solid insulating materials in Japan," *IEEE Electrical Insulation Magazine*, vol. 10, pp. 16-28, 1994.

[65] T. Maeno, H. Kushibe, T. Takada, and C. M. Cooke, "Pulsed electroacoustic method for the measurement of volume charges in E-beam irradiated PMMA," in *1985 Annual Report of Conference on Electrical Insulation and Dielectric Phenomena*, 1985, pp. 389-397.

[66] K. Fukunaga, "Progress and Prospects in PEA Space Charge Measurement Techniques - [Feature Article]," *IEEE Electrical Insulation Magazine*, vol. 24, pp. 26-37, 2008.

[67] J. M. Alison and R. M. Hill, "A model for bipolar charge transport, trapping and recombination in degassed crosslinked polyethene," *Journal of Physics D: Applied Physics*, vol. 27, p. 1291, 1994.

[68] M. Fukuma, M. Nagao, and M. Kosaki, "Computer analysis on transient space charge distribution in polymer," *Proceedings of the 4th International Conference on Properties and Applications of Dielectric Materials*, vol. 1-2, pp. 24-27, 1994.
[69] K. Kaneko, T. Mizutani, and Y. Suzuoki, "Computer simulation on formation of space charge packets in XLPE films," *IEEE Transactions on Dielectrics and Electrical Insulation*, vol. 6, pp. 152-158, 1999.
[70] E. Belgaroui and et al., "A new numerical model applied to bipolar charge transport, trapping and recombination under low and high dc voltages," *Journal of Physics D: Applied Physics*, vol. 40, p. 6760, 2007.
[71] G. Chen and S. H. Loi, "Space charge modelling in solid dielectrics under high electric field based on double charge injection model," *Electroresponsive Polymers and Their Applications*, vol. 889, pp. 235-240, 2006.
[72] S. L. Roy, P. Segur, G. Teyssedre, and C. Laurent, "Description of bipolar charge transport in polyethylene using a fluid model with a constant mobility: model prediction," *Journal of Physics D: Applied Physics*, vol. 37, p. 298, 2004.
[73] J. Tian, J. Zou, Y. Wang, J. Liu, J. Yuan, and Y. Zhou, "Simulation of bipolar charge transport with trapping and recombination in polymeric insulators using Runge-Kutta discontinuous Galerkin method," *Journal of Physics D: Applied Physics*, vol. 41, p. 195416, 2008.
[74] P. Pipinys, A. Rimeika, and V. Lapeika, "DC conduction in polymers under high electric fields," *Journal of Physics D: Applied Physics*, vol. 37, p. 828, 2004.
[75] T. Mizutani, "High field phenomena in insulating polymers," in *Proceedings of the 2004 IEEE International Conference on Solid Dielectrics, ICSD* 2004, pp. 11-16 Vol.1.
[76] S. L. Roy, G. Teyssedre, C. Laurent, G. C. Montanari, and F. Palmieri, "Description of charge transport in polyethylene using a fluid model with a constant mobility: fitting model and experiments," *Journal of Physics D: Applied Physics*, vol. 39, p. 1427, 2006.
[77] T. J. Sonnonstine and M. M. Perlman, "Surface-potential decay in insulators with field-dependent mobility and injection efficiency," *Journal of Applied Physics*, vol. 46, pp. 3975-3981, 1975.
[78] P. W. M. Blom, M. J. M. deJong, and M. G. vanMunster, "Electric-field and temperature dependence of the hole mobility in poly(p-phenylene vinylene)," *Physical Review B*, vol. 55, pp. R656-R659, Jan 1 1997.
[79] G. Chen and Z. Xu, "Charge trapping and detrapping in polymeric materials," *Journal of Applied Physics*, vol. 106, pp. 123707-5, 2009.
[80] G. Mazzanti, G. C. Montanari, and J. M. Alison, "A space-charge based method for the estimation of apparent mobility and trap depth as markers for insulation degradation-theoretical basis and experimental validation," *IEEE Transactions on Dielectrics and Electrical Insulation*, vol. 10, pp. 187-197, Apr 2003.
[81] T.-c. Zhou, G. Chen, R.-j. Liao, and Z. Xu, "Charge trapping and detrapping in polymeric materials: Trapping parameters," *Journal of Applied Physics*, vol. 110, p. 043724, 2011.
[82] I. Kitani, Y. Tsuji, and K. Arii, "Analysis of Anomalous Discharge Current in Low-Density Polyethylene," *Japanese Journal of Applied Physics*, vol. 23, pp. 855-860, 1984.
[83] E. A. Baum, T. J. Lewis, and R. Toomer, "Further observations on the decay of surface potential of corona charged polyethylene films," *Journal of Physics D: Applied Physics*, vol. 10, p. 2525, 1977.

[84] M. Ieda, G. Sawa, and U. Shinohara, "A Decay Process of Surface Electric Charges across Poyethylene Film," *Japanese Journal of Applied Physics,* vol. 6, p. 793, 1967.
[85] Z. Xu, L. Zhang, and G. Chen, "Decay of electric charge on corona charged polyethylene," *Journal of Physics D: Applied Physics,* vol. 40, p. 7085, 2007.
[86] G. Chen, J. Zhao, and Y. Zhuang, "Numerical Modeling of Surface Potential Decay of Corona Charged Polymeric Material," in *Proceedings of 2010 IEEE International Conference on Solid Dielectrics (ICSD)*, Potsdam, Germany, 2010, pp. 549-552.
[87] N. Hozumi, T. Takeda, H. Suzuki, and T. Okamoto, "Space charge behavior in XLPE cable insulation under 0.2-1.2 MV/cm dc fields," *IEEE Transactions on Dielectrics and Electrical Insulation,* vol. 5, pp. 82-90, 1998.
[88] H. Kon, Y. Suzuoki, T. Mizutani, M. Ieda, and N. Yoshifuji, "Packet-like space charges and conduction current in polyethylene cable insulation," *IEEE Transactions on Dielectrics and Electrical Insulation* vol. 3, pp. 380-385, 1996.
[89] K. Matsui, Y. Tanaka, T. Takada, and T. Maeno, "Numerical analysis of packet-like charge behavior in low-density polyethylene under DC high electric field," *IEEE Transactions on Dielectrics and Electrical Insulation,* vol. 15, pp. 841-850, 2008.
[90] D. Fabiani, G. Montanari, L. Dissado, C. Laurent, and G. Teyssedre, "Fast and slow charge packets in polymeric materials under DC stress," *IEEE Transactions on Dielectrics and Electrical Insulation,* vol. 16, pp. 241-250, 2009.
[91] D. Fabiani, G. C. Montanari, E. Siracusano, and L. A. Dissado, "Ultra-fast space charge packets in nanostructured epoxy-based materials," in *IEEE Conference on Electrical Insulation and Dielectric Phenomena (CEIDP '09)*, 2009, pp. 31-34.
[92] N. Hozumi, Y. Muramoto, M. Nagao, and Z. Yewen, "Carrier mobility in ethylene-vinylacetate copolymer estimated by transient space charge," *IEEE Transactions on Dielectrics and Electrical Insulation,* vol. 8, pp. 849-853, 2001.
[93] G. Chen and J. Zhao, "Observation of negative differential mobility and charge packet in polyethylene," *J. Phys. D: Appl. Phys.*, vol. 44, p. 212001, 2011.
[94] J. B. Gunn, "Microwave oscillations of current in III-V semiconductors," *Solid State Communications,* vol. 1, pp. 88-91, 1963.
[95] A. van Roggen, "Electronic Conduction of Polymer Single Crystals," *Physical Review Letters,* vol. 9, p. 368, 1962.
[96] T. J. Lewis and J. P. Llewellyn, "Electron resonance-tunneling, negative differential resistance and positive packet formation in polyethylene," in *2010 10th IEEE International Conference on Solid Dielectrics (ICSD)* 2010, pp. 1-4.
[97] Y. L. Chong, H. Miyake, Y. Tanaka, T. Takada, H. Nakama, and G. Chen, "Space charge in polyethylene under AC electric stress using the pulsed electroacoustic method," *2004 Annual Report Conference on Electrical Insulation and Dielectric Phenomena,* pp. 77-80, 2004.
[98] Y. F. F. Ho, G. Chen, A. E. Davies, S. G. Swingler, S. J. Sutton, R. N. Hampton, and S. Hobdell, "Measurement of space charge in XLPE insulation under 50 Hz AC electric stresses using the LIPP method," *IEEE Transactions on Dielectrics and Electrical Insulation,* vol. 9, pp. 362-370, Jun 2002.
[99] G. C. Montanari, G. Mazzanti, E. Boni, and G. De Robertis, "Investigating ac space charge accumulation in polymers by PEA measurements," *2000 Annual Report Conference on Electrical Insulation and Dielectric Phenomena,* vol. 1-2, pp. 113-116, 2000.

[100] C. Laurent, G. Teyssedre, and G. C. Montanari, "Time-resolved space charge and electroluminescence measurements in polyethylene under ac stress," *IEEE Transactions on Dielectrics and Electrical Insulation,* vol. 11, pp. 554-560, 2004.
[101] G. Chen, M. Fu, X. Z. Liu, and L. S. Zhong, "ac aging and space-charge characteristics in low-density polyethylene polymeric insulation," *J. Appl. Phys.,* vol. 97, p. 083713, 2005.
[102] G. Chen, T. Y. G. Tay, A. E. Davies, Y. Tanaka, and T. Takada, "Electrodes and charge injection in low-density polyethylene using the pulsed electroacoustic technique," *IEEE Transactions on Dielectrics and Electrical Insulation,* vol. 8, pp. 867-873, 2001.
[103] M. Fujii, M. Fukuma, T. Tokoro, Y. Muramoto, N. Hozumi, and M. Nagao, "Numerical analysis of space charge distribution in polypropylene film under AC high field," in *Proceedings of 2001 International Symposium on Electrical Insulating Materials, (ISEIM)*, 2001, pp. 156-159.
[104] K. Kojima, Y. Takai, and M. Ieda, "Electroluminescence in Polyethylene Terephthalate (PET). II. AC Voltage," *Japanese Journal of Applied Physics,* vol. 22, pp. 1436-1438, 1983.
[105] C. Laurent, C. Mayoux, and S. Noel, "Mechanisms of electroluminescence during aging of polyethylene," *Journal of Applied Physics,* vol. 58, pp. 4346-4353, 1985.
[106] C. Laurent, F. Massines, and C. Mayoux, "Optical emission due to space charge effects in electrically stressed polymers," *IEEE Transactions on Dielectrics and Electrical Insulation,* vol. 4, pp. 585-603, 1997.
[107] G. Teyssedre, G. Tardieu, D. Mary, and C. Laurent, "Ac and dc electroluminescence in insulating polymers and implication for electrical ageing," *Journal of Physics D: Applied Physics,* vol. 34, p. 2220, 2001.
[108] S. S. Bamji, M. Abou Dakka, A. T. Bulinski, and L. Utracki, "Electroluminescence and space charge in nanodielectrics subjected to AC voltage," *Journal of CPRI,* vol. 4, pp. 185-194, 2008.
[109] N. Hozumi and et al., "Behaviour of space charge correlated with electroluminescence in cross-linked polyethylene," *Journal of Physics D: Applied Physics,* vol. 37, p. 1327, 2004.
[110] S. S. Bamji, A. T. Bulinski, and R. J. Densley, "The Role of Polymer Interface During Tree Initiation in LDPE," *Electrical Insulation, IEEE Transactions on,* vol. EI-21, pp. 639-644, 1986.
[111] J. Jonsson, B. Ranby, D. Mary, C. Laurent, and C. Mayoux, "Electroluminescence from polyolefins subjected to a homogeneous ac field," *Dielectrics and Electrical Insulation, IEEE Transactions on,* vol. 2, pp. 107-113, 1995.
[112] T. Mizuno, Y. S. Liu, W. Shionoya, K. Yasuoka, S. Ishii, H. Miyata, and A. Yokoyama, "Electroluminescence in insulating polymers in ac electric fields," *IEEE Transactions on Dielectrics and Electrical Insulation,* vol. 4, pp. 433-438, Aug 1997.
[113] P. L. Lewin, S. J. Dodd, and A. M. Ariffin, "Simulation of Electroluminescence using a Bipolar Recombination Model," in *IEEE International Conference on Solid Dielectrics, ICSD '07.*, 2007, pp. 15-18.